D-MEM
PhD-UNIMI

Doctorate program
Milan
EXPERIMENTAL
MEDICINE

Università degli Studi di Milano

PhD Course in
Experimental Medicine

CYCLE XXXVI

PhD thesis

Zebrafish (*Danio rerio*) as a model system for the functional validation of candidate genes for human diseases

---

Candidate: **Dr. Alessia Brix**

Matr. R12846

Tutor: **Prof. Anna Pistocchi**

Director: **Prof. Nicoletta Landsberger**

Academic Year 2023-2024

Table of Contents

Abstract

In recent years, zebrafish (*Danio rerio*) has become increasingly utilized as a model for studying human gene functions and associated diseases. This has been possible due to the very high conservation of genes and of organs and systems which are fully functional within the very first days of embryonic development. The easy and efficient genetic manipulation, the large number of offspring, and the rapid and external development of the embryos make zebrafish ideal for the generation of disease models and for the conduction of large-scale drug screenings. Thus, zebrafish represents a valuable tool to be used as a support, or in particular cases as a substitute, for other animal models in preclinical research. This PhD project aimed precisely at utilizing zebrafish to generate models of human diseases whose pathogenesis is currently poorly understood and for which effective treatments are not yet available.

The main research line focused on the zebrafish model for adenosine deaminase 2 deficiency (DADA2), an auto-inflammatory disease caused by loss-of-function mutations in the *ADA2* (also termed *CECR1*) gene and involving the hematological and vascular compartments. Advances in the comprehension of the molecular mechanisms underlying DADA2 and in the development of effective therapies are hampered by the lack of *in-vivo* models, due to the lack of an ADA2 orthologue in rodents. We generated a zebrafish DADA2 model with loss-of-function of the *cecr1b* gene, the functionally conserved *ADA2* orthologue. We utilized the CRISPR-Cas9 genome editing approach to target *cecr1b* and generated a transient mutant model. We combined several techniques, imaging tools, and transgenic lines to characterize in detail the hematological, inflammatory, and vascular defects of *cecr1b* deficient embryos. We found that they recapitulated the main clinical phenotypes of patients and that they effectively responded to currently used pharmacological therapies. We identified an impairment in adenosine-mediated signaling, which we corrected resulting in a significant improvement in hematological and inflammatory defects. We have therefore developed a valuable zebrafish model for studying the physiological function of ADA2 and the pathogenetic mechanisms of DADA2 and for testing new possible therapeutic strategies. In parallel, we have deepened our knowledge of the possible pathogenesis of this disorder, laying the foundations for new potential correction methods.

A further line of this PhD work was dedicated to the generation of a zebrafish model of MicroCephaly Primary Hereditary 17 (MCPH17), a neurodevelopmental disorder characterized by microcephaly and mental retardation. Mutations in the *CIT* gene have been identified as causative for MCPH17. However, the CIT physiological function and the pathogenesis of MCPH17 are still unclear, and there is currently no curative option. To support and implement the data collected on the murine models and to further investigate the neurodevelopmental mechanisms of MCPH17, which are crucial given the congenital nature of the disorder, we generated a zebrafish model with *cita* deficiency. We induced *cita*-loss-of-function through a morpholino-mediated knockdown approach, which resulted in a significant reduction in head size, behavioral alterations, and impairment of neuronal cell populations. In parallel with the characterization of the *cita* morphants phenotypes, we conducted N-acetylcysteine treatments, which resulted beneficial in treating both the microcephalic condition and the behavioral alterations, as in mice. We demonstrated the potential of the zebrafish in supporting mice models for the comprehension of altered neurodevelopmental processes in MCPH17 and in providing a platform for rapid drug screenings.

A further line of research, as yet unfinished, focuses on the study of the pathogenicity of a mutation in a gene of unknown function, named *GENE-X* in the present thesis. *GENE-X* was identified as possibly responsible for a complex inflammatory/vascular/metabolic syndrome exhibited by a case report. This section of the PhD project aims to characterize the functional role of *GENE-X* and the pathogenicity of the mutation identified in the case report using zebrafish as a model system. We have set up and validated a *gene-x* morpholino-mediated knock-down strategy and started the characterization of the resulting phenotypes. Preliminary analyses, currently extended to the inflammatory and vascular phenotypes only, suggest a significative similarity to the symptoms displayed by the patient under investigation. Once completed the characterization of the model, rescue experiments with the wild-type and mutated *GENE-X* transcripts will be carried out to evaluate, indirectly, the pathogenicity of the disease and investigate its effects.

The last line of research included in this PhD project concerns the generation of a zebrafish model for triadin knock-out syndrome (TKOS). TKOS is a rare, inherited arrhythmogenic cardiac disorder, possibly leading to exercise-induced cardiac arrest in early childhood. Homozygous mutations in the triadin (*TRDN*) gene, encoding for a

muscular protein essential for the structural integrity of the calcium release complex and for the regulation of calcium release during excitation–contraction coupling. However, the precise role of trdn and the mechanism responsible for sudden cardiac events in children suffering from TKOS are not entirely clear, and current anti-arrhythmogenic treatments are often not effective. Hence, there is a need for an *in vivo* TKOS model to further study the function of TRDN and to perform drug screening to rapidly identify new compounds efficient in restoring proper cardiac function. We identified zebrafish as a possible model system for this objective. We generated a *trdn*-deficient zebrafish model by exploiting the morpholino-mediated knockdown. Through morphological and functional analyses, we excluded significant alterations in the structure and function of skeletal musculature and the heart, but identified a dysregulation of cardiac rhythm, as occurs in TKOS patients. We have also demonstrated how our model responds effectively to the modulation of heart rhythm by currently used drugs in human therapies, strengthening the potential of our model in the study of TKOS-related mechanisms and in the identification of possible new therapeutic targets.

Disclosure of research integrity

All the experiments of this PhD work were carried out following the principles of integrity in scientific research, such as reliability, honesty, respect, and responsibility. The University of Milan, where this project was carried out, promotes the knowledge and dissemination of the European Code of Conduct for Research Integrity. Dr. Alessia Brix, together with the other researchers involved in the experimental procedures, was carefully trained on the basic principles of research integrity by her supervisors and senior researchers. Experimental plans and procedures were designed and clearly defined in advance considering the state of the art to avoid unnecessary use of biological samples. Animals and research samples were treated with respect and care according to the National and International Guidelines. All decisions have been made under legal, ethical, and scientific principles, with careful consideration of the impact of the research activity on both the scientific community and society.

Abbreviations

ADAs: Adenosine Deaminases

ADA1: Adenosine Deaminase 1

ADA2: Adenosine Deaminase 2

ADA-SCID: ADA-related Severe Combined Immuno-Deficiency

Ado: adenosine

AGM: Aorta Gonad Mesonephros

ALM: Anterior Lateral Mesoderm

anti-TNF: anti-Tumor Necrosis Factor

ARs: adenosine receptors

bpm: beats per minute

CA: Caudal Aorta

CECR1: Cat Eye syndrome Chromosome Region candidate1

CHT: Caudal Hematopoietic Tissue

CIT: Citron rho-Interacting serine/Threonine kinase

CNS: Central Nervous System

CRC: Calcium Release Complex

CRISPR: Clustered Regularly Interspaced Short Palindromic Repeats

CV: Caudal Vein

CVP: Caudal Vein Plexus

DA: Dorsal Aorta

DADA2: Deficiency of Adenosine Deaminase 2

DC: Duct of Cuvier

DLAVs: Dorsal Longitudinal Anastomotic Vessels

dpf: days post fertilization

DSB: Double-strand Break

eAdo: extracellular adenosine

EHT: Endothelial to Hematopoietic Transition

EMPs: Erythro-Myeloid Precursors

EP: Erythrocytes Precursors

GAPs: GTPase Activating Proteins

GDIs: Guanidine-nucleotide Dissociation Inhibitors

GEFs: Guanidine-nucleotide Exchange Factors

hG-CSF: human Granulocyte-Colony Stimulating Factor

hpf: hours post fertilization

HR: Homology Recombination

HSCs: Hematopoietic Stem Cells

HSCT: Hematopoietic Stem-Cell Transplantation

HSPCs: Hematopoietic Stem and Progenitors Cells

ICM: Intermediate Cell Mass

ICVs: InterConnecting Vessels

ISVs: InterSegmental Vessels

KO: knock-out

MCPH17: Microcephaly Primary Hereditary 17

MO: morpholino

MP: Monocytes Precursors

NHEJ: Non-Homologous End-Joining

PAM: Protospacer Adjacent Motif

PBI: Posterior Blood Island

PCV: Posterior Cardinal Vein

PLM: Posterior Lateral Mesoderm

RBI: Rostral Blood Islands

ROCKs: Rho-associated serine-threonine Kinases

sgRNA: single guide RNA

SIA: Sub-Intestinal artery

SIV: Sub-Intestinal Vein

SIVP: Sub-Intestinal Vein Plexus

sMO: splicing morpholino

TALENs: Transcription Activator-Like Effectors Nucleases

TKOS: Triadin KnockOut Syndrome

tracrRNA: trans-activating crRNA

VDA: Ventral Dorsal Aorta

ZFNs: Zinc-Finger nucleases

Introduction

1. Zebrafish (*Danio rerio*) as a model system for human genetic diseases

Animals have always been fundamental for modeling and studying human physiological and pathological processes, as they share biological and behavioral characteristics with humans (1). Their use has particular relevance in the biomedical and translational fields of scientific research. Indeed, animal models can mimic the development, progression, and treatment of human diseases in a complex environment where all the interactions between different tissues and organs take place (2,3). Thus, they allow a detailed investigation of the pathogenetic mechanisms and represent a platform for testing new drug therapies and their toxicological and pharmacological aspects for future use in humans (4,5). Vertebrates exhibit a very high conservation of genes and of biological processes with humans, representing the ideal models for studying their function in the context of genetic diseases (6,7). Among vertebrates, mammals as mice (*Mus musculus*), rats (*Rattus norvegicus*) and rabbits (*Oryctolagus cuniculus*), together with non-mammalian species like zebrafish (*Danio rerio*) and frogs (*Xenopus laevis*), have been accepted worldwide as standard animal models, due to the similarity of the physiological processes to humans, their relatively small size, the low cost of breeding and ease of reproduction (8). The choice of the proper animal for a particular study should consider several factors which include: the conservation of the pathophysiological processes, the transferability of findings, the feasibility, and the ethical implications (2,9,10).

Zebrafish, a small freshwater teleost, native of South Asia is gaining increasing interest for human disease modelling (11–14). Firstly, human genetic and genomic organization are highly conserved in zebrafish, with approximately 70% of the human genes having a known zebrafish orthologue (15,16). The gene networks regulating the main molecular and cellular processes are also highly conserved, as are most organs and systems (17–19).
Secondly, zebrafish embryos can be very easily genetically manipulated through multiple well-established and efficient chemical and enzymatic techniques (20). This manipulability, combined with the high number of offspring and the transparency of the embryos, makes zebrafish particularly suitable for genetic screens, where phenotypic changes caused by genetic alterations can be easily and quickly identified (21). Thus,

thousands of mutant lines bearing mutations in protein-coding genes have been created over time and are now maintained in the international repositories and available to the scientific community (Zebrafish International Resource Center (ZIRC), European Zebrafish Resource Center (EZRC), China Zebrafish Resource Centre (CZRC)). In addition to this, *ad-hoc* loss-of-function or gain-of-function studies can be performed by targeting transcripts or genes of interest trough several molecular approaches (22–24). These techniques, which will be discussed in detail in the next session, can be applied to the fertilized eggs right after spawning, making it possible to obtain immediately embryos with transient or stable genetic deregulations. Also, zebrafish offers the possibility of working easily both with individuals at embryonal and larval stage or with juveniles and adult individuals, with considerable advantages. Zebrafish larvae up to 5 days of development are not considered in the new EU Directive 2010/63/EU on the protection of animals used for scientific purposes, opening the way for a wide use of this model system in line with the 3R principles (i.e. refine, reduce, replace) (25). In fact, most of the main organs and systems develop and become functional within the very first days of embryonic development, reducing the time needed for experimental procedures and analyses (26). Moreover, the optical clarity of the embryos and their external development allow to easily visualize the morphogenetic processes and their possible pathological alterations. Such abnormalities are largely diffused especially in congenital disorders, but cannot be easily studied in animals that, like mammals, have an intrauterine development (27). Transgenic reporter lines, which are largely diffused and utilized among the zebrafish community, are a valuable tool for this type of studies. Indeed, they allow the expression of fluorescent proteins in tissues in a promoter-specific way, highlighting anatomical or developmental variations with respect to the physiological condition (28). As regards the test of new drugs for pharmacological therapies, zebrafish embryos can be utilized for high-throughput drug screenings to simultaneously test hundreds of compounds and identify the most effective ones (29,30). The findings from the embryo studies can then be supplemented and integrated with other important information that zebrafish adult models can provide. The use of stable adult mutant lines makes it possible to study late-onset diseases or phenotypes, and degenerative disorders (31). It also provides a platform to analyse complex aspects of pharmacokinetics and toxicity of new drugs and allows to analyse separately the effects on the organs that metabolise them (32).

In conclusion, although not as immediately translational as mammals, zebrafish represents a powerful pre-clinical model for studying the pathogenesis and treatments of human diseases, mediating between *in vitro* models and mammalian ones.

1.1. Methods for the generation of zebrafish disease models

In recent decades, next-generation sequencing (NGS) techniques have generated massive amounts of high throughput whole-genome data (33,34). These techniques make it possible to rapidly sequence whole genomes or specific target regions by identifying mutations in specific genes, quantify mRNAs for gene expression analysis and study rare somatic variants and epigenetic factors (35,36). Although these data can be invaluable for studying pathogenetic mechanisms, the pathogenetic role of a specific gene must be functionally validated. Zebrafish have always been used for genetic screenings, for identification of genotype-phenotype correlations and for the study of gene functions especially during development (37–39). Such studies can be conducted by means of a forward or of a reverse genetic screening approach (18,40). Forward genetic approaches are based on the identification of genes involved in a specific biological process or pathway by screening individuals carrying random mutations and exhibiting particular phenotypes (18,40). Mutations are initially induced by treating embryos with mutagenic agents, such as the typical N-ethyl-N-nitrosourea (ENU) treatment, or by injecting insertional mutagenic agents, such as retroviruses or transposons (41–44). Mapping of the modified alleles within the genome of affected individuals reveals genes responsible for those specific phenotypes (18,40). Reverse genetic approaches, instead, involve targeting of a specific gene followed by the analyses of the resulting phenotypes (18,40). Over the years, numerous molecular approaches have been developed to create loss-of-function or gain-of-function zebrafish models for a specific gene. Such techniques can modulate the function of a gene transiently or stably, depending on whether the transcript or the genome is targeted. Each of these methods offers advantages and poses limitations, which need to be carefully evaluated to select the most appropriate methodology for the research objective.

1.1.1. Modulation of gene expression through transient approaches

Transient approaches are based on the modulation of the transcript of a specific gene, which can be downregulated or over-expressed as described in detail in the following paragraphs (24). These strategies are applied directly from the earliest stages of embryo development (1-2 cells stage). They provide an immediate effect, but they action is limited to the first few days of development. They can therefore be used to analyse physiological and pathological aspects of gene function in processes occurring in the early stages of development but not to investigate long-term aspects of a disease.

1.1.1.1. Morpholino-mediated knock-down

The standard approach to interfere with gene expression in zebrafish is the use of specific morpholinos (22,45). Morpholinos are synthetic antisense oligomers complementary to the sequence of a target transcript (46). Their stable, RNAse-H insensitive molecular structure is composed of 25 subunits methylenemorpholine rings linked to nitrogen bases and joined by phosphorodiamidate interlinkages (47,48). Upon binding to their complementary sequence on the transcript, they create a steric hindrance that prevents proper processing or translation (49,50) (Figure 1) . In fact, morpholinos can be designed to pair either to the regions surrounding splicing sites (splicing morpholinos) or to the translation-start region (ATG-morpholino) (51) (Figure 1). Splicing morpholinos act by preventing the correct splicing process, leading to intron retention or exon skipping (Figure 1A,B). By using them, it is possible to induce the expression of altered transcripts, leading to the production of truncated or out-of-frame non-functional proteins (52,53) (Figure 1A,B). Because of their mechanism of action, splicing morpholinos can act only on pre-mRNAs before maturation of the transcript has occurred. It is fundamental to consider they have no effect on maternally expressed genes, whose mature transcripts are already present in the yolk (51,54). ATG-morpholinos impede the correct assembly of the ribosome subunits at the translation initiation site, thus preventing the production of the protein (Figure 1C). In this case, both mature and unprocessed transcripts can be targeted (55). Morpholinos are micro-injected in 1-4 cells stage embryos and, following cell divisions, they are

uniformly distributed to all the cells of the developing organism leading to a ubiquitous knock-down (56). The extent in the downregulation depends on the amount of endogenous transcript that morpholinos can bind and consequently on the dose administrated. Thus, it is possible to modulate the effects of morpholinos by varying the injection dose, which can be a great advantage especially for diseases whose phenotypes are dose-dependent (51). Despite its ubiquitous action, the amount of morpholino molecules available in the cells dilutes as the organism proceeds with cell divisions, making this approach time limited.

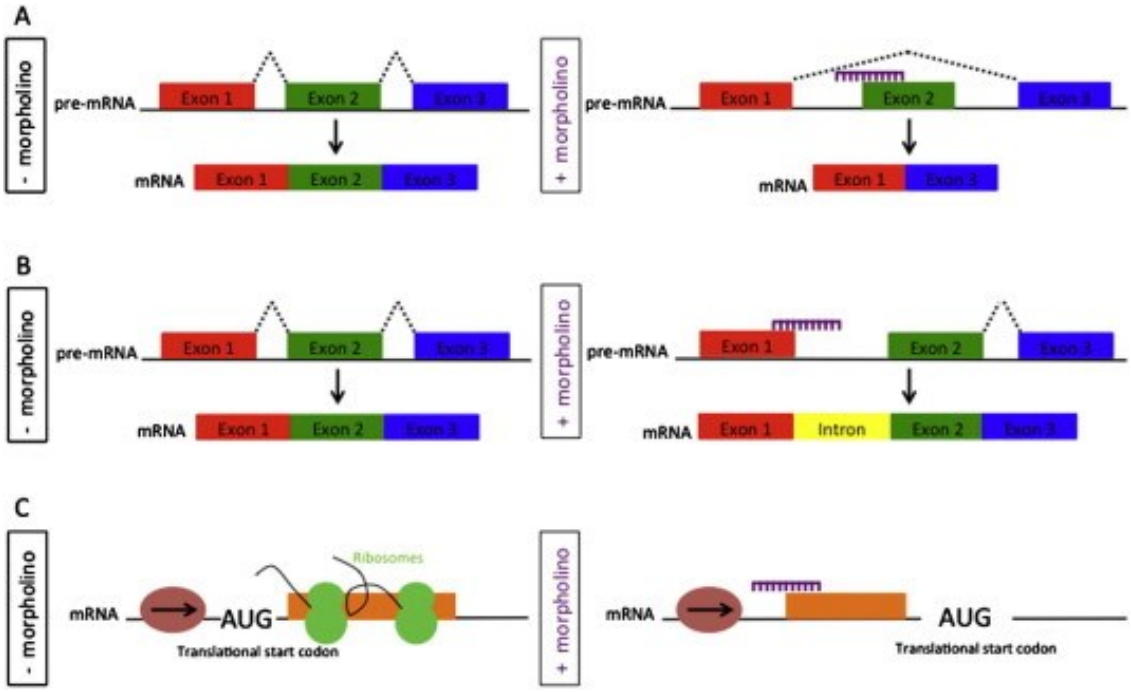

Figure 1. schematic representation of the action mechanisms of morpholinos. (A,B) Action of splicing morpholinos: transcripts are normally spliced to create a mature mRNA through removal of introns and linkage of exons as depicted in the left side of the figure. Splicing morpholinos shown in the right side of the figure can target intron-exon boundaries **(A)** or exon-intron boundaries **(B)**, preventing proper splicing and leading either to exon skipping **(A)** or intron retention **(B)**. **(C) Action of splicing morpholinos:** mRNAs are normally translated as illustrated in the left side of the picture, with ribosomes assembled over the mature transcript and translating it. Translation-blocking morpholinos create a steric hindrance on the translation initiation region, impeding translation as shown in the right side on the figure. Modified from (57)**.**

To ensure the validity and reliability of a morpholino-mediated knock-down, a few considerations must be made. First, it is necessary to validate the efficiency of the morpholino action by checking for the appearance of altered transcripts or for the reduction of the protein levels, depending on the type of utilized morpholino(50).

The ubiquitous action of the morpholino, which is not restricted to the tissues where the transcript is expressed, could lead to increased risk of off-target effects (58). The specificity of phenotypes must therefore be verified, to ensure that they are due to the knockdown of the gene of interest. It is recommended to combine sub-critical doses of non-overlapping morpholinos targeting different regions of the same transcript, known to give a synergistic and highly specific effect (54,59). To further exclude non-specific targeting, rescue experiments with the wild-type and with mutant mRNAs should be performed, to check the efficacy and the specificity in rescuing the morpholino-induced phenotypes (51,60). Moreover, a proper scrambled, inverted or no-target morpholino should be injected at the highest used dose as a control (51,60).

More recently, non-conventional modified morpholinos have been developed to perform gene downregulation in a more spatiotemporal-specific manner. These are the caged morpholinos and the vivo-morpholinos. Caged morpholinos are composed by a standard antisense oligomer enveloped in a photocleavable protection layer (61,62). The action of caged morpholinos can be precisely activated in specific tissues or organs or at specific developmental stages, bringing a great advantage to functional genomics studies (63). In vivo-morpholinos the antisense oligomer is covalently linked to a delivery macromolecule composed of an octa-guanidine dendrimer, which facilitates entry into cells (64) Vivo-morpholinos can be injected systemically or locally into adult organisms providing an efficient diffused or localized gene knock-down (65–67).

Morpholinos-mediated knock-down, performed with the appropriate controls and following an accurate experimental design, thus offers a valuable tool for transient loss-of-function studies in zebrafish.

1.1.1.2. Transient gene overexpression

Knock-down techniques are not suitable for the study of diseases linked to hyper-regulation of specific pathways, gain-of-function mutations, or dominant negative and constitutively active variants. In these cases, gene overexpression can be achieved by introducing the specific mRNA encoding the wild-type or mutant protein of interest in

the zebrafish embryos (22). By injecting the wild-type zebrafish or human transcripts, it is possible to mimic pathologic conditions driven by hyper-activation of specific pathways (13,24). Alternatively, the pathogenicity of human disease alleles can be tested by injecting the mRNA bearing the desired mutation (68,69). Like the morpholino-mediated knock-down, direct mRNA injection also leads to a wide effect, resulting in ectopic expression of the transcript. Moreover, as for morpholinos, the dose of mRNA is diluted with progressive cells divisions and the amount of functional transcript decreases over time due to its limited stability (70). As an alternative to direct mRNA injection, expression plasmids are also used. Cell-type-specific promoters and enhancers can be combined to provide tissue-specific distribution. They enable a more stable and long-lasting expression but are unequally distributed between cells and thus create a mosaic organism in which only few cells express the protein of interest (70). Knock-down and overexpression techniques can be combined so that a specific gene is downregulated and substituted by a mutant variant, thus providing and efficient and rapid development of a disease model.

1.1.2. Genome editing techniques for stable mutagenesis

International repositories hold thousands of mutant lines that were generated mainly through large scale chemical mutagenesis (21,37,38). However, in some cases it is necessary to generate *ad-hoc* mutant lines with specific mutations in precise genic regions. In these instances, several sequence-specific mutagenesis techniques can be exploited to develop the desired mutant model (20,23). Such reverse genetic methodologies allow the generation of stable mutant lines, which, in contrast to transient approaches, enable the investigation of long-term pathological and therapeutic aspects (71). Genome editing technologies allow genetic manipulation by modifying, deleting, or inserting sequences in a site-specific manner. Methods for targeted mutagenesis in zebrafish include Zinc-Finger nucleases (ZFNs), transcription activator-like effectors nucleases (TALENs) and the CRISPR-Cas9 system (72–76). Both ZFNs and TALENs are based on the activity of the FokI endonuclease, which is fused with the DNA-binding domain of zinc-finger proteins or with TALE repeats domains, respectively (Figure 2A,B) (77–82). Such DNA-binding domains can be engineered to recognize specific target sequences, providing specificity to the action of FokI cleavage (83–86). Upon binding of two ZFN or TALEN units to DNA sequences

in proximity, the FokI domains dimerize reconstituting their catalytical activity and introducing double strand breaks (DSBs) (Figure 2A,B) (87–89). Following DNA rupture, error-prone DNA-repair mechanisms are activated inducting mutations in the cleaved region. These two methods thus enable sequence-specific and efficient mutagenesis. However, the complexity and high cost of designing protein domains, together with raised concerns about specificity and off-target effects, have led to a shift towards the use of the CRISPR-Cas9 (Figure 2C) (90,91).

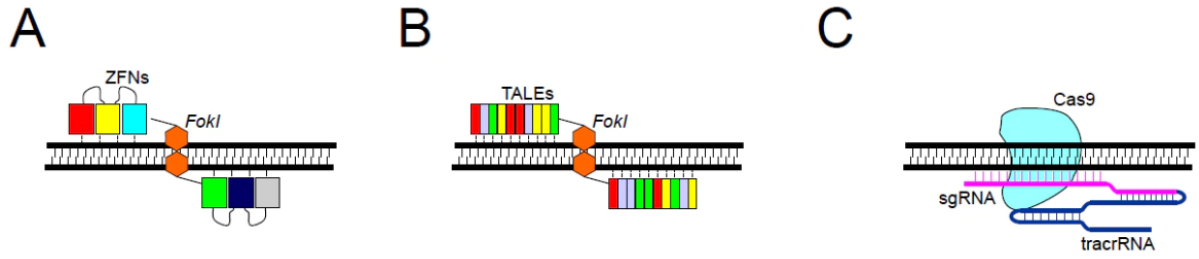

Figure 2. Schematic representation of genome editing nucleases. (A) Zinc-Finger nucleases (ZFNs): two ZFNs (coloured blocks) recognizing the target genomic region bind at opposite DNA strands allowing dimerization of the FokI domains (orange hexagons) leading to DNA cleavage. **(B) transcription activator-like effectors nucleases (TALENs):** like ZFNs, TALEN domains recognize and bind the DNA target sequence inducing FokI dimerization and DNA cleavage. **(C) The CRISPR-Cas9 system:** The Cas9 nuclease is guided and loaded to the genomic target region by the specific sgRNA, associated with the stabilizing tracrRNA. (ttps://www.ptglab.com/news/blog/crispr-cas9-talens-and-zfns-the-battle-in-gene-editing/).

1.1.2.1. Targeted mutagenesis with CRISPR-Cas9

The CRISPR-Cas9 system is based on bacterial acquired immunity, which induces the degradation of invading foreign viral DNA by RNA-guided DNA cleavage (92–94). Procaryotes possess the CRISPR (Clustered Regularly Interspaced Short Palindromic Repeats) loci, which are constituted by short palindromic repeats alternating with exogenous viral DNA sequences, named “spacers” (95). (Figure 3A). CRISPR loci comprise a set of additional conserved genes, encoding for the CRISPR-associated (Cas) proteins essential for proper functioning of the system (96,97) (Figure 3A). Following transcription, a long precursor CRISPR-RNA (pre-crRNA) forms and is then processed and cleaved by the Cas proteins into a series of mature crRNAs, each containing a spacer sequence (98,99). Processed crRNAs function as guides to drive the Cas endonucleases to the specific complementary sequences, the “protospacer”

where they initiate target degradation (98,100). The recognition of the exogenous target to be cleaved is achieved, firstly, by the complementarity between the protospacer sequence of the target DNA and the spacer sequence of the crRNA and, secondly, by the presence of the Protospacer Adjacent Motif (PAM) sequence, a three bases-long sequence which is adjacent to the protospacer. Among the bacterial CRISPR/Cas systems, the *Streptococcus pyogenes* type II system has been selected and adapted for genome editing across species, including zebrafish (101) (Figure 3). This adapted system utilizes RNA guides (gRNAs) consisting of a crRNA with a sequence complementary to the one of interest and a tracrRNA (trans-activating RNA) that mediates the interaction between the crRNA and the endonuclease Cas9 (102,103) (Figure 3B). Once the gRNAs and the Cas9 have been introduced into eucaryotic cells, the DNA DSBs activate the error-prone non-homologous end-joining (NHEJ) or the homology recombination (HR) repair mechanisms (104,105) (Figure 3C). During the NHEJ process, small insertion or deletions are usually inserted into the target genomic region. If they are found in the coding sequence, they can lead to frameshifts or to the formation of premature termination codons, resulting in loss-of-function alleles (106). In HR a homologous DNA strand is utilized as a template for the repair of the damaged one (107). Such mechanism can be exploited to introduce precise point mutations or to perform knock-in by simply providing an exogenous single stranded DNA oligonucleotide as a donor (108,109).

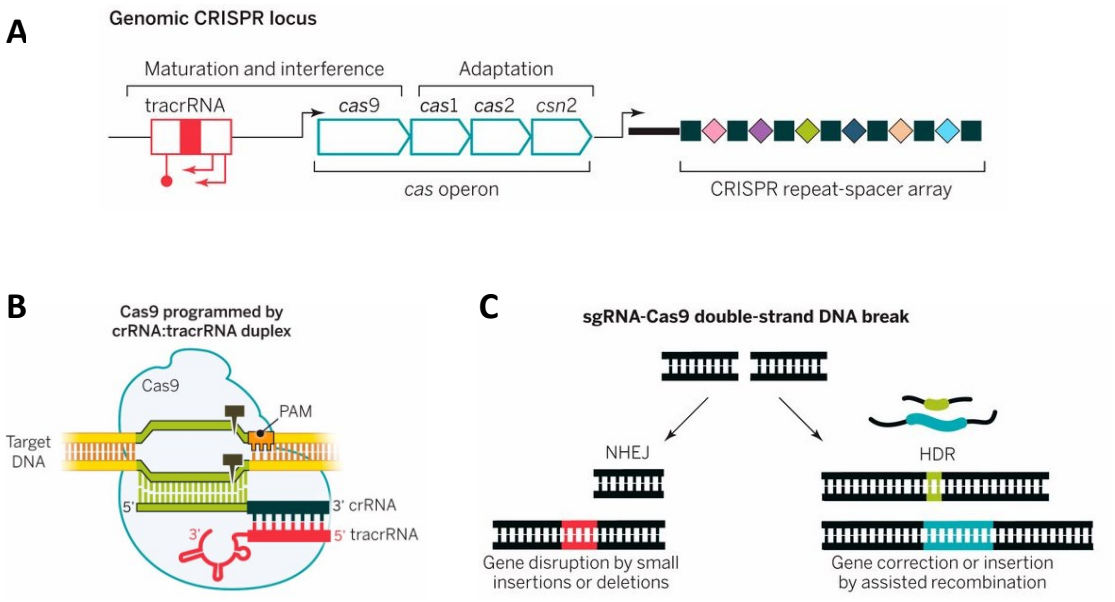

Figure 3. Structure and function of CRISPR-Cas system in *S. pyogenes*. (A) The genomic CRISPR locus: the CRISPR-Cas locus is composed of a tracrRNA encoding sequence, Cas proteins encoding genes, and the CRISPR array composed of short repeats (black squares)

alternating with spacers (coloured rhombi). **(B) Detailed mechanism of target DNA cleavage:** the crRNA-tracrRNA complex forming the sgRNA leads the Cas9 protein to the target genomic region. Here, a DSB is induced in the precise site 3 bases apart from the PAM sequence. **(C) DNA repairing mechanisms induced by sgRNA-Cas9 mediated DSBs:** DSBs induced by Cas9 endonuclease can activate nonhomologous end joining (NHEJ) or homology-directed repair (HDR) mechanisms leading to small indels or to insertion of homologous sequences. Adapted from (101).

Multiple gRNAs can be combined to target different sequences simultaneously or to delete specific genomic regions (e.g. promote sequences or entire coding sequences of genes) resulting in null alleles (110,111). The gRNAs and the Cas9 can be microinjected directly in zebrafish zygotes to create the first F0 generation of mosaic embryos. Indeed, mutations induced by the CRISPR-Cas9 action are not inherited by all cells, thus generating an organism where the gene knock-out is uncomplete (112). These F0 mosaic embryos can be directly used for analyses, or they can be grown to adulthood. The so-called “founders” bearing the mutation in their germinal line can be selected through crosses with wild-type individuals and genotyping of their progeny (113). Founders can be then out-crossed with wild-type fish to generate the F1 heterozygote stable mutant line. In turn, this line can then be maintained in heterozygosity, or the homozygous line can be generated (113).

The CRISPR-Cas9 method thus offers the possibility of creating customised stable mutant zebrafish lines relatively easily and quickly, with very high precision and efficiency. However, some considerations must be made for the generation of disease models with this technique. First, gene compensation must be considered during the experimental design. This aspect is particularly relevant for zebrafish, which possesses paralogues for most of its genes due to teleost whole genome duplication (15,114). In 70% of cases mutants and morphants show discordant phenotypes, with increased severity in morphants (115,116). This was initially attributed to off-target effects of the morpholinos but was later found to be related to transcriptional adaptation (117). Transcriptional adaptation consists in nuclear translocation of mRNA degradation fragments that activate or upregulate the transcription of the related “adapting genes”. These genes can compensate for the absence of the mutant one masking its phenotypes (118–120). mRNA degradation is triggered by premature or lacking termination codons or by secondary structures interfering with ribosome translocation (121–123). All these transcript alterations frequently occur with the CRISPR-Cas9

mutagenesis process, as described above. Therefore, it is preferable to design the mutagenesis strategy to achieve complete deletion of the gene locus or of promoters or regulatory elements (leading to RNA-less alleles), or to obtain in-frame deletion of functional domains (119,124,125). Alternatively, if small indels are introduced during the mutagenesis process, the possible contribution of gene compensation should be always considered. In this case, the comparison of the phenotypes emerged from the knock-down of the gene of interest can provide valuable information. Another fundamental aspect to consider is the recessive or dominant inheritance pattern of the alleles and of the disease to be modelled. In the case of recessive mutations, the stable mutant line is often bred in heterozygosis, especially if the homozygotes are not viable and fertile or are suffering (126,127). Following heterozygotes crossing, the offspring has mixed genotypes (wild-type, heterozygotes and homozygotes), and each embryo must therefore be genotyped after analysis for genotype-phenotype correlation. This complicates and lengthens the time needed for analyses compared to knock-down techniques in which loss-of-function embryos are obtained immediately and in greater numbers. The maternal genic contribution should also be considered. The maternal wild-type transcripts in the yolk of embryos might replace the function of the mutated ones, masking any early phenotypes (128,129). In the case of dominant, sub-lethal or lethal alleles, it may be very difficult or impossible to create a viable and fertile stable line. Ethical considerations should also be carefully evaluated in these cases, as described in international guidelines (EU Directive 2010/63/EU).
In conclusion, zebrafish disease models can be generated through several approaches, which can be combined to obtain a comprehensive view of the biological processes to be investigated (130).

2. Human diseases models

In this section the human genetic diseases covered by this project will be described. For each of them, a brief description of the genetics, clinical phenotypes and currently available therapies will be given. Following this, the knowledge of the biological function of the gene involved, and the possible pathogenetic mechanisms known to date will be summarised, together with reference to the available animal models.

2.1. Deficiency of adenosine deaminase 2 (DADA2)

2.1.1. Clinical manifestations and treatments

Deficiency of adenosine deaminase 2 (ADA2) (OMIM entry: 615688) is a rare and potentially lethal genetic disorder caused by recessive loss-of-function mutations in adenosine deaminase 2 (*ADA2*) gene (previously named *CECR1*) (131,132). Patients affected by DADA2 present a wide spectrum of clinical phenotypes including immuno-haematological manifestations (e.g., neutropenia and bone marrow aplasia), chronic systemic auto-inflammation and endothelial dysfunction leading to recurrent intracranial leakages (133,134). If untreated, DADA2 is life-threatening mostly due to recurrent haemorrhagic strokes and unresolved infections (135). Current therapies are mainly based on anti-TNF agents and granulocyte mobilizers (hG-CSF) and successfully mitigate symptoms but are not resolutive (134,136). Allogenic hematopoietic stem-cell transplantation (HSCT) has proved to be promising in severe DADA2 cases, resulting in immuno-haematological reconstitution and resolution of inflammation (137,138). However, this curative option is limited by the scarcity of donors and by the high risk of severe complications (139). Advances in DADA2 treatment are mostly hampered by the lack of stable animal models to study it. Indeed, rodents do not have an ADA2 orthologue, and the sole DADA2 *in-vivo* model generated so far is a zebrafish *cecr1b* knock-down model exhibiting neutropenia and intracranial haemorrhages (131).

2.1.2. ADA2 biological function and DADA2 pathogenesis

To date, the physiological role of ADA2 remains unclear and no cellular or molecular pathways responsible for DADA2 pleiotropic manifestations have been identified. ADA2, together with the isoenzyme ADA1 constitute the family of human adenosine deaminases (ADAs) which are capable of degrading adenosine (Ado) through deamination (140,141). The role of ADA1 is closely linked to its catalytical function. ADA1 is ubiquitously expressed and exhibits a 100-fold higher affinity for Ado with respect to ADA2, making it the main responsible for Ado degradation (142,143). Indeed, ADA1 deleterious mutations are directly linked to profound impairments in Ado intracellular homeostasis, resulting in the well-known ADA-related severe combined immuno-deficiency (ADA-SCID) (142,143). To elucidate ADA2 physiological function, it is of extreme importance to consider its structure, expression pattern and localization which differ significantly from the ones of ADA1, making them unlikely to play redundant roles (134,141). Unlike the intracellular, monomeric ADA1, ADA2 is secreted as a homodimer prevalently by myeloid cells and localizes in the extracellular environment (134,143–146). In addition to the catalytic domain, ADA2 possesses a receptor binding domain with high sequence conservation to adenosine deaminase growth factors, suggesting a possible double enzymatic/growth-factor function (141,145–147). Although the specific ligands of this receptor domain have not been fully identified, it appears that it may interact with proteoglycans and adenosine receptors on immune cells, mediating their maturation and function (145,146)(141). Indeed, it is well-known that ADA2 regulates proper maturation of monocytes and maintenance of macrophages in an anti-inflammatory M2 status (145,148,149). Moreover, while ADA1 is most likely implicated in Ado deamination under physiological conditions, ADA2 might be required for resolution of inflammatory states. Increased ADA2 levels have been found in patients with auto-inflammatory immune disorders and cancer, where extracellular Ado (eAdo) levels are substantially increased due to ATP turnover (150–152). Emerging evidence suggests that dysregulation of extracellular Ado (eAdo) homeostasis may be implicated in DADA2 pathogenesis. Indeed, DADA2 patients show marked reduction of ADA2 residual enzymatic activity, whose level correlates with the type and severity of clinical manifestations (153). Elevated plasmatic Ado levels have been reported in DADA2 patients in one study (154). Notably, eAdo directly regulates hematopoietic stem-cells (HSCs) homeostasis,

which play a key role in DADA2 context given the haematological manifestations of patients and the curative potential of HSCT (155–157).

2.2. Microcephaly Primary Hereditary 17 (MCPH17)

2.2.1. Clinical manifestations and treatments

Microcephaly primary hereditary 17 (MCPH17) (OMIM entry: 617090) is an autosomal recessive neurodevelopmental disorder associated to mutations in the citron rho-interacting serine/threonine kinase (*CIT*) gene (158–161). Patients affected by MCPH17 present with a congenital, severe reduction of head circumference with simplified brain gyral pattern, agenesis of the corpus callosum and hypoplasia (158–162). These neuroanatomical defects are often associated to short stature and dysmorphic features, delayed psychomotor development, spasticity, and intellectual disability of variable degree (158–162). To date, there is no preventive treatment to correct MCPH-associated neurodevelopmental abnormalities. Only secondary symptoms such as spasticity or seizures can be treated (163). Mutant mouse and rat models with CIT-deficiency are available, and well recapitulate the clinical phenotypes of MCPH17 patients. They both display the microcephaly together with a severe neuronal depletion and a complex neurological syndrome characterized by ataxia and epilepsy (lethal seizures) (164–166). Both these models are extremely valuable for the study of MCPH17 in its post-natal aspects. However, rodent models are not easily exploitable for the investigation of the neurodevelopmental processes due to their internal and relatively long embryonic development. Such pathogenetic developmental processes, which are directly linked to MCPH17, are currently unknown, thus leaving an important gap in knowledge of the disease that needs to be filled.

2.2.2. CIT biological function and MCPH17 pathogenesis

CIT encodes for the citron rho-interacting kinase, a large, multidomain protein. In addition to the N-terminal kinase domain, the CIT structure comprises an internal coiled-coil domain with a Rho/Rac interacting site, a C-terminal region consisting of a Zn finger, a pleckstrin homology domain, Citron homology domain and a putative SH3

binding domain (167–169). Such a complex structure bearing several interaction domains gives CIT, in addition to the kinase activity, a putative role as a molecular interactor with multiple players (170,171). Mammalian CIT proteins derive from two main isoforms: CIT-K and CIT-N (163). CIT-K is the complete mammalian isoform, it is ubiquitously expressed in proliferating cells and regulates cytokinesis (164,167,168). The short isoform, CIT-N, lacks the kinase domain, is specifically expressed in the central nervous system (CNS) and its function is currently unclear (172–174). Converging evidence demonstrate that, despite its ubiquitous expression, CIT-K is required only in the developing CNS (164,166). Indeed, mutant mice with depletion of CIT-K but physiological levels of CIT-N develop a microcephalic condition and recapitulate the neuro-developmental defects typical of MCPH17 (164). Accordingly, the partial and defective development of the CNS has been directly linked to impaired cytokinesis both in patients and in rodent models. Histological cerebellar sections of MCPH17 patients and neuronal progenitors derived from induced pluripotent stem cells showed numerous multinucleated cells and increased apoptosis (159,160). These two phenotypes were also observed in mouse and rat CIT-K deficient models (164–166,175,176). The precise role of CIT-K during cytokinesis has not yet been fully elucidated. However, it is now proved that CIT-K is required for proper shaping and stabilization of the midbody architecture (163,177,178). Recent findings show that CIT-K maintains the proper arrangement of the midbody proteins and links the different components of the contractile ring and of the central spindle (170,171,179–181). Here it also appears to stabilize microtubules and ensures genomic stability (182,183).

2.3. *GENEX*-deficiency – Case Report

2.3.1. Clinical manifestations and treatments

GENE-X has been identified as a highly probable causative gene of a syndromic disorder presented by a paediatric patient being treated at the Istituto Giannina Gaslini in Genova.

The patient presented at the age of 10 with a complex clinical situation. She exhibited a short stature with growth delay and psychotic disorder. She suffered from chronic inflammation, hypergammaglobulinemia, and swollen, granulomatous lymph nodes with high lymphoproliferation suggesting immune system involvement. She also presented with dyslipidaemia, reduced high-density lipoproteins, progressive occlusion of medium-calibre arteries, and recurrent cerebral ischaemia. Compromised vessels showed an altered structure, resembling atherosclerotic plaque. Treatments with immune-suppressive agents (glucocorticoids and anti-interleukin6 monoclonal antibodies) led to recovery of inflammation, hepatosplenomegaly, and lymph node swelling, but not of the vascular impairments, excluding vasculitis. The patient, together with her consanguineous parents underwent whole exome sequencing which revealed a homozygous missense mutation in the functional domain of *GENE-X* (T518K).

2.3.2. GENE-X biological function

GENE-X encodes for an unknown GTPase activating protein (GAP), belonging to the family of the Ras-Homologue (Rho) GTPase regulators. Rho-GTPases are involved in a wide series of molecular and cellular processes including cytoskeleton regulation, cell differentiation and cell cycle regulation (184–186). They are usually located at the plasma membrane where they mediate signal transduction of numerous signalling pathways (187,188). Alternance between an active GTP-bound and an inactive GDP-bound conformation allows them to regulate effector proteins thus inducing specific cellular responses (185,189). This cycling is finely regulated by the guanidine nucleotide exchange factors (GEFs), the GTPase activating proteins (GAPs) and the guanidine nucleotide dissociation inhibitors (GDIs) (189). GEFs activate Rho GTPases

by promoting the release of GDP and the uptake of GTP, while GAPs induce their intrinsic GTPase activity, inactivating them (190). GDIs sequester the GDP-bound of GTPases in the cytoplasm, preventing their proper localisation in the membrane or their activation by GEFs (191). The direct downstream effectors of Rho-GTPases are the Rho-associated serine-threonine kinases (ROCKs), which are involved in cancer and in many other pathological processes associated to the cardiovascular, nervous, and muscular compartments (192,193). The precise biological function of GENE-X is currently unknown as are possible pathological mechanisms associated to it.

2.4. Triadin KnockOut Syndrome (TKOS)

2.4.1. Clinical manifestations and treatments

Triadin KockOut Syndrome (TKOS) (OMIM entry: 603283) refers to a rare, inherited arrhythmogenic condition associated to null mutations in the triadin (*TRDN*) gene (194–196). TKOS is manifested in early childhood and causes a series of arrhythmias with T-wave inversions, transient long QT, and life-threatening exercise-induced cardiac arrest (195,197–200). In addition to the arrhythmogenic phenotype, patients with TKOS exhibit mild proximal muscle weakness and myopathy in absence of gross anatomical abnormalities (194,201). Conventional therapy for TKOS is based on β-blockers combined with sodium or calcium channel blockers but is often insufficient to prevent recurrent breakthrough cardiac events (194). A high proportion of refractory patients underwent cardiac sympathetic denervation or device implantation as additional treatment, highlighting the importance of developing novel, non-invasive, therapeutic strategies (194). Mice models with Trdn loss-of-function have been developed over time and have contributed to the study of TRND physiological function and pathological aspects. Complete knock-out of Trdn in mice resulted in cardiac arrhythmias and reduced strength of skeletal muscles, combined with altered excitation-contraction coupling and impaired function of the calcium release complex (CRC) (202–204). To date, these models have not been directly used for development of new therapies. Therefore, a TRDN loss-of-function model enabling drug screening for identification of novel therapeutic compounds is still missing.

2.4.2. TRDN biological function and TKOS pathogenesis

Triadin is a transmembrane protein composed of an N-terminal cytosolic domain, a transmembrane domain crossing the membrane of the junctional sarcoplasmic reticulum and a long, positively charged C-terminal tail protruding into the lumen of the sarcoplasmic reticulum (205,206). TRDN was demonstrated to play an essential role in the regulation of calcium release from the sarcoplasmic reticulum during the excitation–contraction coupling mechanism, both in cardiac and in skeletal muscle cells (196). Excitation-contraction coupling, essential for proper muscular contraction,

is regulated by a multiprotein complex composing the CRC (207,208). Several evidence demonstrate that TRDN binds to multiple proteins of the CRC, providing structural stabilization of the complex and mediating proper calcium release from the sarcoplasmic reticulum (208–211). Ablation of Trdn in mice causes alterations in the structure and composition of the cardiac CRC and increases sarcoplasmic reticulum calcium overload (202,204). This calcium excess is thought to increase the frequency of spontaneous ectopic Ca2+ release from the sarcoplasmic reticulum leading to arrhythmias and decreased muscle strength (202,204). Electron microscope analyses of muscular biopsy from TKOS patients also revealed alterations in the ultrastructure of the sarcoplasmic reticulum, which are predictive of altered CRC function (201).

3. Morphological and physiological features of the developing zebrafish

The human diseases described in the previous section involve numerous organs and systems. In the case of DADA2 and GENE-X deficiency, the vascular and immune compartments are primarily affected, while for TKOS and MCPH17, the cardiac and nervous systems respectively are of primary relevance. They are all highly conserved between mammals and zebrafish. Indeed, numerous studies demonstrated how zebrafish can be utilized for the study of the cardiovascular, immuno-haematological, and nervous systems (212–217). They all develop within the first days of embryonic development, through closely interconnected processes which need to be perfectly timed and regulated. They are fully functional in the zebrafish larvae even if still simplified with respect to their adult counterparts (26). This gives zebrafish the unique advantage of studying physiological and pathological processes in a complete but simplified *in-vivo* model.

3.1. Zebrafish cardiovascular system

As mammals, zebrafish has a closed cardiovascular system which forms very early during embryonic development to support growth and development (218,219). Despite relevant differences such as lack of a pulmonary circulation and a two-chambered instead of a four-chambered hearte, zebrafish is widely utilized as a model for cardio-vascular pathologies. Indeed, the cardiovascular systems between zebrafish and mammals are highly similar in terms of anatomy and physiology (220–222). Embryos small size enables oxygen diffusion, allowing survival and development in presence of compromised cardiovascular systems (223–225). This permits the study of severe cardio-vascular human diseases that are typically embryonic lethal. Development and function of the zebrafish embryonic cardiovascular system is described in the next section.

3.1.1. Zebrafish vasculature

A primitive, completely functional vascular tree develops in the first 24-26 hours post fertilization (hpf) trough vasculogenesis, the de-novo formation of blood vessels

(226,227). Endothelial cells progenitors, the angioblasts, originate during early gastrulation from an endothelial-hematopoietic bipotential progenitor located in the mesoderm: the hemangioblast (228). At around 12 hpf angioblasts became specified and migrate to the embryonic midline anteriorly to posteriorly (229). Here they give rise to two chord-like structures which then originate the two main axial vessels of the embryo (229). The two axial vessels primordia lumenize by 24 hpf, before the onset of circulation (230). At around 26 hpf, the primary vascular system is completely functional. The primary circulatory loop starts with the two lateral dorsal aortae, conveying blood from heart and converging into the dorsal aorta (DA). From there, blood passes into the caudal aorta (CA), the caudal vein (CV) and finally into the posterior cardinal vein (PCV), which returns blood to the rostral region of the embryo (Figure 4A). Blood is then drained back to the heart through the duct of Cuvier (DC) to start a new circulatory loop (Figure 4A) (226). This primitive vascular tree is remodelled and expanded through angiogenic processes which originate specialized vascular structures (231,232). As early as 3 days post fertilization (dpf) multiple specialized vascular structures can be recognized including the intersegmental vessels (ISVs), the dorsal longitudinal anastomotic vessels (DLAVs), the complex brain vasculature, the sub-intestinal vein plexus (SIVP), and the caudal vein plexus (CVP) (226,231) (Figure 4B). Of these, the last two have relevance to this project and will be further discussed in the next sections.

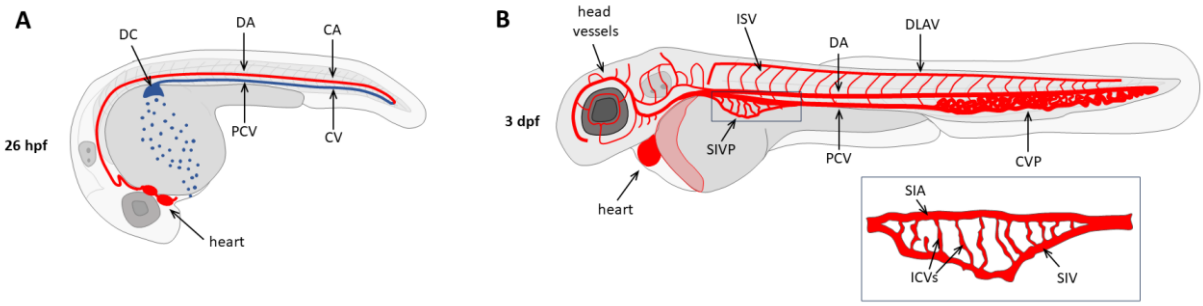

Figure 4. Vascular system of the developing zebrafish embryo at 26hpf (A) and 3 dpf (B). (A) Primitive circulatory loop at 26 hpf: blood flows from heart to the caudal region of the embryo through the dorsal aorta (DA) and the caudal aorta (CA). Then, it is conveyed back to the rostral region through the caudal vein (CV) and posterior cardinal vein (PCV). Finally, it returns back to the heart through the Duct of Cuvier (DC), spreading over the yolk sac. **(B) Vascular tree of a 3 dpf embryo:** the primitive vascular system has expanded and further developed via angiogenesis. Several vascular structures can be recognized; rostrally to caudally: the complex head vasculature, the sub-intestinal vein plexus (SIVP), the intersegmental vessels (ISVs), the bilateral dorsal longitudinal anastomotic vessels (DLAVs) and the caudal venous plexus (CVP). The bottom right rectangle shows the detail structure of the SIVP, composed of a sub-intestinal artery (SIA), a sub-intestinal vein (SIV) and several interconnecting vessels (ICVs).

3.1.1.1. The sub-intestinal vein (SIVP) and the caudal vein plexus (CVP)

The sub-intestinal vein plexus (SIVP) is the vascular structure responsible for absorption of nutrients from the yolk and, subsequently, for the blood supply to the digestive system (226,233). The mature SIVP at 3 dpf lays on the yolk and is composed of the supra-intestinal artery (SIA), the two bilateral sub-intestinal veins (SIVs) and the interconnecting vessels (ICVs) forming the typical honeycomb-shaped structure (Figure 4B) (233). SIVP is prevalently composed by venous vessels which are profoundly remodelled through complex angiogenic processes and is therefore an excellent structure for studying angiogenesis (233). A direct link between regulation of the SIVP angiogenesis and lipidaemia has been demonstrated (234–236). The yolk is the unique source of lipids and proteins for the developing embryo up to 5 dpf, when it begins to feed independently (237–239). Thus, correct patterning and extension of the SIVP is essential for conveying nutrients from the yolk and sustain proper embryo growth and development. Changes in lipid balance are sensed by endothelial cells which respond increasing or decreasing SIVP angiogenic processes accordingly (234). Therefore, during early stages of development, regulation of lipidaemia and of angiogenesis are closely linked. Impairments in one of the two processes necessarily affects the other.

The caudal vein plexus (CVP) hosts the caudal hematopoietic tissue and serves as a vascular niche for hematopoietic stem cells (HSCs) during development (240–242). The CVP develops from angiogenic sprouts emerging from the caudal vein by 24-25 hpf and progressively remodels to form a network of interconnecting vessels (231,243). At 2 dpf, the CVP appears as a complex, well perfused vascular bed being colonized by definitive HSCs (231,243). Once in the perivascular portion of the CVP, HSCs are embedded in pocket-like structures by endothelial cells, which protect them and regulate their function (240). The complex environment of the CVP niche tightly regulates HSCs function, proliferation, and differentiation, as described in detail in the Section 3.2.

3.1.2. The zebrafish heart

The zebrafish heart is the first organ to develop and become functional, appearing as a contracting linear bilayer tube as early as 24 hpf (26,244). From 28 to 36 hpf the heart undergoes a leftward looping pushing the ventricular chamber to the right of the atrium (Figure 5A,B) (245,246). At around 36 hpf, the heart slow, peristaltic contractions switch to sequential chamber contraction activity, indicating the onset of cardiac conduction system (246). By 48 hpf, the cardiac looping has completed, and the two contracting chambers are clearly distinguishable and separated by an atrioventricular canal (Figure 5C)(244,247). At 3-5 dpf, the heart is composed of an inflow tract, an atrium and a ventricle separated by an atrioventricular valve, and an outflow tract ending with the bulbus arteriosus (Figure 5D) (244).

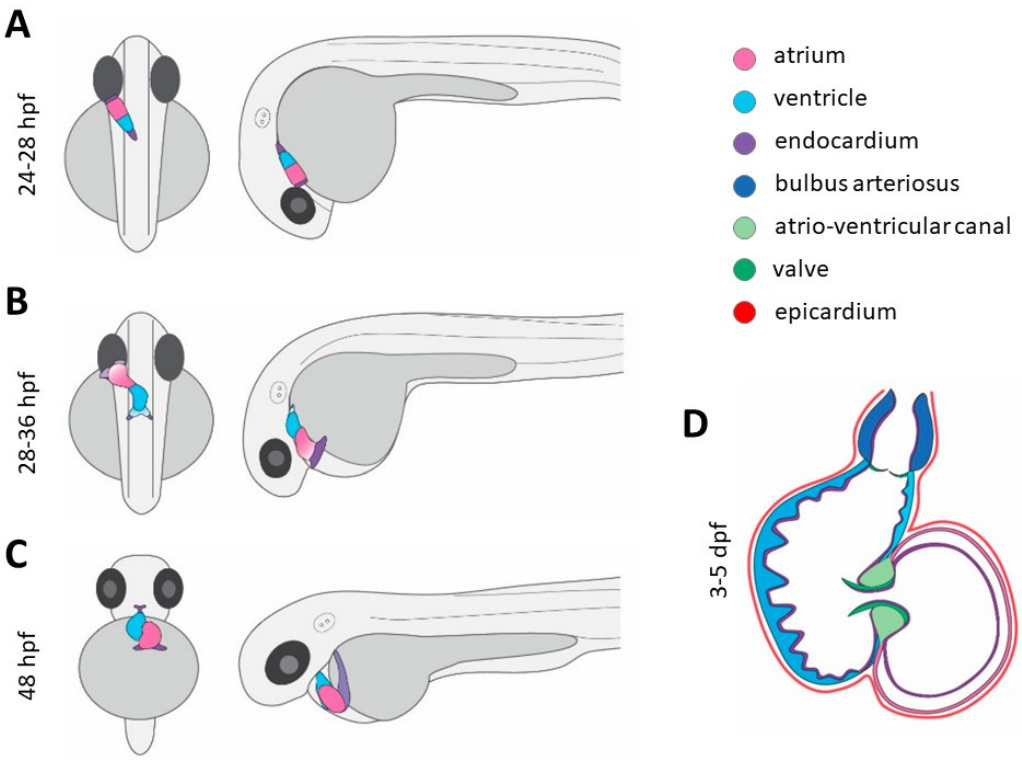

Figure 5. Steps of zebrafish cardiac development from 24 hpf to 5 dpf. (A-C) dorsal and lateral views of the zebrafish embryo with the different cardiac anatomical components: (A) at 24-28 hpf the zebrafish heart appears as a tubular contractile structure, where atrial and ventricular regions have already specified. (B) between 28 and 36 hpf the heart structure undergoes partial looping acquiring an "S" shape and the sequential contractions of the cardiac chambers start. (C) By 48 hpf the cardiac looping is complete, and the two chambers are completely distinguishable. **(D) Schematic representation of zebrafish heart at 3-5 dpf:** by 3-5 dpf the zebrafish heart has acquired a complete structure with all the anatomical elements of the adult heart, as depicted in (D). Colour code of the different cardiac structures and tissues is reported in the right side of the figure. Modified from (248).

Zebrafish heart rate is regulated, as in mammals, by pacemaker cells located at the sinoatrial boundary and responsible of inducing spontaneous and synchronous myocardial contractions (249–251). The basal heart rate of zebrafish embryos is 130-180 beats per minute (bpm) at 28°C, which is much more similar to the human one (60-70 bpm) compared with that of mice (500-600 bpm) (252–255). Of note, cardiac electrophysiology is remarkably similar between humans and zebrafish, largely due to the similarities in heart rate and electrical properties (256,257). Electrocardiogram recordings in zebrafish showed clearly recognizable P (atrium depolarization), QRS-complex (ventricular depolarization) and T (ventricular repolarization) waves, with a QT duration similar to humans (258,259). Resting membrane potential and action potential are also comparable between humans and zebrafish hearts in terms of both amplitude and duration (259). Moreover, most of the ion channels and regulatory proteins required for human cardiac function are conserved in zebrafish and allow easy genetic and chemical modelling of human heart pathological conditions (259–261).

3.2. Hematopoiesis and development of immune cells

Hematopoiesis is the process of generation and maturation of blood cells. It entails the formation, proliferation and maintenance of hematopoietic stem and progenitor cells (HSPCs) and their differentiation into multilineage progenitors then originating specific blood cell types (262). Processes and cell types involved in hematopoiesis are highly conserved among vertebrates, making zebrafish a valuable model for the study of the molecular bases and steps of such developmental process and associated diseases (263–266). Vertebrate hematopoiesis occurs in three different steps: the primitive, transient and definitive steps (265). The primitive hematopoietic wave supplies erythrocytes and monocytes precursors (EP and MP), required for facilitation of oxygen provision to the tissues and for immune protection during early developmental stages of the embryo (267). Primitive hematopoiesis takes place in the blood islands of the yolk sac in mammals and in the corresponding zebrafish rostral blood island (RBI) and intermediate cell mass (ICM), originated from the anterior and posterior lateral mesoderm (ALM and PLM), respectively (Figure 6A) (268,269). Blood islands host the hemangioblasts, the common endothelial-hematopoietic bipotential progenitors originating from embryonic mesoderm and giving rise to either angioblasts (*Kdrl*+) or

erythrocyte/monocyte progenitors (*Gata1+/Spi1b+*) (268–271). In zebrafish, *gata1+* erythrocytes precursors and *spi1b+* myeloid precursors emerge by 12 hpf in the RBI and ICM, respectively (272–274). By 16-18 hpf, myeloid progenitors initiate the expression of the pan-leucocyte *l-plastin* marker, together with more specific monocyte or neutrophil genes (214). At the same time, *gata1+* erythrocyte precursors in the ICM start expressing embryonic haemoglobin, originating mature erythrocytes which start circulation at 24 hpf (214). Primitive erythrocyte and myeloid progenitors do not exhibit self-renewal capacity and are therefore only transiently available during embryonic development (265). A second, brief and transient hematopoietic wave occurs in most vertebrates in blood islands and originates erythro-myeloid precursors (EMPs). The bipotential EMPs differentiate either in Gata1 expressing erythrocytes or in Spi1+ expressing myeloid progenitors (275,276). Zebrafish EMPs arise from 24 hpf in posterior blood island (PBI) and differentiate to *gata1+* erythroid and *spi1+* myeloid cells by 30 hpf (276). Lastly, definitive hematopoiesis consists in the formation of hematopoietic stem and progenitor cells (HSPCs), multipotent stem cells which differentiate into all adult blood cell lineages, sustaining long-term hematopoiesis (265,277). Both in mammals and in zebrafish, HSPCs originate from the hemogenic endothelium (HE), a particular endothelial portion located in the aorta-gonad-mesonephros (AGM) or in the ventral portion of the dorsal aorta (VDA), respectively (Figure 6A) (214,278–280). Activation of the hematopoietic transcriptional program in hemogenic endothelial cells requires the essential transcription factors Runx1 and cMyb both in zebrafish and in mammals (281). The process of specification of definitive HSPCs from the endothelium is termed endothelial to hematopoietic transition (EHT) and is driven and finely regulated by a complex network of molecular interactors (281–284) (Figure 6B). A series of transcription factors such as Scl/Lmo2/Gata2 and SoxF family members regulate the expression of Runx1/cMyb by interacting with each other and with elements of the Notch, Wnt and TGF-β signalling pathways, as extensively reviewed by (Figure 6B) (282). A further level of regulation involves sterile pro-inflammatory stimuli, purinergic signalling, and blood flow mechanical forces (Figure 6B) (285–292). Once specified, zebrafish HSPCs start emerging and budding from the HE at 30-32 hpf and colonize by 2-3 dpf the caudal-hematopoietic tissue (CHT), equivalent to the mammalian foetal liver (Figure 6B) (293,294). As mentioned in Section 3.1.1.1., the CHT provides the proper micro-environment for HSPCs expansion, maturation, and differentiation into the main different blood cell lineages

(241,295,296). By 3-3.5 dpf definitive erythropoiesis and myelopoiesis begin in the CHT, originating definitive erythroid and myeloid cells which gradually substitute the primitive ones (Figure 6A) (297–300). The CHT cell population at this stage of development is composed of numerous blood cell types, which include, in addition to HSPCs, mature *gata1+/hbbe3+* erythrocytes, *spi1b/pu.1+* myeloid progenitors, *mpx+* neutrophils, and *mpeg+* macrophages (301). By 4 dpf, HSPCs colonize the thymus where they start lymphopoiesis, and the kidney marrow, the analogue of the mammalian bone marrow, where adult hematopoiesis occurs (294) (Figure 6A). Lymphocyte development begins immediately after erythroid and myeloid cells emergence as in mammals, with early lymphoid progenitors starting to form in the developing thymus and kidney as early as 72 hpf (302). Despite the appearance of these lymphoid progenitors during the larval stage, the full maturation of lymphocytes takes several weeks. At around 3 weeks post fertilization mature and fully functional T-cells and B-cells reside in the kidney marrow, after having developed in the thymus and pronephros, respectively (303).

All the types of white blood cells just described, make up the zebrafish immune system. Zebrafish immunity is highly similar to the human one, as besides cell lineages, also cytokines, chemokines, receptors, and soluble elements (e.g. antibodies, complement system) are conserved (304–307) As in the other vertebrates, an innate and an adaptive immunity can be distinguished in zebrafish (308–310). As mentioned above, adaptive immunity is fully mature at 4-6 weeks post-fertilization, making zebrafish embryos particularly suitable for studying innate immunity alone (308,311). Primitive monocytes and neutrophils, the two major cell types involved in innate immunity are differentiated very early during zebrafish development and are comparable to their mammalian counterparts (214). They both display phagocytic capacity, cytokines expression and motility (312,313). Additionally, macrophages also exhibit M1-M2 polarisation and granuloma formation, while neutrophils are capable of generating extracellular traps (314). Apart from their purely immune role in the body's defence against pathogens, innate immune cells, and in particular macrophages, play essential roles during early embryonic development. Indeed, macrophages release several cytokines, growth factors and matrix-remodelling metalloproteinases which contribute to development of many organs and systems. For instance, contribution of primitive macrophages is essential for definitive hematopoiesis itself, for vascular development and for neurogenesis (242,315–319).

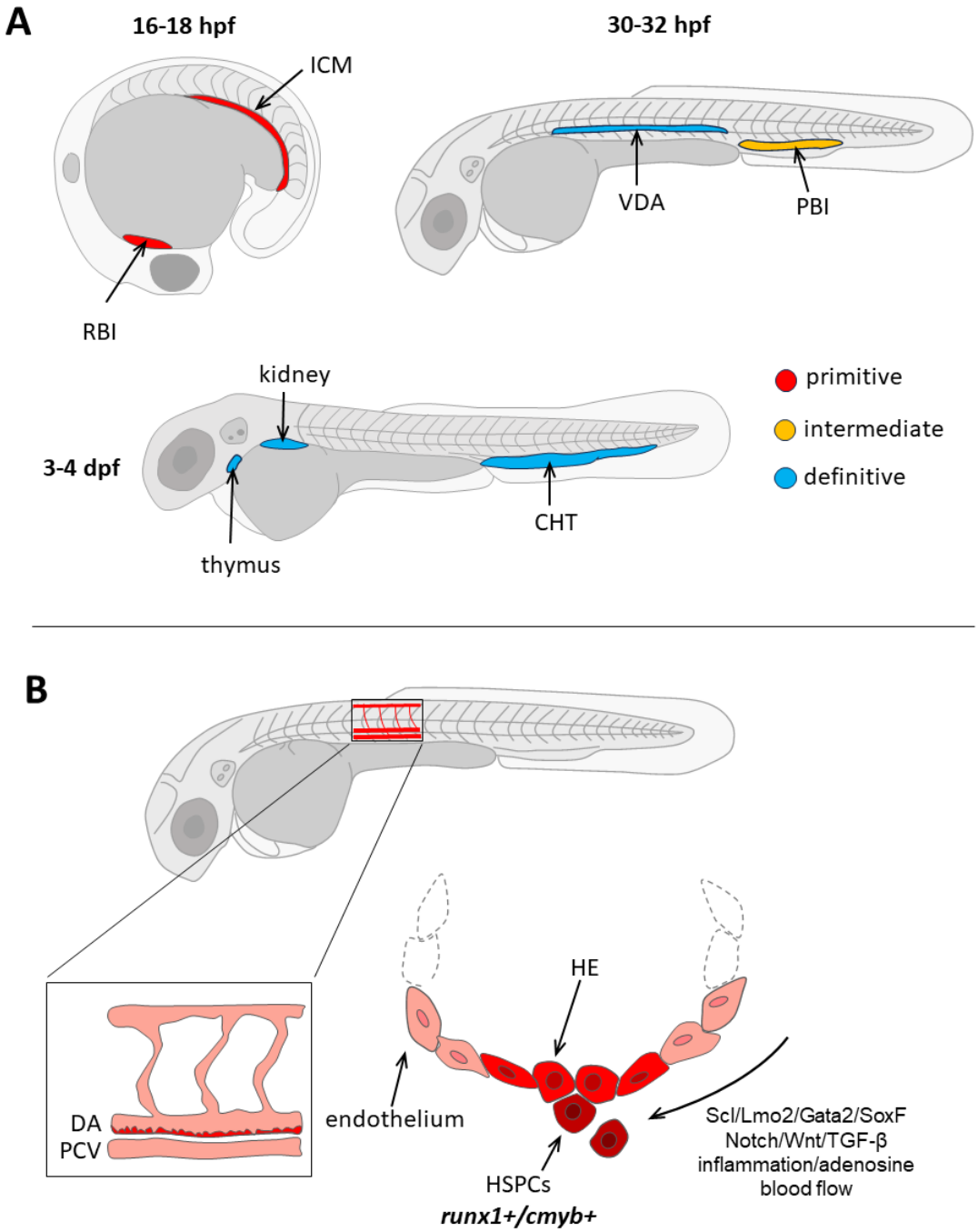

Figure 6. Zebrafish hematopoiesis. (A) Scheme of the anatomical regions where the different hematopoietic waves occur: each hematopoietic process (primitive, intermediate and definitive wave) is highlighted by a different colour, as indicated in the colour legend. RBI: rostral blood island; ICM: intermediate cell mass; PBI: posterior blood island; VDA: ventral dorsal aorta; CHT: caudal hematopoietic tissue. **(B) Details of the endothelial to hematopoietic transition (EHT) process:** endothelial cells of the ventral dorsal aorta constitute the hemogenic endothelium (HE) and, starting from 30-32 hpf activate the hematopoietic transcriptional program through a complex series of molecular players. Specified HSPCs emerge and bud from the endothelium. DA: dorsal aorta; PCV: posterior cardinal vein.

3.3. Zebrafish neurogenesis

The development of the zebrafish central nervous system (CNS) begins during early gastrulation. At around 6 hpf the neuroectoderm is already organized in a series of overlapping but independent regions which are the precursors of the major mature brain subdivisions (320). By 10 hpf the neural tube becomes distinguishable, and by 13 hpf it undergoes a folding process forming the neural keel, which further develops into the neural rod by 16 hpf (26,321). Afterwards, the rod undergoes cavitation to create a lumen and transforms into a neural tube around 24 hpf (321). The neural tube, along with the neuroepithelial neural progenitors, then gives rise to the entire CNS through symmetric and asymmetric cell divisions (321,322) By 24 hpf, the major brain regions, such as the forebrain, midbrain, hindbrain, and spinal cord, become morphologically distinguishable (Figure 7A,B) (323). Between 18 and 32 hpf, the neural signaling systems including catecholaminergic, GABAergic, and glutamatergic systems begin to form (324,325). As a result, 2 dpf zebrafish are already capable of sensing and reacting to diverse sensory stimuli (326,327). By 3 dpf, the major adult neuronal cell types, nuclei, and circuits have formed and become functional. Similar to mammals, zebrafish possess a forebrain, a midbrain, and hindbrain already during early development (321). These embryonic structures later differentiate to give rise to the main structures of the adult brain: the telencephalon, the diencephalon, the mesencephalon and metencephalon (321). Additionally, zebrafish also possesses all the main neural cell types such as astrocytes, microglia, oligodendrocytes, cerebellar Purkinje cells, myelin and motor neurons (328–332).

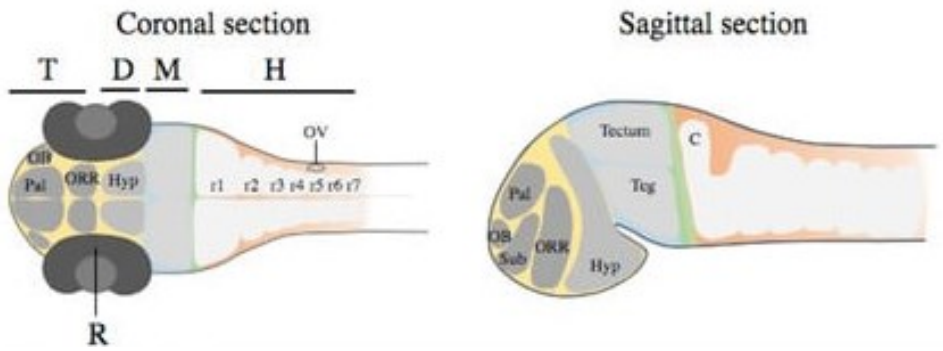

Figure 7. Zebrafish embryos central nervous system. (A) schematic representation of the zebrafish central nervous system at 30 hpf: forebrain, midbrain (M) and midbrain-hindbrain boundary (MBH) and the hindbrain (H) are labelled in yellow, blue, green and red, respectively. Schemes of the coronal and sagittal sections highlight the internal organization

of brain structures primordia. The forebrain is subdivided in the telencephalon (T) (darker grey) and the diencephalon (D) (lighter grey). Adapted from(323).

Therefore, the remarkable anatomical and physiological resemblance between human and zebrafish nervous systems, together with the high conservation of genes involved in neurodevelopment, make zebrafish a potent tool for the study of neurodevelopmental and behavioural studies (217,333).

Aim of the thesis

This PhD project aims to generate and characterize zebrafish disease models for the functional study of genes involved in human genetic diseases. In particular, four zebrafish disease models have been developed for four different diseases: adenosine deaminase 2 deficiency (DADA2), microcephaly primary hereditary 17 (MCPH17), GENE-X deficiency (a complex syndrome exhibited by a case report and never described before) and triadin knock out syndrome (TKOS). These genetic disorders, very different in terms of symptoms, are linked by a lack of knowledge of the causative gene functions and of the pathogenetic mechanisms involved, and by the unavailability of effective therapies. For each of the genes examined, we generated and validated a transient zebrafish loss-of-function model with loss of function and subsequently characterized their phenotypes, paralleling them with those exhibited by the patients.

The aim of creating the DADA2 model is to generate a currently non-existent animal model to study the pathogenetic mechanisms and perform drug screenings. For the DADA2 model, we have investigated in detail the possible mechanisms responsible for the onset of the main phenotypes, trying to understand the complex, tight link between the immune-hematological, inflammatory, and vascular defects exhibited by the patients. The generation of the MCPH17 and TKOS zebrafish models aimed to support and validate the data collected in murine models, to contribute to the comprehension of the causative molecular mechanisms to identify new drug targets. For the GENE-X-deficient model, the twofold objective is to validate the pathogenicity of the mutation found in the case report under review and to identify, the biological function of GENE-X, which is yet unknown, and consequently, possible therapeutic strategies.

Each line of research was conducted in collaboration with research groups with expertise in the specific fields. The DADA2 project was initiated and continued in collaboration with the research group of Dr. Alessandra Mortellaro, group leader of the “Mechanisms of Inflammation in Health and Disease Unit” at San Raffaele Institute for Gene Therapy. The MCPH17 project was carried out in collaboration with Prof. Enrica Boda, group leader at the Department of Neuroscience Rita Levi Montalcini, Institute Cavalieri Ottolenghi (NICO) of the University of Turin. The GENE-X deficiency project is being developed in collaboration with the group of Dr. Stefano Volpi of the Rheumatology and Autoinflammatory Diseases Department of the Giannina Gaslini

Institute in Genoa. Lastly, the TKOS project was run in collaboration with the group of Dr. Chiara di Resta, University Vita Salute San Raffaele.

Materials and Methods

1.1. Animals' husbandry

Adult zebrafish were bred according to international (EU Directive 2010/63/EU) and national guidelines (Italian decree 4th March 2014, n. 26) on the protection of animals used for scientific research. Briefly, adult zebrafish were raised in tanks in a recirculating water system at constant temperature of 28°C and following a 14/10 h light/dark cycle.

Crosses of breeding pairs were set up in specific breeding tanks and fertilized eggs were collected following natural spawning. Embryos were maintained at 28 °C in standard 90 mm × 15 mm Petri dishes in fresh E3 medium up to 24 hours post-fertilization (hpf) (E3 50X stock solution: 73.0 g of NaCl, 3.15 g of KCl, 9.15 g of CaCl2, and 9.95 g of MgSO4 in 5 L of distilled H2O. E3 stock solution was diluted in distilled water supplemented with 200 µl of 0.05% methylene blue). Starting from 24 hpf embryos were grown in E3 medium added with 0.003% 1-phenyl-2-thiourea (PTU, Sigma-Aldrich) to prevent pigmentation. Before analyses, chorions were mechanically removed with thin needles or tweezers, and they were anesthetized with a 0.016% tricaine solution (ethyl 3-aminobenzoate methanesulfonate salt; Sigma-Aldrich). For all experiments reported, the embryos were grown to the maximum stage of 5 days post fertilization (dpf) while adult fish were used for breeding use only. The following zebrafish lines were used for the experiments: AB wild-type (European Zebrafish Resource Center, EZRC), tg(CD41:GFP), tg(*kdrl*:GFP);tg(*gata1*:dsRed); tg(*kdrl*:GFP); tg(*mpeg1*:mCherry);tg(*tnfα*:GFP), tg(*runx1*:citrin; *kdrl*:mCherry) (334–337).

1.2. Bioinformatic analyses

Pairwise alignments for transcripts and protein sequences were performed utilizing the Needle-EMBOSS tool (Clustal, EMBL-EBI) (338). Sequences were obtained from the Ensembl database. The reference codes of the sequences used for the analyses are reported in the table below. Synteny analyses for ADA2 and Cecr1 were performed using the 'PhyloView' tool of the Genomicus Browser (Version 110.01), which allows to identify pairwise synteny blocs between species as previously described (339,340).

Gene	Species	Transcript ID	UniProt Match
ADA2	human	ENST00000399837.8 (NM_001282225.2)	Q9NZK5-1
CIT	human	ENST00000392521.7 (NM_001206999.2)	O14578-4
Cit	mouse	ENSMUST00000102560.7	D3YU89
cecr1a	zebrafish	ENSDART00000073416.6	F1R9S0
cecr1b	zebrafish	ENSDART00000144048.4	F6NKG5
cita	zebrafish	ENSDART00000122274.3	E7FGD8
citb	zebrafish	ENSDART00000122454.3	F1QN82

1.3. Morpholino-mediated knock-down

Morpholino-mediated knockdowns were obtained by injecting the transcript-specific morpholinos as listed in the table below:

Morpholino	Targeted region	Sequence 5'-3'	Dose injected per embryo	
***cecr1b*-ATGMO**	ATG region	GCTTATGCTACTCATTGCTCCCAGC	0.15 pmol	0.3 pmol total
***cecr1b*-sMO**	exon3-intron3	TAACTTTGATGTTCGCTCACCTGTT	0.15 pmol	
***$a_{2b}r$*-ATGMO**	ATG region	CAATGGCGATGTAGAGCGAATCCAT	0.15 pmol	
***tnfα*-ATGMO**	ATG region	AGCTTCATAATTGCTGTATGTCTTA	0.3 pmol	
***cita*-ATGMO**	ATG region	ATATTTAAACTTCAACATCACTGCAGG	0.0625 pmol	0.125 pmol total
***cita*-sMO**	Intron1-exon2	CACTTCCCTGGTGAAACACAAAATA	0.0625 pmol	
***gene-X*-ATGMO**	ATG region	ACGGGTGTAAACCCATTTTTACTGG	0.125 pmol	0.25 pmol total
***gene-X*-sMO**	Intron1-exon1	CCAAAATGACAGGACACTTACGTTT	0.125 pmol	
***trdn* ATGMO**	ATG region	TCCATCTCTCTCATGCACTAACAGG	0.3 pmol	0.6 pmol total
trdn-sMO	Intron1-exon1	ATGAAGTTCACAGTACCTTCCATCT	0.3 pmol	

All the morpholinos were obtained from Gene Tools and injected in 1-2 cells embryos. The splicing morpholinos (sMO) were validated by RT-PCR; briefly, total RNA was extracted from 24 hpf control and sMO injected embryos (~ 30 embryos per condition) using the NucleoZOL one phase RNA purification Reagent according to the

manufacturer's instructions (Macherey-Nagel). Following quantification, the extracted RNAs were treated with DNase to avoid endogenous genomic DNA contamination using the RQ1 RNase-Free DNase kit (Promega) and retrotranscribed with the High-Capacity cDNA Reverse Transcription Kit (Applied Biosystems) (for *cecr1b* sMO validation) or with the GoScript™ Reverse Transcriptase cDNA Synthesis kit (Promega) (for *cita*, *gene-X* and *trdn* morpholinos). cDNA for validation of *cecr1b*-sMO was pre-amplified using the TaqMan PreAmp Master Mix (Applied Biosystems). The cDNAs were next amplified by standard PCR reactions using the GoTaq® G2 DNA Polymerase (Promega) with *β-actin* primers and specific primers for validation of exon skipping or intron retention, designed with the Open Source Primer3 softwareand reported in the following table:

primer name	Sequence (5'-3')	Purpose
β-actin Fwd	TGTTTTCCCCTCCATTGTTG	Housekeeping gene for RT-PCR ctrl
β-actin Rev	TTCTCCTTGATGTCACGGAC	Housekeeping gene for RT-PCR ctrl
cecr1b-E2Fwd	CAAAGTGCGGCACATCATACA	RT-PCR for *cecr1b*-sMO validation
cecr1b-E4Rev	TGTGATCAGCCCAGACAGAG	RT-PCR for *cecr1b*-sMO validation
cita-FwdE1	CTCGACTCAATCAGCTGCTG	RT-PCR for *cita*-sMO validation
cita-RevI1	TCTACCGTTGTGCCTCCAAT	RT-PCR for *cita*-sMO validation
gene-X-FwdE1	CGGGATTTAAACGCTAGCTAGT	RT-PCR for *geneX*-sMO validation
gene-X-RevI1	TGACCTTGACCAAACACACA	RT-PCR for *geneX*-sMO validation
trdn-FwdE1	CTGGACCCGGGGAATTGACT	RT-PCR for *trdn*-sMO validation, and for *trdn* expression analyses
trdn-RevE2	CTTCAAGACCCTTGCTGTCGAG	RT-PCR for *trdn*-sMO validation, and for *trdn* expression analyses

For *cecr1b* and *cita*, PCR bands were cut from a 2% agarose gel, extracted, and purified for sequencing (Wizard® SV Gel and PCR Clean-Up System (Promega). *trdn*-ATG morpholino (ATG-MO) was validated by western blot analysis. Proteins were extracted from control and *trdn*-ATGMO injected embryos in RIPA buffer (10 mM Tris-HCl pH 8.0, 1 mM EDTA, 0.5 mM EGTA, 1% Triton X-100, 0.1% sodium deoxycholate, 0.1% SDS, 140 mM NaCl) added with protease inhibitor (Roche). After 3 cycles of sonication at 30 Hz for 5s lysates were centrifuged at 16,000 Xg at 4 C° fpr 10 min. Supernatants were collected and quantified by using the Quantum Micro Protein Assay (EuroClone). 40 µg of lysates were loaded in a 10% acrylamide/polyacrylamide gel

and for electrophoresis. Proteins were then transferred to polyvinylidene fluoride (PVDF) membranes and incubated in blocking solution (5% skimmed powder milk in TBS with 0.1% Tween-20) for 1 h at room temperature (RT) before o/n incubation at 4 C° with primary antibodies diluted in blocking solution. mouse anti-TRDN (dilution of 1:500, Sigma-Aldrich) and mouse anti-tubulin (dilution of 1:2500, Merck-Millipore,) were utilized as primary antibodies. Tubulin served as the internal housekeeping control. Membranes were then incubated for 1-hour at RT with a horseradish peroxidase (HRP) conjugated secondary antibody in blocking solution (Cell Signaling Technology) at dilutions of 1:4000 and 1:8000 for Tubulin and Trdn detection, respectively. The anti-TRDN antibody specifically targeted the longest TRDN isoform and was selected based on prior evidence demonstrating its reactivity against zebrafish Trdn (341). Protein bands were visualized using the WESTAR ECL detection system (Cyanagen). Imaging was performed using the Alliance MINI HD9 AUTO Western Blot Imaging System (UVItec Limited), and subsequent analysis was conducted using the associated software. *cecr1b*, *cita* and *gene-X* ATGMOs were validated trough comparison of the related phenotypes with those induced by the validated splicing morpholinos, as no antibodies efficiently targeting the zebrafish proteins were available. *a2br*-ATGMO and *tnfα*-ATGMO action was previously described and validated (288,342).

1.4. Genome editing with the CRISPR-Cas9 system

For CRISPR-Cas9 genome editing the web tool crispor.tefor.net was used to design 20 bp long crRNAs *S. pyogenes* Cas9 (SpCas9), using zebrafish GRCz11 genome assembly as a reference. All the synthetic sgRNAs were synthesized by IDT (Integrated DNA Technologies) as Alt-R CRISPR-Cas9 crRNA (2 nmol/ml) and Alt-R CRISPR-Cas9 tracrRNA (5 nmol/ml). 100 µM stock solutions of crRNAs and tracrRNA were prepared in IDT Nuclease-Free Duplex Buffer. For injection, 1 µl of each crRNA stock solution was added to 1 µl of tracrRNA stock solution, incubated at 95°C for 5 min, cooled down at room temperature and added with 0,2 µl of 10X CRISPR buffer (20 mM Hepes-NaOH pH 7.5, 0.15M KCl). The injection mix was prepared with 0.5 µl of each crRNA/tracrRNA solution and 1 µl of of Alt R *S.p*. Cas9 nuclease V3 (10 µg/µl) protein (IDT). 3 µl of the injection mix were micro-injected in 1-cell embryos.

crRNA name	Sequence (5'-3')
cecr1a-crRNA1	GATGCAAATTTTTGCCATACAAAATTTGAAAAGGTAATTGAGAAG
cecr1a-crRNA2	AAGAAACGGTTAATTAAGATCTTATCGATTCAGATTGGTATTTAA
cecr1b-crRNA1	TAATCATATGTTGTTCTGTTTAGGCATATGAACTGGACGGCACTA
cecr1b-crRNA2	AGATGTTTAAATAGCATTTTTTGGCATTGTCAGGAAGTTACCTTG

Genome editing was validated by PCR as following: genomic DNA was extracted by pools of 16 randomly chosen 24 hpf embryos by proteinase K (0.17 mg/mL, Roche Diagnostics) digestion in lysis buffer (10 mM Tris, pH 8.0, 10 mM NaCl, 10 mM EDTA) with 1 hour and 30 minutes incubation at 55˚C and inactivation for 15 min at 95˚C; each target genomic locus was PCR-amplified using Phusion High-Fidelity DNA polymerase (ThermoFisher Scientific) (see the following table for primers sequences) and run on a 1% agarose gel to check for the presence of a smaller aberrant band**.**

primer name	Sequence (5'-3')	Purpose
cecr1a-Fwd-gDNA	GCAACTCAA ATCTGTCAGAGGAA	genotyping
cecr1a-Rev-gDNA	GTATACTTACAAAGTCAAAACC	genotyping
cecr1b-Fwd-gDNA	GAGATGATTCATCTTAAGGTGC	genotyping
cecr1b-Rev-gDNA	CCTGTTAGACTAGAAGTGCC	genotyping

The T7 endonuclease I assay was performed utilizing the EnGen® Mutation Detection Kit (New England Biolabs), according to the manufacturer' instructions. Variations in the sizes of digested and undigested PCR fragments were examined by agarose gel electrophoresis.

1.5. Neutrophils staining and count

Mature neutrophils were stained using the Leucognost-POX colorimetric assay (Merck,) as previously described (343). Briefly, 3 dpf or 5 dpf embryos were fixed in 4% paraformaldehyde (pfa) (Sigma-Aldrich) in Phosphate Buffer Saline (PBS) for 2 hours at room temperature (RT), washed in PBS, moved into the staining solution prepared according to the manufacturer's indications for 10-15 min under constant monitoring and finally washed in PBS. Images of each stained embryo were acquired

with a stereomicroscope equipped with a digital camera with LAS Leica imaging software (Leica). Acquired images were processed and analysed using the Fiji (ImageJ) software. A region of interest (ROI) including the CHT area was set, and neutrophils included in the ROI were counted manually.

1.6. Whole mount *in-situ* hybridization (WISH) and quantifications

Whole mount *in-situ* hybridization (WISH) experiments were performed following the standard Thisse protocol (344), optimized for each probe.For probe preparation, we referred to the procedure described in (344). Briefly, to generate the *trdn* antisense probe, the *trdn* cDNA was amplified via PCR utilizing the specific primers: *trdn*-probe-Fwd (5'-CTGGACCCGGGGAATTGACT-3') and *trdn*-probe-T7-Rev (5'-GCGTAATACGACTCACTATAGGGCATCCTCCTCTTCTTCCGGC-3'). For *cmyb, runx1, scl1, efn2b2, efnb4, olig, rag1, ckma* and *cmlc2* antisense probes, vectors were linearized with enzymatic digestion utilizing the appropriate restriction enzyme as indicated in the Table. Each probe was synthetized by using the T7 RNA polymerases kit (Promega) and the digoxigenin (DIG) RNA labeling mix (Roche). Images of stained embryos were acquired with a stereomicroscope equipped with a digital camera with LAS Leica imaging software (Leica). Acquired images were processed and analysed using the Fiji (ImageJ) software. Signal intensity and area were quantified as previously described (345).

1.7. RT-PCR for expression analyses

Total RNA was isolated embryos at different developmental stages (~ 30 embryos) using the NucleoZOL one phase RNA purification Reagent according to the manufacturer's instructions (Macherey-Nagel). Following quantification, the extracted RNAs were treated with DNase to avoid endogenous genomic DNA contamination using the RQ1 RNase-Free DNase kit (Promega, Madison, WI, USA) and retrotranscribed with the GoScript™ Reverse Transcriptase cDNA Synthesis kit (Promega). *trdn* expression was then assessed by PCR using the GoTaq DNA polymerase (Promega) and the primers reported in the morpholino-mediated knock-

down section. PCR conditions were optimized according to the manufacturer's instructions.

1.8. Chemical treatments

The conditions used for drug treatments are shown in the table below:

Compound	Company	Stock	Dose
CGS15943	Tocris, BioTechne	10 mM, DMSO	10 µM
NECA	Merck Millipore	50 mM, DMSO	20 µM
H89 (2HCl)	Tocris, BioTechne	25 mM, distilled water	10 µM
N-acetylcysteine (NAC)	In-house	100 mg/ml distilled water	1 mg/mL
Y-27632 (2HCl)	StemCell technologies	100 mM, DMSO	20 µM
adrenaline	Galenica Senese S.r.l.,	0,5 mg/ml solution for injection	50 µg/ml
isoprenaline chlorhydrate	S.A.L.F. S.p.A.	0,2 mg/ml solution for injection	25 µg/ml
atropine sulphate monohydrate	S.A.L.F. S.p.A.	0,5mg/ml, solution for injection	50 µg/ml
metoprolol	Recordati S.p.A.	16.5 mg/ml in distilled water	16.5 µg/ml
flecainide	DOC Generici S.r.l.	13 mg/ml in distilled water	13 µg/ml

Embryos were treated in 6 multi-well plates with a maximum of 30 embryos/well in E3 medium supplemented with PTU. For drugs resuspended in DMSO, a volume of DMSO equivalent to that of the drug was added to the control embryos. For treatments lasting several days, the drug was changed daily to ensure efficacy. CGS, H89 and NECA treatments were performed from 5-8 somites stage to 34-36 hfp, from 50% epiboly to 26-32 hpf, or from 24 hpf and 36 hpf to 3 days post fertilization (dpf) according to the experiment, as described in the Result section. NAC and Y-27632 treatments were performed from 50% epiboly to the final experimental time point (24 hpf, 48 hpf, 72 hpf or 5 dpf according to the experiment, as described in the Result section). Adrenaline, isoprenaline and atropine were administrated to 3 dpf embryos for 100 min. For metopropolol and flecainide, 48 hpf embryos were treated overnight.

1.9. Real-time qPCR analyses

For real-time quantitative-PCR (RT-qPCR) analyses, total RNA was extracted from the embryos (~30 embryos per condition) using the NucleoZOL one phase RNA purification Reagent according to the manufacturer's instructions (Macherey-Nagel).

Following quantification, 1 µg of RNA for each sample was treated with RQ1 RNase-Free DNase kit (Promega) to avoid genomic contamination and retro-transcribed to cDNA using GoScript Reverse Transcription system (Promega). qPCR reactions were performed using the iQ SYBR Green Super Mix (Promega) and the 384-well QuantStudio™ 5 Real-Time PCR System (Applied Biosystem). Expression levels of each analysed gene were normalized to the zebrafish *rpl8* housekeeping gene and estimated with the $2^{-\Delta\Delta Ct}$ comparative method. Primers used for the analyses are listed in the following table:

primer name	Sequence (5'-3')	Purpose
rpl8-Fwd	CTCCGTCTTCAAAGCCAATG	RT-qPCR
rpl8-Rev	TCCTTCACGATCCCCTTGAT	RT-qPCR
a2br-Fwd	GATATCTGGCGGTCAAAATCC	RT-qPCR
a2br-Rev	CTCTCTCGCCCTTTTACCTG	RT-qPCR
cxcl8-Fwd	CGACGCATTGGAAAACACAT	RT-qPCR
cxcl8-Rev	TGTCATCAAGGTGGCAATGA	RT-qPCR
runx1-Fwd	CTCTGAGCAGTTGAGGCGAA	RT-qPCR
cmyb-Fwd	GACACAAAGCTGCCCAGTTG	RT-qPCR
cmyb-Rev	GCTCTTCCGTCTTCCCACAA	RT-qPCR
runx1-Rev	CTGCCGGGAGTCGGGAAT	RT-qPCR
il1β-Fwd	TGGACTTCGCAGCACAAAATG	RT-qPCR
il1β-Rev	CGTTCACTTCACGCTCTTGGATG	RT-qPCR
tnfα-Fwd	CTTCACGCTCCATAAGACCC	RT-qPCR
tnfα-Rev	GCCTTGGAAGTGAAATTGCC	RT-qPCR
il6-Fwd	TCAGAGACGAGCAGTTTGAG	RT-qPCR
il6-Rev	GAGAGGAGTGCTGATCCTGA	RT-qPCR
il10-Fwd	TTCAGGAACTCAAGCGGGAT	RT-qPCR
il10-Rev	GACCCCCTTTTCCTTCATCTTT	RT-qPCR
edn1-Fwd	GACCATGCTGACATCTGGATT	RT-qPCR
edn1-Rev	CTTATTCCTGGAGTGACGTGC	RT-qPCR
vcam1a-Fwd	TGACATTGGGATTGAGCGAAG	RT-qPCR
vcam1a-Rev	GCAGGTATTATGGCTACAGGC	RT-qPCR
olig2-Fwd	CACCTGCTACCGGCAATATC	RT-qPCR
olig2-Rev	CAGAGTCCATGGCGTTCAGT	RT-qPCR
gfap-Fwd	GGAGAGGAAAGCAGAATCACT	RT-qPCR
gfap-Rev	TCACGGGTCTCAACAGTTCG	RT-qPCR
mpb-Fwd	AAGGGAAAGAGACCCCACCA	RT-qPCR
mbp-Rev	GCTTTCTCCCCTCGACTTAGG	RT-qPCR
aif1-Fwd	GACTTACAAGGCGGAAAAGC	RT-qPCR
aif1-Rev	ACTTCTGATCTTCCATGAACTCC	RT-qPCR
ccr2-Fwd	CAAGTACTGTGGCTGCTACAA	RT-qPCR

ccr2-Rev	TGTTTGGCCATTGTTGCATG	RT-qPCR

1.10. rhADA2, h-GCSF anti-TNFα intravascular injections

The recombinant human ADA2 protein (rhADA2) (CECR1 Protein, CF, R&D) was diluted in sterile PBS1X (1:100, 1:75 and 1:50) immediately before injection. 1 nl of the rhADA2 dilution was injected intravascularly in the duct of Cuvier of previously anesthetized and fully circulating 26-28 hpf larvae. A corresponding dilution of the rhADA2 resuspension vehicle (20mM HEPES, 200 mM NaCl, 20% glycerol) was injected in ctrl and *cecr1b*-LoF embryos as a control. For the human granulocyte-colony stimulating factor (hG-CSF, Zarzio®, Sandoz GmbH) and for the anti-Tnfα (Enbrel®, Pfizer), 2 nl of the stock solution was injected intravascularly in the duct of Cuvier of previously anesthetized and fully circulating 48 hpf larvae.

1.11. *In-vivo* analyses

Brightfield and birefringence images of living embryos were captured using a Leica stereomicroscope equipped with a digital camera with LAS Leica Imaging software version 4.13 (Leica). For head size measurements, 24 hpf embryos were anesthetized and imaged from a lateral and a dorsal view; the same parameters of image acquisition were maintained throughout all the experiments. Dorsal and lateral head areas were measured using Fiji (ImageJ) software selecting a region of interest (ROI) around the head. For heart rhythm detection analyses, the larvae heart-beat frequency was counted manually for 15s for each larva. The number of beats/15s was then multiplied by 4 to obtain the beats per minute (bpm) (346). To minimise heart-beat alterations related to the ambient temperature 5 embryos per time were taken from the 28 C incubator. For birefringence analyses, 3 dpf anesthetized larvae were positioned on a polarizing filter, with a second polarizing filter placed over the objective lens, as previously described (347,348). Embryos were oriented to enhance the brightness of the trunk and tail when viewed through the crossed filters. Subsequently, images were processed using Adobe Photoshop software version 22.2.0. Fluorescence analyses with the Tg(*kdrl*:GFP);Tg(*gata1*:dsRed), Tg(CD41:GFP), tg(*mpeg1*:mCherry);tg(*tnfα*:GFP), and Tg(*runx1*:citrin;*kdrl*:mCherry) transgenic lines

were performed with a epifluorescence stereomicroscope M205FA (Leica) equipped with a digital camera. Acquired images were processed and analysed using the Fiji (ImageJ) software.

1.12. Time-lapse confocal microscopy

Time-Lapse experiments were performed utilizing a Yokogawa spinning Disk (ECLIPSE Ti2-E) confocal microscope with W1-SoRa module (Nikon). 30 hpf embryos were anesthetized in 0.016% tricaine solution and included laterally in 1% low-melting point agarose in in 35 mm confocal Petri dishes to provide stability during imaging. Included embryos were soaked in 0.016% tricaine solution to prevent the gel from drying out. Embryos were acquired for 6 hours every 5 minutes (magnification 20X, step size 0.5µm). Images were processed and analyzed using the NIS Element Analysis Software (Nikon) and the Fiji (ImageJ) software.

1.13. Immunofluorescences and apoptosis staining

HSPCs proliferation rate was estimated by double anti GFP/phoshohistone-H3 (p-H3) immunofluorescences in Tg(CD41:GFP) embryos; Tnfα/*mpeg1* colocalization in Tg(*tnfα*:GFP);Tg(*mpeg1*:mCherry) was analysed following signal amplification via anti GFP/mCherry immunostaining. Briefly, embryos were fixed in 4% pfa in PBS for 2 hours at RT and rinsed several times in PBS and in washing buffer (PBS 1X, TritonX 1%, DMSO 0,2%). After incubation in blocking buffer (PBS1X, TritonX 0,1%, DMSO 1%, sheep serum 5 %) for 2 hours at RT the following primary antibodies were added for overnight incubation at 4°C: mouse anti-GFP (dilution 1:2000, Sigma-Aldrich), rabbit anti p-H3 (dilution 1:200, Sigma-Aldrich) and rabbit anti mCherry (dilution 1:50, Abcam). The following secondary antibodies were added following washing and incubation in blocking buffer: Alexa Fluor 488 conjugated goat-anti-mouse antibody (dilution 1:1000) and Alexa Fluor 546 conjugated goat-anti-rabbit antibody (dilution 1:200) (Invitrogen Life Technologies). Fluorescence was visualized and acquired by confocal microscopy. Proliferation rates were estimated by counting the number of double positive (GFP+/p-H3+) cells normalized on the total GFP+ cells in the CHT

region**.** Apoptotic cells in Tg(CD41:GFP) fixed larvae were stained using the Click-iT Plus TUNEL Assay with the Alexa Fluor 647 picolyl azide dye according to the manufacturer's instruction (Invitrogen Life Technologies). For both the stainings, fluorescence images were acquired using a Leica, TCS-SPII confocal microscope following inclusion of the embryos in 1% low melting point agarose gel in 35 mm confocal Petri dishes. Images were processed and analysed using the Fiji (ImageJ) software.

1.14. Fluorescence activated cell sorting (FACS) analyses

Embryos dissociation was obtained as previously described (349). GFP+ cells were sorted from Tg(*fli1a:*GFP)^{y1} (350) embryos at 32-34 hpf using a BD FACSMelody Cell Sorter (BD Bioscience, Franklin Lakes, NJ, USA). To ensure accuracy in fluorescence detection and to eliminate the interference of auto-fluorescence, embryos of the wild-type AB strain were used to set the gate and exclude auto-fluorescence of cells.

1.15. Light/dark transition test

The monitoring and quantification of motor activity and swimming behavior of the *cita*-deficient larvae were conducted using the DanioVision system with the EthoVision XT software (Noldus). Larvae were grown to 5 dpf in PTU-free E3 medium to allow pigmentation, essential for visual recognition by the DanioVision system. Each larva was transferred to a 24-well plate with one single larva in each well. The multi-well plate was inserted into the observation chamber of DanioVision, with the temperature control unit adjusted to 28.5°C. Zebrafish underwent a 10-minute acclimation period in the chamber before recording. Employing the EthoVision XT software, light/dark cycles were established, comprising a 20-minute dark phase succeeded 10 minutes of white light exposure. The entire recording duration spanned 1 hour and 10 minutes. For each larva, the distance moved and the velocity parameters were calculated at 1 min intervals (351). Raw data were then analysed using the GraphPad Prism 8.0 software. Average distance moved and average velocity of the larvae were calculated at each time point and plotted to obtain the final graphs showing the light/dark trends.

1.16. Endogenous alkaline phosphatase assay

3 dpf larvae were fixed in 4%PFA (in PBS) for 2 hours at RT and then washed in PBS 1X. Larvae were then incubated in MeOH 100% for 2 hours at RT and rehydrated in solutions of decreasing MeOH concentration (75%, 50%,25%) in PBS 1X a RT, 5 min each. After washing in PBT, larvae were incubated in filtered NTMT staining solution (100 mM NaCl, 100 mM Tris HCl pH 9.5, 50 mM MgCl2, 1% Tween20) for 30 min. The staining was developed by incubating the larvae in NTMT added with the chromogenic substrates NBT (Nitro Blu Tetrazolium, Roche; 4,5 µl/ml) and BCIP (5-bromo-4-chloro-3-indolyl phosphate, Roche; 3.5 µl/ml), in the dark, in agitation under constant monitoring. Following stainig, embryos were washed twice in PBT and post-fixed in PFA 4% in PBS for 30 min and then maintained in PBS1X.

1.17. Semithin sections

For sections, 48 hpf zebrafish embryos were fixed overnight in a 2.5% glutaraldehyde, 4% paraformaldehyde, and cacodylate buffer (pH 7.2) solution at RT. Subsequently, the embryos were postfixed in 1% osmium tetroxide, dehydrated using increasing EtOH 100% series, and embedded in epoxy resin. Samples were then sectioned with an ultramicrotome, producing semithin sections (1 µm), which were stained with toluidine blue. Imaging was conducted using the Hamamatsu slide scanner (OSI optoelectronics in Hawthorne, CA, USA).

1.18. Statistical analyses

All data were shown as means ± standard deviation (SD) or standard error of the mean (SEM), as indicated in the figure legends. The Unpaired t-Student test, Chi-square test and Ordinary One-way ANOVA (with Tukey's correction) were used to compare different experimental groups. The p values < 0.05 were considered statistically significant, $p < 0.05$ (*); $p < 0.002$ (**); $p < 0.001$ (***). All analyses were conducted with the software package GraphPad Prism 8.0 Software.

Results

1. Generation of the DADA2 zebrafish model

1.1. Analysis of Cecr1a and Cecr1b paralogues

Zebrafish (*Danio rerio*) possesses two *ADA2* orthologues: *cecr1a* (GRCz11, Chr25:16.689.633-16.700.924) and *cecr1b* (GRCz11, Chr4:5.225.552-5.240.128). *cecr1b* was identified as the paralogue with conserved function to the human *ADA2.* Indeed, a morpholino-mediated *cecr1b* knock-down resulted in neutropenia and brain hemorrhages, while insertional mutagenesis for *cecr1a* did not cause any overt phenotype (131). However, sequence and structure conservation between the two paralogues had not been thoroughly described, and functional analyses were performed based on two different loss-of-function techniques, which are not fully comparable. Therefore, we examined in detail both the paralogues in terms of sequence identities and genomic organization. We verified sequence conservation between the human and the zebrafish ADA2 transcripts and proteins. We performed multiple pairwise sequence alignments with the Needle (EMBOSS) tool (Clustal, EMBL-EBI (338)). The results of the alignments, reported in the table of Figure 1A, show that sequence conservation to the human ADA2 appears quite similar for *cecr1a* and *cecr1b*, both in terms of transcripts and of protein identity and similarity. Additionally, we analyzed in detail the amino-acid sequence conservation of the regions encoding the catalytic domain, essential for proper ADA2 enzymatic function. We utilized the Geneious Prime Software (Geneious Prime 20- 2023,1.2) to align and compare the human (hADA2) and the zebrafish (z_*cecr1a* and z_*cecr1b*) catalytic domain sequences. The resulting consensus sequence outlined a high conservation of aminoacidic identity in the catalytic portion of both the zebrafish Cecr1 proteins, impeding a simple identification of the most conserved paralogue (Figure 1B). Finally, we assessed the synteny between the human and zebrafish ADA2 genes in order to identify the 'conserved order of aligned genomic blocks', which are indicative of gene conservation between two species. We visualized the synteny between the human and the zebrafish ADA2 orthologues by using the Genomicus Software (339) (Figure 1C). However, analysis of the ADA2 flanking genomic regions again showed no particular differences between the two paralogues (Figure 1C).

From the data collected through these bioinformatic analyses, we were unable to identify whether either of the two paralogues of Cecr1 was the only one with conserved function with the human ADA2. Consequently, we proceeded to generate a loss of function for both paralogues.

A

Sequence1	vs	Sequence2	cDNA sequence identity	Protein identity	Protein similarity
zf cecr1a		*zf cecr1b*	52.3%	53.3%	73.7%
human *ADA2*		*zf cecr1a*	34.0%	47.7%	65.2%
human *ADA2*		*zf cecr1b*	29.7%	44.7%	67.1%

B

C

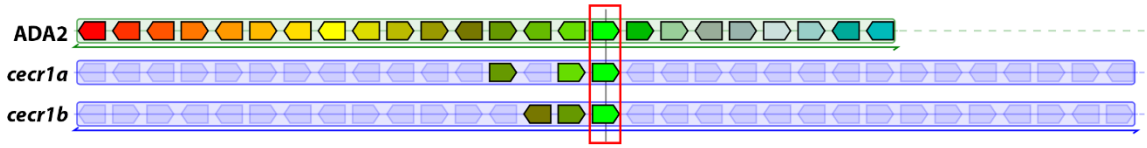

Figure 1. Analysis of sequence conservation between the human *ADA2* and the zebrafish *cecr1a* and *cecr1b*. (A) Table reporting the results of pairwise alignments for transcript and protein sequences (Needle-EMBOSS tool - Clustal, EMBL-EBI)*:* cDNA sequence identity, and protein sequence identity and similarity are reported. **(B)** Output of the multiple alignment results of ADA2 catalytic domain sequences aligned with Geneious Prime Software*:* the three aminoacidic portions encoding for the catalytic domain are highlighted by coloured rectangles. The consensus sequence shows conservation levels for each residue: green = 100% identity across all the three sequences, yellow =. 30% to 99% identity, red = less than 30% identity (Geneious Prime 20- 2023,1.2). **(C)** Genomicus "PhyloView" of the analysed *ADA2* synteny between humans and zebrafish. Genes are represented by coloured blocks and their orientation is indicated by the arrowed end. Each different gene is marked with a specific colour along the species. The *ADA2* gene is represented by the light green block and is highlighted by the red rectangle (339).

1.2. Set up of the loss-of-function strategy and characterization of the *cecr1b*-deficient zebrafish model

To verify the biological role of *cecr1b* and *cecr1a* we set up a CRISPR-Cas9 knock-out strategy for both the paralogues. We designed and validated specific sgRNAs to delete exon5, encoding for a portion of the catalytic domain thus disrupting Cecr1 function (Figure 2A-E). Two sgRNAs were designed for each *cecr1* gene in intronic regions flanking exon 5. We tested the ability of the guides to cut the region of interest by performing PCR with specific genotyping primers mapping upstream and downstream of exon 5. As expected, we found a shorter, aberrant amplification band in PCR reactions performed on genomic DNA of embryo injected with the *cecr1* sgRNAs, confirming the excision of exon5 (Figure 2 B,D). Such excision event was gained by the simultaneous action of the two guides. The efficiency of such double DNA cleavage appears higher for *cecr1a* sgRNAs that for *cecr1b* sgRNAs. However, the action of each single sgRNA must be considered for the total loss-of-function efficiency. Each guide leads to micro-deletions/insertions undetectable by simple PCR assays in the "will-type-like". We therefore conducted additional T7 endonuclease assays to demonstrate the presence of mutations in the wild-type like PCR band of *cecr1b*-sgRNAs injected embryos (Figure 2E). After validating the efficacy of our genome editing strategy, we began to characterise the phenotypes resulting from *cecr1* loss of function. We decided to consider neutropenia as the reference phenotype for the first functional validation and comparison of *cecr1* crispants. Indeed, as cited above, a morpholino-mediated *cecr1b* knock-down resulted in a neutropenic condition in zebrafish embryos (131). We took advantage of these previously described *cecr1b* morpholinos, that we validated and co-injected, to obtain our neutropenic "reference" phenotype (Figure 2F-G). We stained myeloperoxidase positive (Mpx+) mature neutrophils employing the Leucognost-Pox colorimetric assay (343) and we quantified the number of Mpx+ cells in the caudal hematopoietic tissue (CHT) of 3 dpf morphants and crispants. We observed the insurgence of neutropenia following the downregulation of *cecr1b* but not of *cecr1a*, further confirming the functional conservation between ADA2 and Cecr1b (Figure 3A-B). Therefore, all experiments were performed targeting the *cecr1b* paralogue only.

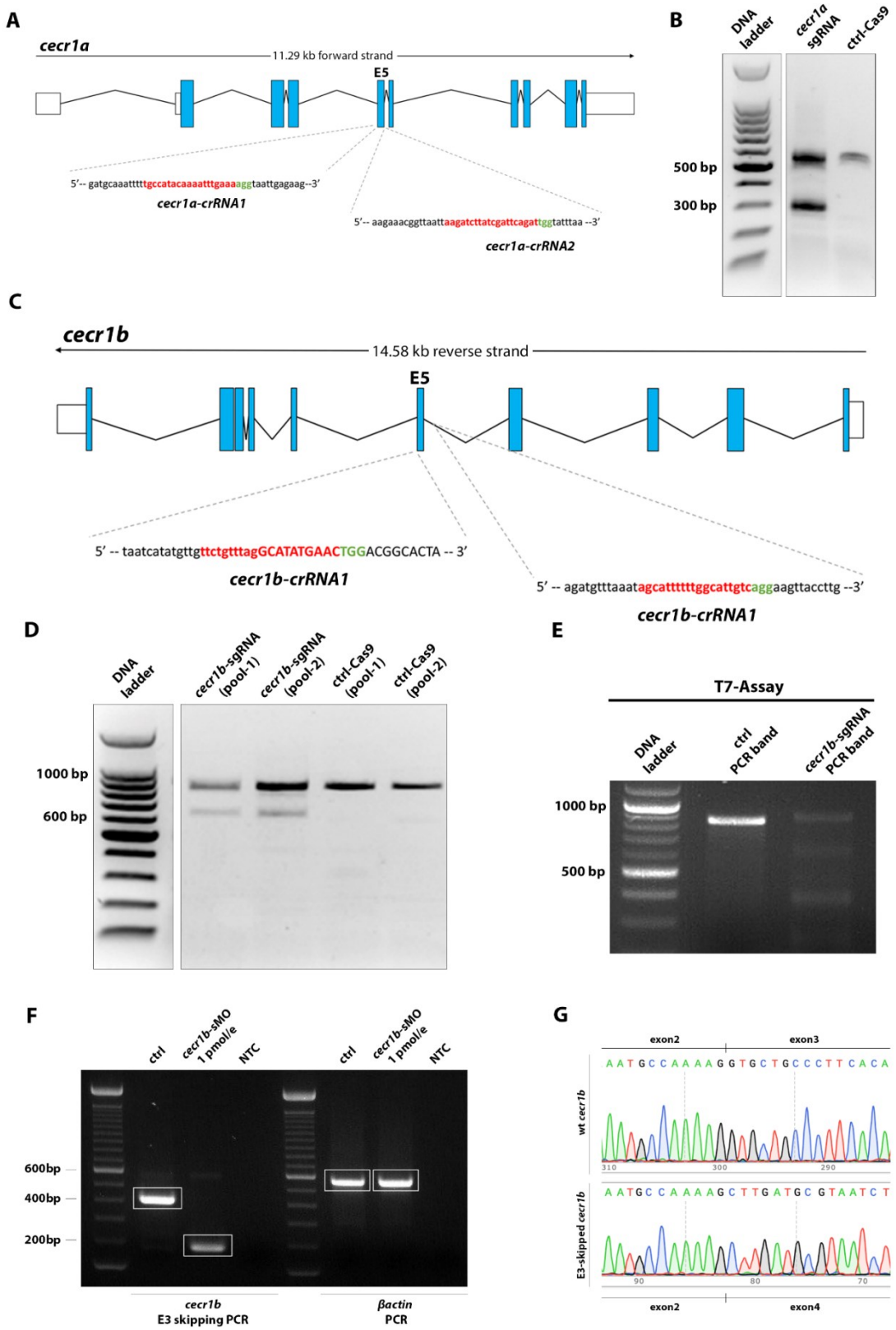

Figure 2. Molecular validation of *cecr1a*- and *cecr1b*-deficient zebrafish models.
(A) Schematic representation of the *cecr1a* genomic region, which we targeted with two different *cecr1a* crRNAs 1 and 2(*cecr1a*-sgRNA) flanking exon5 (E5). Exons = blue boxes; UTRs = white boxes; introns = black lines; crRNA sequence and PAM sequence are highlighted in red and green, respectively; lowercase = intronic region. **(B)** gel-electrophoresis

of the PCR amplicon obtained with *cecr1a* primers flanking the targeted genomic region in *cecr1a*-sgRNAs in ctrl Cas9 and *cecr1a*-sgRNAs injected embryos. (**C**) Schematic representation of the *cecr1b* genomic region, which we targeted with two different *cecr1b* crRNAs 1 and 2 (*cecr1b*-sgRNA) flanking exon5 (E5). Exons = blue boxes; UTRs = white boxes; introns = black lines; crRNA sequence and PAM sequence are highlighted in red and green, respectively; lowercase = intronic region, uppercase = exonic region. **(D)** gel-electrophoresis of the PCR amplification products obtained with *cecr1b* primers flanking the targeted genomic region of ctrl Cas9 and *cecr1a*-sgRNAs injected embryos belonging to two different pools. **(E)** Gel electrophoresis showing the results of the T7 endonuclease I assay performed on the "wild-tipe-like" amplification product of *cecr1b*-sgRNAs injected embryos and revealing multiple bands indicative of mutations. **(F)** agarose gel showing molecular validation of the *cecr1b*-sMO; left side of the gel: cDNA amplification bands obtained by PCR with *cecr1b*-specific E2Fwd-E4Rev primers for testing exon3 skipping (as described in detail in the methods section). Right side of the gel: cDNA amplification bands obtained by PCR with the housekeeping gene *βactin* primers, used as a positive control for the quality and integrity of cDNA in each sample. NTC = no template control. **(G)** Electropherogram obtained from Sanger Sequencing of the wild-type and aberrant bands extracted from the validation agarose gel and showing complete exone3 skipping in embryos injected with the *cecr1b*-sMO.

To further characterise the zebrafish *cecr1b*-Lof model and its parallels with human DADA2, we tested the effects of human granulocyte colony stimulating factor (hG-CSF; Zarzio®) and anti-TNF therapy (Enbrel®), the most common treatments for patients. We administrated both hG-CSF and anti-TNFa to 2 dpf embryos by systemic intravascular injection and analysed their effect on Mpx+ neutrophils population at 5 dpf (Figure 3C-E). hG-CSF significantly corrected neutropenia as in patients, and anti-TNF ameliorated it, even if only partially (Figure 3C-E). The ability of the anti-TNF therapy to mitigate neutropenia in *cecr1b*-Lof larvae suggested us a possible early involvement of inflammation in the development of this phenotype. Therefore, we analysed the inflammatory profile of *cecr1b*-LoF embryos by means of RT-qPCR analyses and of the transgenic line Tg(*tnfα*:GFP). We observed an augmented expression of the pro-inflammatory cytokines *il1-β* and *tnfα* along with a decrease in the level of the anti-inflammatory cytokine *il10* in *cecr1b*-LoF embryos (Figure 3F)**.** Additionally, we observed a significant increase of Tnfα+ cells in the trunk-tail region of *cecr1b*-LoF embryos starting from 24-26 hpf (Figure 3G,H), further confirming the inflammatory state of *cecr1b*-LoF embryos**.** In addition to neutropenia and inflammation, *cecr1b*-LoF embryos exhibited sporadic hemorrhagic events occurring mainly in the head and in the sub-intestinal vein region at 2-3 dpf (Figure 3I'-J''). However, no gross morphological defect was observed in the vascular tree nor in the circulation of these embryos (Figure 3 J',J''). Given the association between vascular fragility, vasculitis, and altered endothelial function in patients (131,133,134) we analyzed the expression levels of the endothelial activation markers *edn1* and *vcam1a*

by RT-qPCR. Both *edn1* and *vcam1a* expression was upregulated in *cecr1b*-LoF embryos, at 32-34 hours post fertilization (hpf) and at 3 dpf, indicating endothelial dysfunction over time, as in patients (Figure 3K).

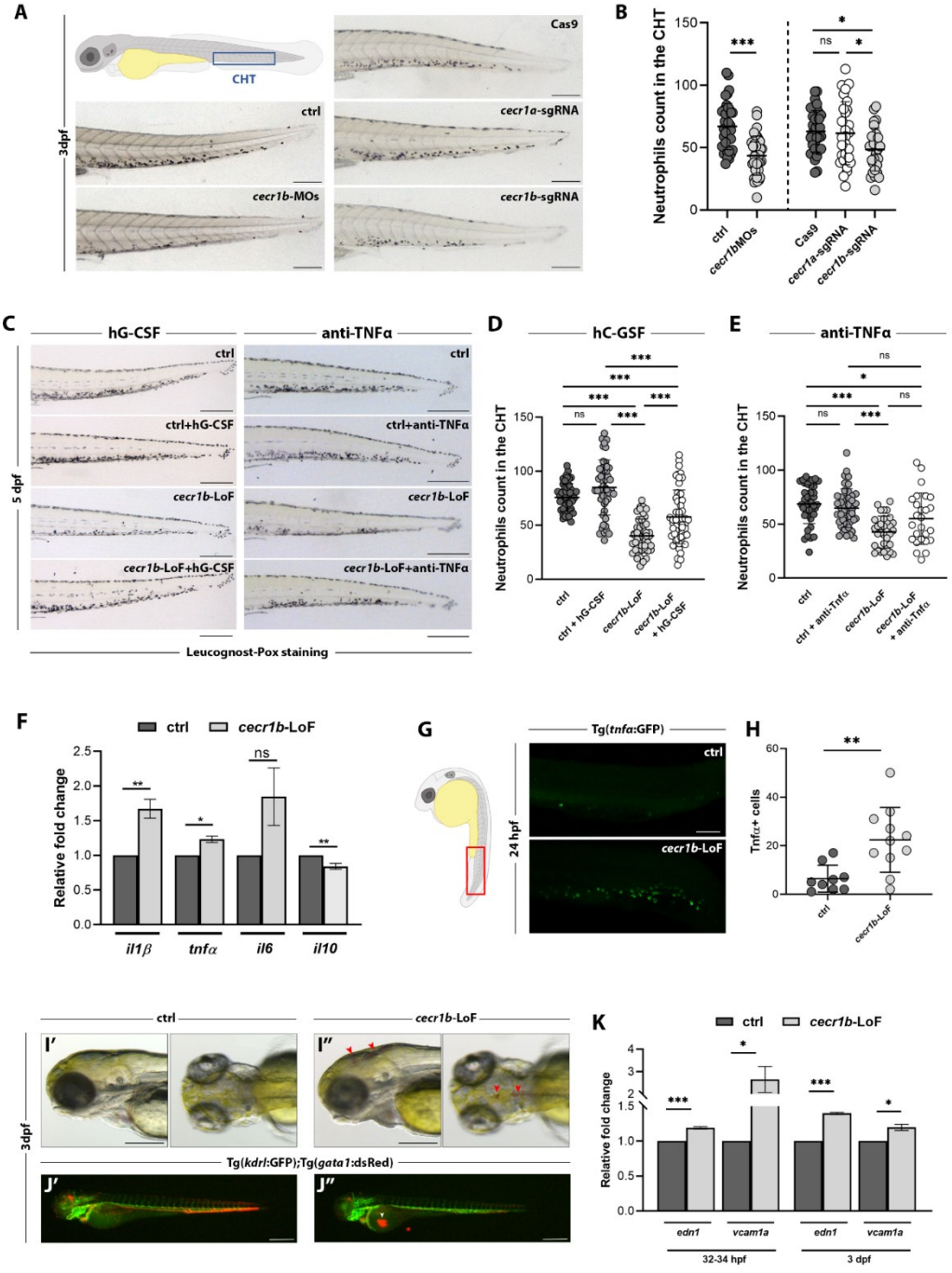

Figure 3. Characterization of the *cecr1b*-LoF zebrafish model (A) Brightfield representative images of the caudal hematopoietic tissue (CHT) of 3 dpf embryos of the different experimental conditions stained with the leucognost-POX assay. Sale bar: 300 µm. **(B)** Quantification graphs of neutrophils count in the CHT. Statistical significance was assessed by Unpaired t-Student test and Ordinary one-way ANOVA test with Tukey's correction. ***p<0.0*01*; *p < 0.05; ns: not significant. **(C)** Representative bright-field images of the CHT region of 5 dpf larvae belonging to the different experimental categories, stained for Mpx+ mature neutrophils with the Leucognost-Pox assay. **(D,E)** Quantification graphs of Mpx+ neutrophils in the different

experimental conditions. Scale bar: 300 μm. Statistical significance was assessed by Ordinary one-way ANOVA test with Tukey's correction ***p<0.001; *p < 0.05; ns: not significant. **(F)** RT-qPCR analyses of pro-inflammatory (*il1β, tnfα, il6*) and anti-inflammatory cytokines (*il10*) in 3 dpf embryos, showing enhanced inflammation compared to controls. **(G,H)** Representative confocal images and quantification graph of Tnf*α* expressing cells in the trunk-tail region of 24 hpf embryos. Magnification: 20X. Scale bar: 100 μm. Statistical significance was assessed by Unpaired t-Student test; **p<0.002. **(I'-I'')** Representative brightfield images of the head region of control embryos and of *cecr1b*-LoF embryos showing hemorragic events. Scale bar: 100 μm **(J'-J')** Extravasating red-labeled erythrocytes are visible in 3 dpf *cecr1b*-LoF Tg(*kdrl*:GFP);Tg(*gata1*:dsRed) embryos, in which *kdrl*+ endothelium and *gata1*+ erythrocytes are labeled in green and red fluorescence, respectively. Sale bar: 300 μm. **(K)** RT-qPCR analyses of *end1* and *vcam1a*, markers of vessel-endothelial activation, at 32-34 hpf and 3 dpf. Statistical significance is assessed by Unpaired t-Student test. ***p<0.001; *p < 0.05.

1.3. *cecr1b* deficiency leads to defective hematopoietic stem and progenitor cells (HSPCs) formation due to deregulation of the A_{2b}r pathway

Given the central role of hematological manifestations in DADA2 patients and the curative potential of hematopoietic stem cell transplantation, we decided to analyse in detail this cell population. In vertebrates, hematopoietic stem and progenitor cells (HSPCs) specify from hemogenic endothelial cells during a process termed endothelial to hematopoietic transition (EHT) (214,352). EHT is driven by a complex network of molecular interactors, which in zebrafish comprise eAdo signalling mediated by the A_{2b}r, the AR enriched in the endothelium of the developing embryo (288,353,354). Activation of the A_{2b}r/cAMP/Pka/*cxcl8* axis in the hemogenic endothelium (HE) initiates the hematopoietic transcriptional program, leading to the expression of the HSPCs specific markers *runx1* and *cmyb* (Figure 4A) (288). Given the catalytical ability of ADA2 to degrade eAdo and to interact with A_bR modulating its affinity for eAdo (134,145), we investigated whether *cecr1b* deficiency could lead to a dysregulation of the A_{2b}r pathway by measuring the expression levels of the two A_{2b}r downstream, genes *cxcl8* and *cmyb* (Figure 4B-C) (288). RT-qPCR analyses on sorted endothelial cells (ECs) showed that both of them were upregulated in *cecr1b*-LoF embryos at 32-34 hpf, when EHT initiates, (355) suggesting an hyperactivation of the pathway (Figure 4B-C). Treatment of *cecr1b*-LoF embryos with the A2 adenosine receptor antagonist CGS-15943 (herein referred to as CGS) (Figure 5A-A') effectively mitigated the expression of *cxcl8* and *cmyb* genes, thus validating the dependency of their upregulation on eAdo signaling (Figure 4B,C). Dysregulation of this pathway was

further corroborated through expression analyses conducted on whole embryos (Figure 5D-F). Remarkably, administration of H89, a selective protein kinase A (PKA) inhibitor, to *cecr1b*-LoF embryos also attenuated the expression of A2bR-associated genes, whereas the introduction of the eAdo analog NECA resulted in their further augmentation, thereby affirming the involvement of this pathway in the observed phenotype (Figure 5B-C', Figure 5E,F). Expression analyses of *scl* and *runx1*, pivotal genes for HE specification, was conducted via *in-situ* hybridization analyses (283,356,357). Concordant with the upregulation of $A_{2b}R$ signalling, an increase in both *scl* and *runx1* expression was observed in the ventral wall of the dorsal aorta (VDA) – the site of HE localization – in 24-26 hours hpf *cecr1b*-LoF embryos (Figure 4D). Similarly, the *cmyb* signal in the HE exhibited an increase in *cecr1b*-LoF embryos compared to controls. Chemical modulation of the $A_{2b}r$ pathway affected the expression of these markers, further confirming the role of $A_{2b}r$ in their regulation (Figure 4D, Figure 5G-J). Thus, these data indicate increased expression of HSPCs specification markers in the hemogenic endothelium of *cecr1b*-LoF embryos.

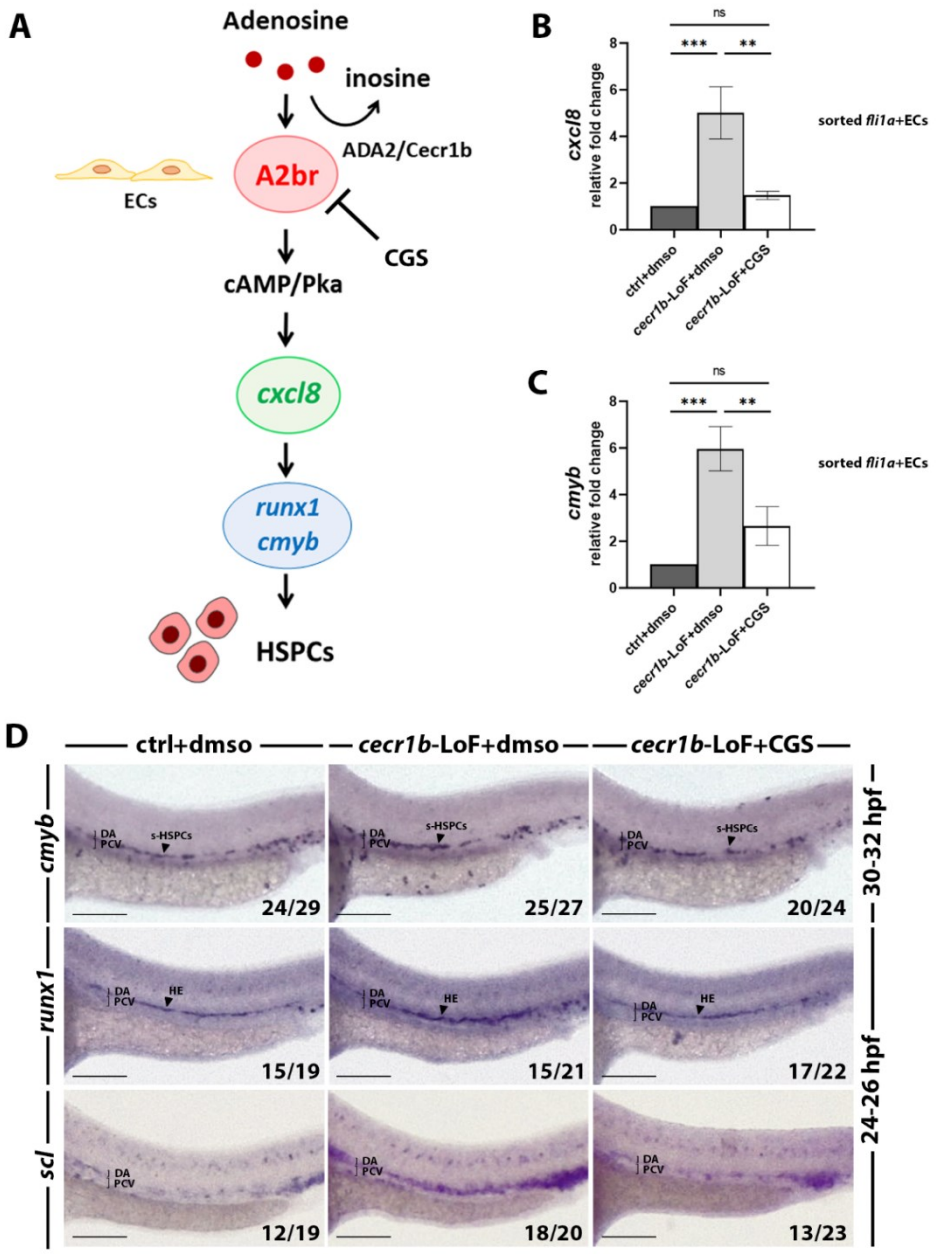

Figure 4. Analysis and modulation of the A_{2b}r pathway, which is dysregulated in the HE of *cecr1b*-LoF embryos. (A) Schematic representation of the A_{2b}r-dependent eAdo signalling pathway and of its modulators. A_{2b}r activation in endothelial cells leads to the expression of HSPCs-specific genes (*runx1* and *cmyb*). **(B-C)** RT-qPCR analyses of *cxcl8* and *runx1* in sorted endothelial cells of 32-34 hpf embryos. Statistical significance was assessed by Ordinary one-way ANOVA test with Tukey's correction; ***p<0.001; **p<0.002; ns: not significant. **(D)** Representative brightfield images of the trunk region of 32-34 hpf or 24-26hpf embryos of the different experimental conditions, stained for the HE/HSPCs markers *cmyb, runx1* and *scl* via WISH. Scale bar: 100 µm. DA = dorsal aorta; PCV = posterior cardinal vein; s-HSPCs = specifying HSPCs; HE= hemogenic endothelium. Numbers indicate the embryos belonging to the representative phenotype of each category, shown in the image.

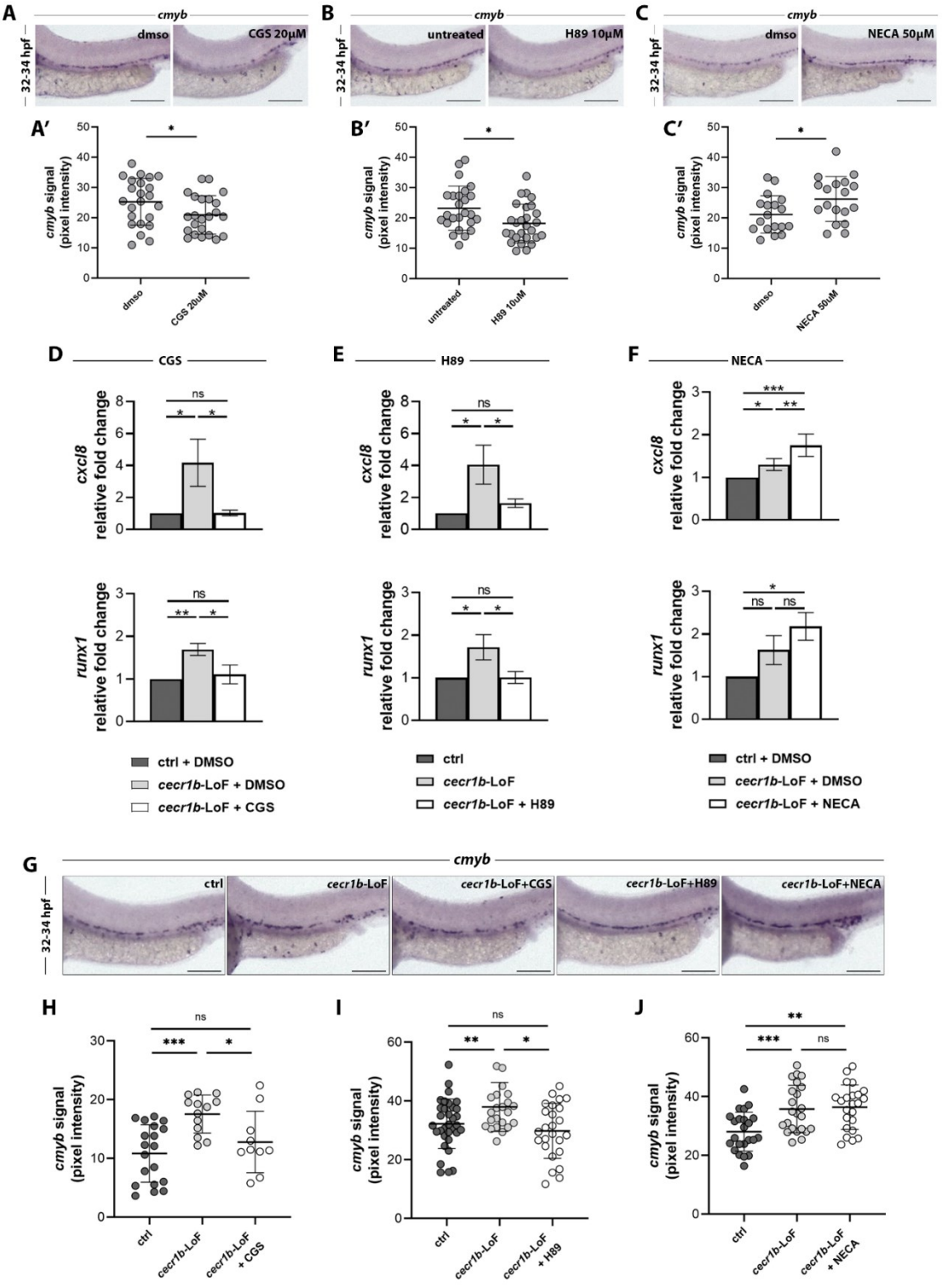

Figure 5. Modulation of the A_{2b}r pathway. (A-C) Representative WISH images of the *cmyb* signal in the trunk region of 36 hpf wild-type embryos treated with CGS (A), H89 (B) and NECA (C). Scale bar: 100 µm. **(A'-C')** Quantification graphs of *cmyb* signal intensity in the HE, which is decreased following CGS and H89 administration, and enhanced following NECA administration, confirming the successful modulation of the A_{2b}r pathway. Statistical significance was assessed by Unpaired t-Student test. *p < 0.05. **(D-F)** RT-qPCR analyses for expression of *runx1* and *cmyb* genes in the different experimental conditions. Statistical significance was assessed by Ordinary one-way ANOVA test with Tukey's correction; ***p<0.001; **p<0.002; *p<0.05; ns: not significant. **(G)** Representative WISH images of the trunk region of 32-34 hpf control embryos and *cecr1b*-LoF embryos of the different experimental cathegories stained for the HSPCs marker *cmyb*. Scale bar:

100 µm. **(H-J)** Quantification of *cmyb* signal intensity in the HE of *cecr1b*-LoF embryos of the different experimental categories. Statistical significance was assessed by Ordinary one-way ANOVA test with Tukey's correction; ***, p<0.001; **, p<0.002; *, p < 0.05; ns, not significant.

To find out whether the increase in the HSPCs markers *runx1* and *cmyb* was due to an upregulation of their expression levels or to an increased number of HSPCs, we took advantage of the double transgenic line *Tg*BAC(*runx1*:Citrine);*Tg*(*kdrl*:mCherry). We performed *in vivo* time point analyses between 26 and 34 hpf, to directly look at specifying HSPCs in the *cecr1b*-deficient background (Figure 6). The total number of VDA-associated Runx1-citrine+ HE cells was reduced in *cecr1b*-LoF embryos. The reduction in Citrine+ HE cells was efficiently rescued by CGS treatment at all the analysed time points (Figure 6).

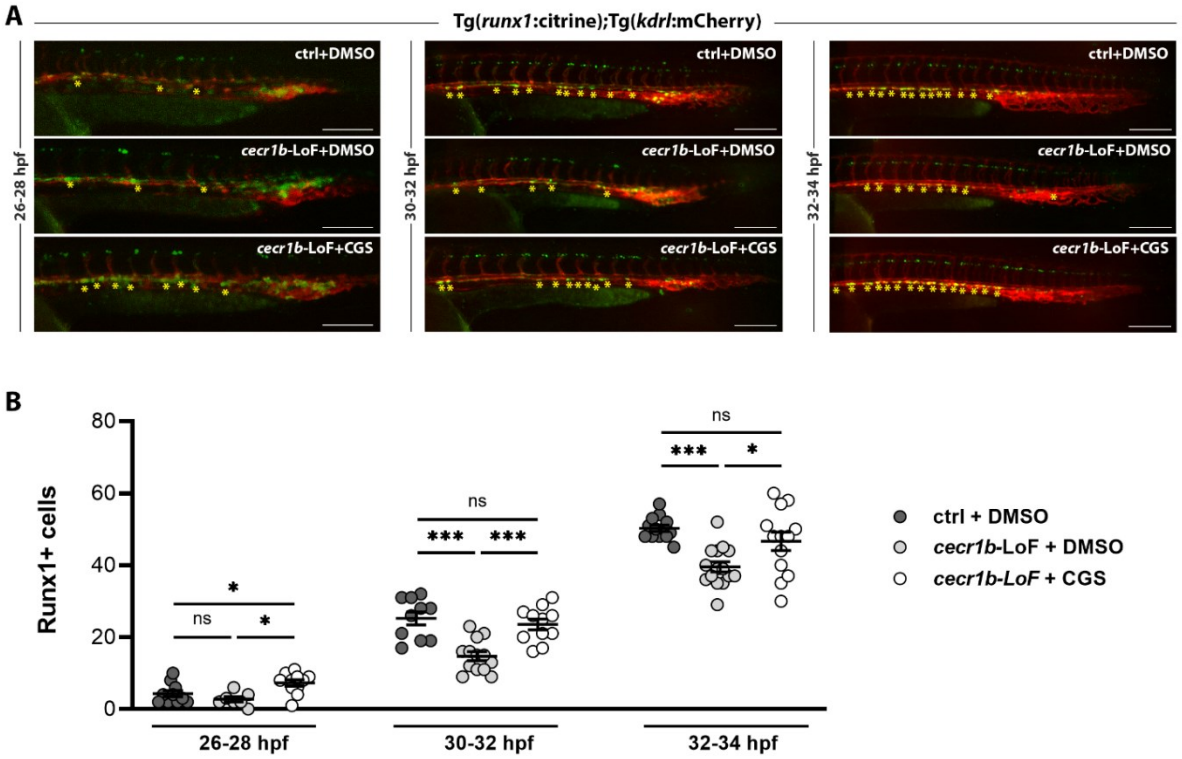

Figure 6. Time point analysis of specifying Runx1+ HSPCs revealing a decrease in their number, rescued by A_{2b}r pathway modulation. (A) Representative fluorescence images of the trunk-tail region of Tg(*runx1*:citrine);Tg(*kdrl*:mCherry) embryos of the different experimental conditions at 26-28 hpf, 30-32 hpf and 32-34 hpf. Specifying Runx1+ HSPCs are indicated by asterisks. Scale bar: 150 µm. **(B)** Quantification graphs of Runx1+ HSPCs at the different time points. Statistical significance was assessed by Ordinary one-way ANOVA test with Tukey's correction; ***p<0.001; *p < 0.05; ns: not significant.

1.4. Defects in the population of HSPCs are related to impaired endothelial functionality

The emergence of HSPCs is closely linked to endothelial function, given the endothelial origin of this cell population. Moreover, expression of *runx1* in HE down-regulates the arterial program allowing differentiation of HSPCs (280). We therefore decided to the evaluate arterio-venous specification of the axial vessels. The arterial marker *efnb2* was downregulated in *cecr1b*-LoF, as expected from the increased expression of *runx1* (Figure 7A). Similarly, the venous marker *efnb4* was slightly decreased, suggesting incorrect specification of axial vessels (Figure 7A). The modulation of the A_2R pathway through CGS administration also restored these defects, further demonstrating the role of the $A_{2b}R$ pathway in *cecr1b*-induced phenotypes (Figure 7A) (358). To further analyse the emergence and budding of HSPCs from the HE, we conducted *in vivo* time-lapse analyses using Tg(*kdrl*:GFP) (336) embryos from 30 to 34 hours post-fertilization (hpf) (Figure 8B). Normally, from 32 hpf onwards, endothelial cells undergo contraction, initiating endothelial-to-hematopoietic transition (EHT), detach from the aorta floor, and enter the bloodstream to seed the caudal hematopoietic tissue (CHT) (359). In *cecrb*-LoF embryos, we observed abortive EHT events characterized by HSPCs fragmenting as they bud from the HE (Figure 7B). Subsequently, using the transgenic line Tg(CD41:GFP) to label HSPCs (335), we observed a significant reduction in CD41+ cells in the CHT of 3 dpf *cecr1b*-LoF larvae compared to controls (Figure 7C,D). Moreover, *cecr1b*-deficient CD41+HSPCs displayed a partial and atypical CHT colonization, with most of them accumulating in the anterior region (Figure 7C,E). To exclude potential defects in HSPC migration from the HE to the CHT, we conducted time-point whole-mount in situ hybridization (WISH) analyses for the *cmyb* marker from 36 hpf to 3 dpf. Staining for *cmyb* in *cecr1b*-LoF embryos revealed migration kinetics to the CHT similar to that of controls (Figure 8). Proper homing and expansion of HSPCs in the CHT rely on the caudal vein plexus (CVP), which provides a supportive and protective microenvironment for HSPCs (240–242). Analysis using endothelial-specific Tg(*kdrl*:GFP) (336). transgenics in *cecr1b*-LoF embryos revealed an altered architecture of the CVP despite circulation, explaining the abnormal CHT colonization (Figure 7F-H). The CVP vascular network appeared reduced both in the anterior and, to a greater extent, in the posterior regions of the CHT of*cecr1b*-LoF embryos, with some areas completely lacking vascularization (Figure 7F-H).

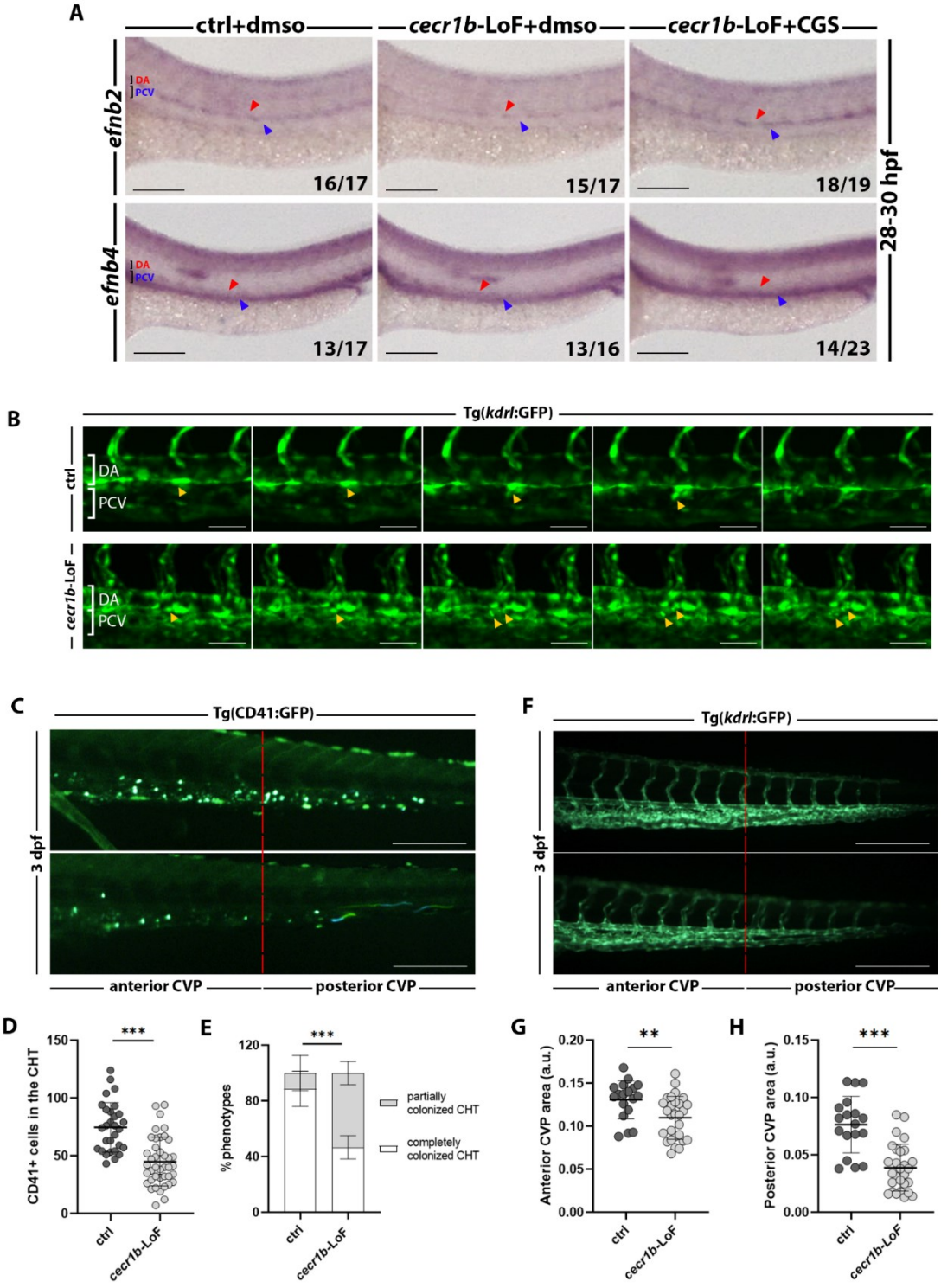

Figure 7. Analysis of the vascular structures associated to HSPCs origin and expansion. **(A)** Representative WISH images of the trunk region of 28-30 hpf of the different experimental conditions stained for the arterial (*efnb2*) and venous (*efnb4*) markers. DA = dorsal aorta; PCV = posterior cardinal vein, Red arrowheads indicate the region of the DA, blue arrowheads indicate the region of the PCV. Scale bar = 100 µm. **(B)** Sequential images from time-lapse analyses on Tg(*kdrl*:GFP) ctrl and *cecr1b*-LoF embryos from 30 to 36 hpf. Yellow arrowheads indicate HSPCs emerging from the ventral wall of the dorsal aorta in the trunk region. DA = dorsal aorta; PCV = posterior cardinal vein. Magnification 20X, scale bar = 50 µm. (**C**) Representative fluorescence images of the CHT region of 3 dpf Tg(CD41:GFP) ctrl and *cecr1b*-LoF embryos. The anterior and

posterior regions of the CHT are divided by the red dotted line. Scalebar = 150 µm. (**D**) Quantification graph of the CD41+HSPC number in the CHT region of 3 dpf ctrl and *cecr1b*-LoF embryos. Statistical significance was assessed by Unpaired t-student test. ***p < 0.001 (**E**) Histograms showing the proportion of embryos with complete or partially colonization of the CHT. Statistical significance was assessed with Chi-square test (Fisher's exact test, confidence interval 95%). ***p < 0.001. (**F**) Representative fluorescence images of the CVP region of 3 dpf Tg(*kdrl*:GFP). The red dotted line divides the CVP region into the anterior and posterior region. (**G-H**) Quantification graph of the GFP+ area in the anterior **(G)** and posterior **(H)** region of the CVP. Statistical significance was assessed with unpaired t-student-test. ***p<0.001; **p<0.002.

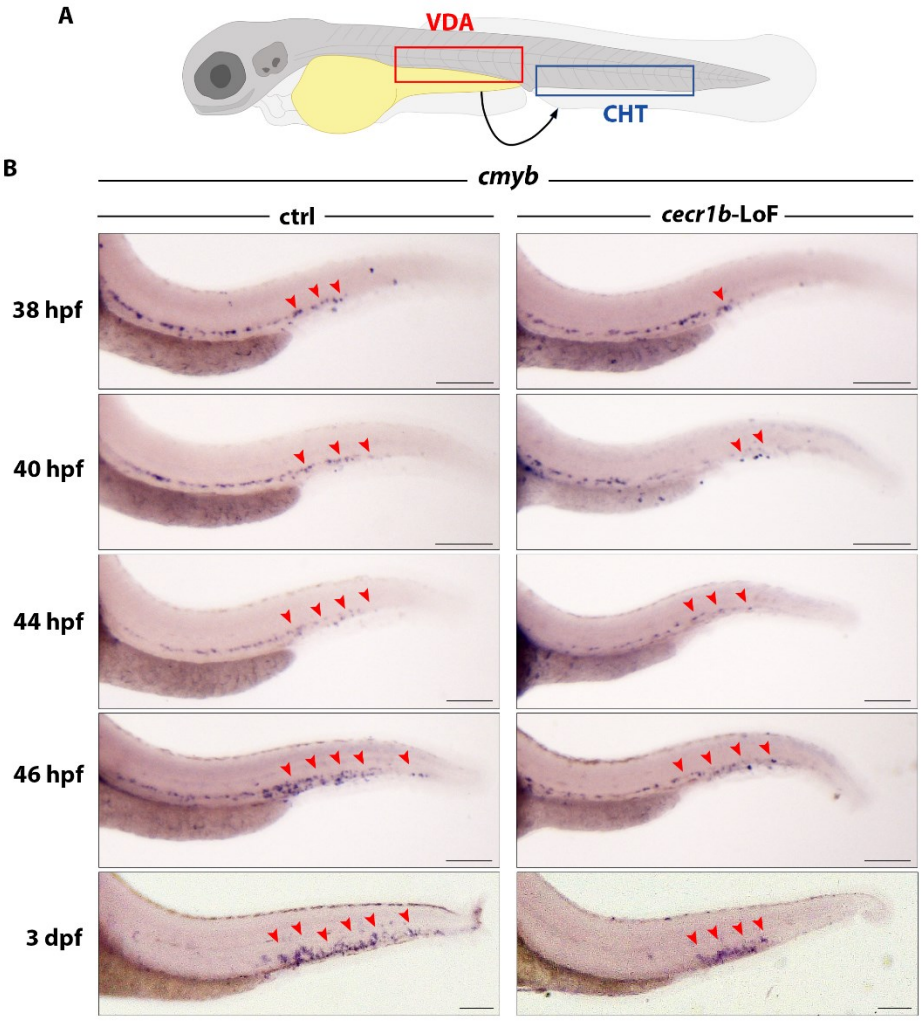

Figure 8. Migration kinetics of HSPCs in *cecr1b*-LoF embryos, revealing no defects in their migration capacity. (A) Schematic representation of a 3 dpf embryo: the ventral dorsal aorta (VDA, red rectangle) and the caudal hematopoietic tissue (CHT, blue rectangle) are highlighted. **(B)** Representative images of time-point WISH analyses for the *cmyb* marker in controls and *cecr1b*-LoF embryos from 38 hpf to 3 dpf. *cymb*+ HSPCs are indicated by red triangles. Scale bar: 150 µm.

1.5. Defects in definitive HSPC population are recovered both by A_{2b}r modulation and by mitigation of inflammation.

After emergence from the HE HSPCs migrate to the caudal hematopoietic tissue (CHT), and completely colonize it by 3 dpf (294). Here they proliferate and give rise to myeloid and erythroid progenitors (293).
Since we successfully rescued HSPCs number with CSG and H89 at earlier stages we investigated whether this early A_{2b}r modulation was sufficient to correct long-term HSPCs defects. However, because CGS treatment resulted toxic for embryos from 48 hpf, we performed H89 treatments only. We tested an "early" treatment starting it from 24 hpf, before HSPCs specify, and a "late" treatment, starting it at 36 hpf, after HSPCs have emerged. We then analysed the CD41-GFP+ HSPCs population in the CHT at 3 dpf (Figure 9 B,C). Notably, H89 administration successfully restored HSPC numbers and ameliorated CHT colonization only when embryos were treated from 24 hpf (Figure 9 A-C). To further confirm that HSPCs defects are specifically consequent to a dysregulation of the A2br pathway, we injected a subcritical dose of *a2br*-ATG morpholino in *cecr1b*-LoF embryos, to obtain a partial decrease of A_{2b}r, as it is required for HSPCs production. As expected, we found a significant rescue both in HSPCs numbers and in CHT colonization (288) (Figure 9 D-F) further confirming that A_{2b}r hyperactivation mediates the hematopoietic defects of *cecr1b*-LoF embryos. Moreover, our data demonstrate that only early modulation of A2br-mediated eAdo signalling can rescue *cecr1b*-dependent hematopoietic defects, suggesting the role of this pathway only during a specific time window in which HSPCs are emerging from the HE.

The emergence of HSPCs relies on inflammatory signaling in the HE (287). To explore whether hyper-activation of the A_{2b}R pathway triggers endothelial inflammation, we assessed the expression of pro-inflammatory cytokine in both whole embryos (Figura 10 A-D) and in sorted *fli1a*-GFP+ endothelial cells (Figure 10 E,F). We observed elevated levels of *il1β* and *tnfα*, which were normalized upon A_{2b}R pathway modulation. We next investigated the potential connection between inflammation and the reduction of HSPC population. We employed a *tnfα*-ATG morpholino (*tnfα*-ATG-MO) to modulate inflammation in *cecr1b*-LoF embryos. Downregulation of *tnfα* led to the recovery of HSPC numbers and improved CHT colonization (Figure 10G-I). Likewise, modulation of *tnfα* restored neutrophil populations in *cecr1b*-LoF embryos (Figure 10J-K). These

findings suggest a direct involvement of endothelial inflammation in generating hematopoietic defects in *cecr1b*-LoF embryos.

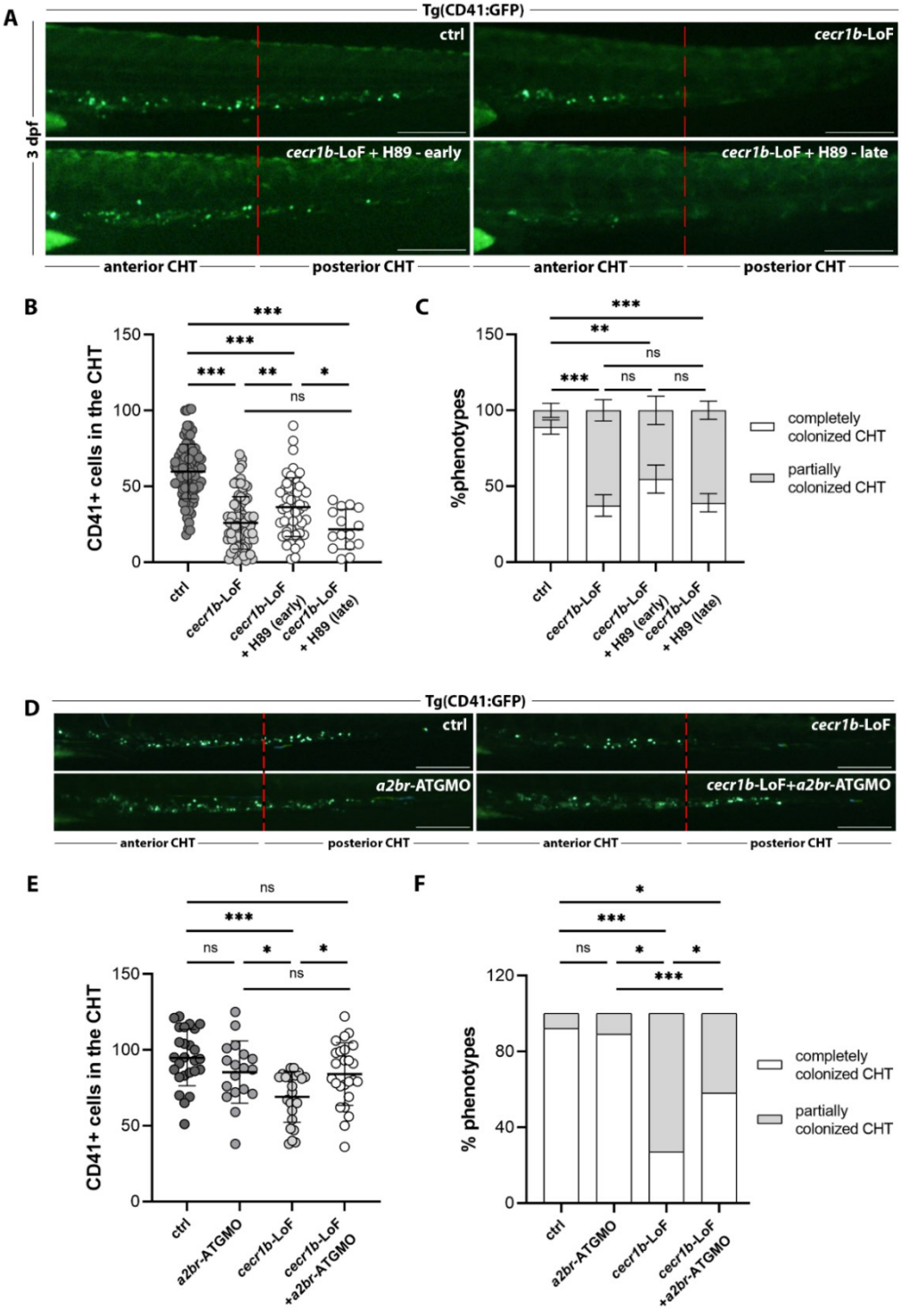

Figure 9. Analysis of HSPCs population in the CHT of *cecr1b*-LoF embryos and correction trough A_{2b}r modulation. (A) Representative fluorescence images of the CHT region of 3 dpf Tg(CD41:GFP) embryos of early and late H89 treatment experiments. The anterior and the posterior regions of the CHT are separated by a red dashed line. Scale bar: 150 µm. **(B)** Quantification graph of CD41+ HSPCs in the CHT, for early and H89 treatments. Statistical significance was assessed by Ordinary one-way ANOVA test with Tukey's correction; ***p<0.001; **p<0.002; *p < 0.05; ns: not significant. **(C)** Proportion of embryos showing complete or defective

CHT colonization in the different experimental conditions for H89 treatment experiments. Statistical significance was assessed by Chi-Square analysis (Fisher's exact test; ***p<0.001; **p<0.002; *p < 0.05; ns: not significant. **(D)** Representative fluorescence images of the CHT region of 3 dpf Tg(CD41:GFP) embryos of the *a2br*-ATGMO injection experiments. The anterior and the posterior regions of the CHT are separated by a red dashed line.Scale bar: 150 µm. **(E)** Quantification graphs of CD41+ HSPCs in the CHT of 3 dpf embryos of the *a2br*-ATGMO injection experiments. Statistical significance was assessed as for (B). **(E)** Proportion of embryos showing complete or defective CHT colonization in the different experimental conditions for the *a2br*-ATGMO injection experiments. Statistical significance was assessed as for (C).

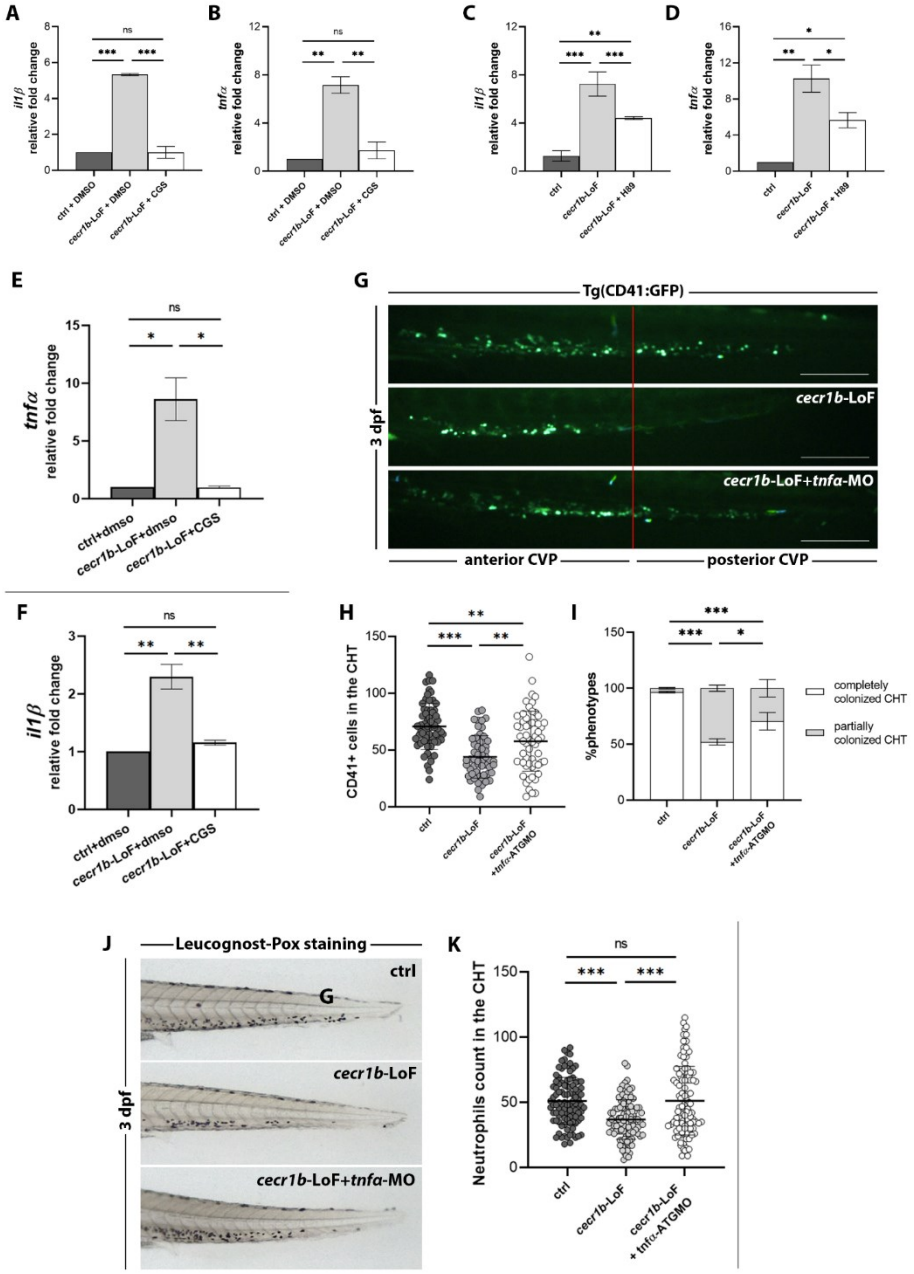

Figure 10. The role of inflammation in HSPCs defects (A-D) RT-qPCR analyses for the pro-inflammatory cytokines *il1β* and *tnfα* in 32-34 hpf embryos treated with CGS **(A-B)** and H89 **(C-D)**. Statistical significance was assessed by Ordinary one-way ANOVA test with Tukey's correction; ***p<0.001; **p<0.002; *p < 0.05; ns, not significant. (**E-F)** RT-qPCR analyses for the pro-inflammatory cytokines *il1β* and *tnfα* in sorted endothelial cells of 32-34 hpf embryos

Statistical significance was assessed by Ordinary one-way ANOVA test with Tukey's correction; **p<0.002; *p < 0.05; ns, not significant. **(G)** Representative fluorescence images of the CHT region of 3 dpf Tg(CD41:GFP) embryos belonging to the different experimental categories. Scale bar: 150 μm. The red dotted line divides the CHT region into the anterior and posterior parts. **(H)** Quantification graph of the CD41+ HSPCs number in the CHT of 3 dpf embryos of the *tnfα*-ATGMO experiments. Statistical significance was assessed by Ordinary one-way ANOVA test with Tukey's correction; ***p<0.001; **p<0.002; *p < 0.05; ns: not significant. **(I)** Proportion of embryos showing complete or defective CHT colonization in the different experimental conditions for *tnfα*-ATGMO experiments. Statistical significance was assessed by Chi-Square analysis (Fisher's exact test; ***p<0.001; **p<0.002; *p < 0.05; ns: not significant. Representative bright-field images (**J**) and quantification graph (**K**) of neutrophils stained with the Leucognost-Pox colorimetric assay in the CHT of 3 dpf embryos. Scale bar: 300 μm. Statistical significance statistical significance was assessed by Ordinary one-way ANOVA test with Tukey's correction; ***p<0.001, ns, not significant.

1.6. Administration of the human recombinant ADA2 protein (hADA2) rescues the haematopoietic defects of *cecr1b*-LoF embryos.

Since we hypothesised a direct role of Cecr1b in DADA2 pathogeny, we asked if the haematological phenotypes shown by *cecr1b*-LoF embryos could be corrected through administration of the recombinant human ADA2 (rhADA2). We tested different doses of the rhADA2 (17pg, 23 pg and 35 pg), administrating it by systemic intra-vascular injection at 26-28 hpf, right after the onset of circulation. We analysed the CD41-GFP+ HSPCs population and the Mpx+ neutrophils at 3 dpf and found a dose-dependent rescue of cell numbers, which enabled us to select the most effective rhADA2 dose as 35 pg/embryo (Figure 11). Once the optimal dose was selected, we analysed the population of CD41+HSPCs in more detail and observed a significant rescue in HSPCs number and in their CHT colonization capacity (Figure 12A-C). Furthermore, considering that ADA2 may play a role as a growth factor responsible for proliferation and differentiation of HSPCs (146) we decided to investigate whether *cecr1b*-LoF affected either HSPC proliferation or survival (Figure 12C-D). Staining with the proliferation marker phopsho-histone H3 (p-H3) by immunofluorescence in *Tg*(CD41:GFP) embryos at 3 dpf showed an almost complete absence of p-H3 staining in cecr1b-LoF embryos (Figure 12C). We estimated the proliferation rates by counting the number of double positive (GFP+/p-H3+) HSPCs vs the total GFP+ cells in the CHT**.** Proliferation of HSPCs was almost completely absent in most of *cecr1b*-LoF embryos and was restored by rhADA2 administration (Figure 12C,D). We excluded cell death events by performing TUNEL assays, which revealed that survival of *cecr1b*-deficient HSPCs was not affected (Figure 12E). rhADA2-mediated restoration of the

HSPCs compartment was accompanied by correction of the neutropenic condition as measured by Mpx+ neutrophils staining (Figure 12F,G), further indicating conservation of ADA2 function between the two species.

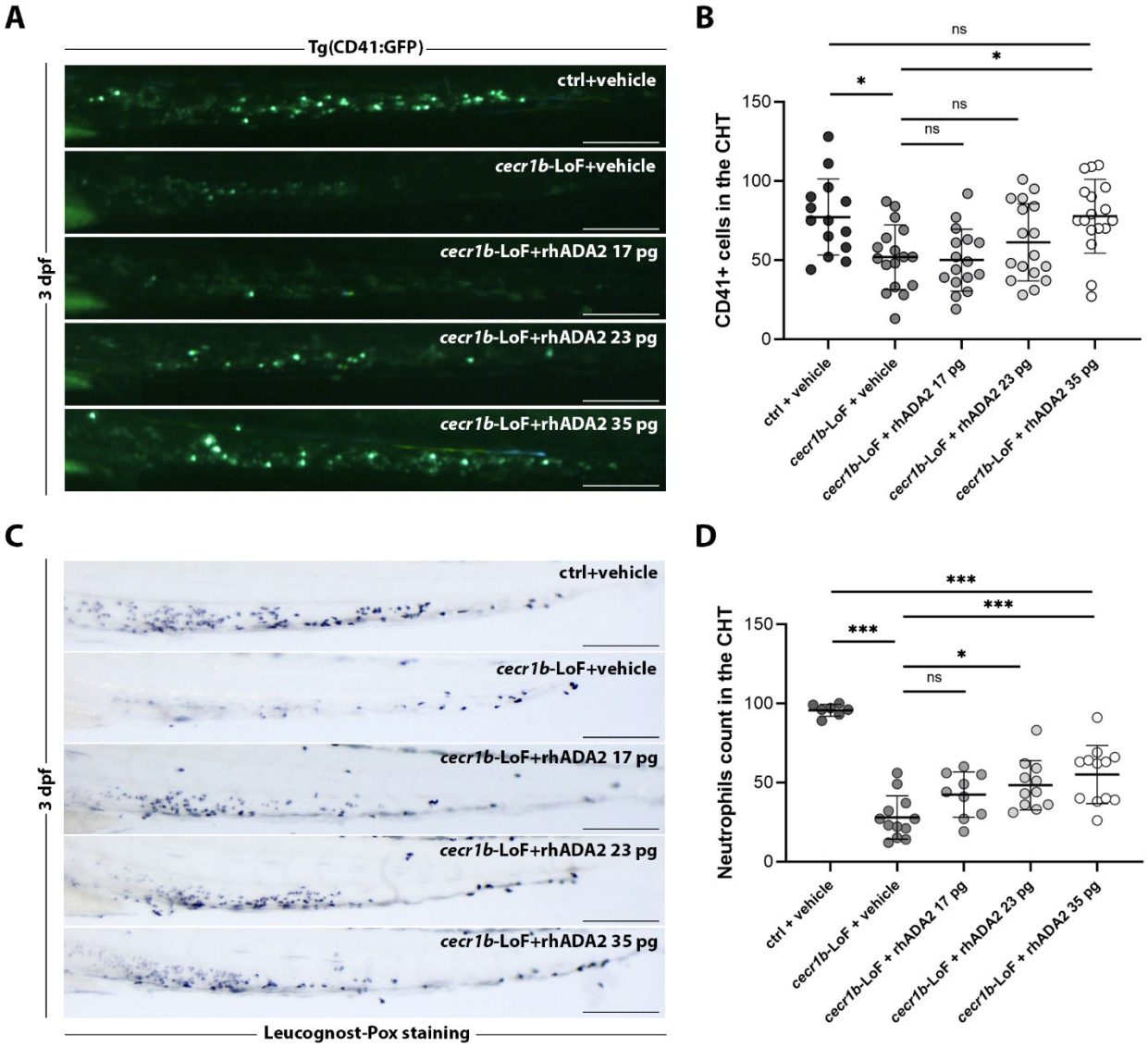

Figure 11. Dose-dependent rhADA2 mediated rescue of HSPCs and neutrophils. (A,B) Representative fluorescence images of the CHT region of 3 dpf Tg(CD41:GFP) embryos and quantification of the CD41+ HSPCs cells in controls, *cecr1b*-LoF and *cecr1b*-LoF embryos administrated with different doses of the rhADA2. Scale bar: 300 µm. Statistical significance was assessed by Ordinary one-way ANOVA test with Tukey's correction; ***p<0.001; **p<0.002; *p < 0.05; ns: not significant. **(C,D)** Representative bright-field images and quantification of neutrophils stained with the Leucognost-Pox colorimetric assay in the caudal hematopoietic tissue (CHT) of 3 dpf embryos. Scale bar: 300 µm. Statistical significance was assessed by Ordinary one-way ANOVA test with Tukey's correction; ***p<0.001; **p<0.002; *p < 0.05; ns: not significant.

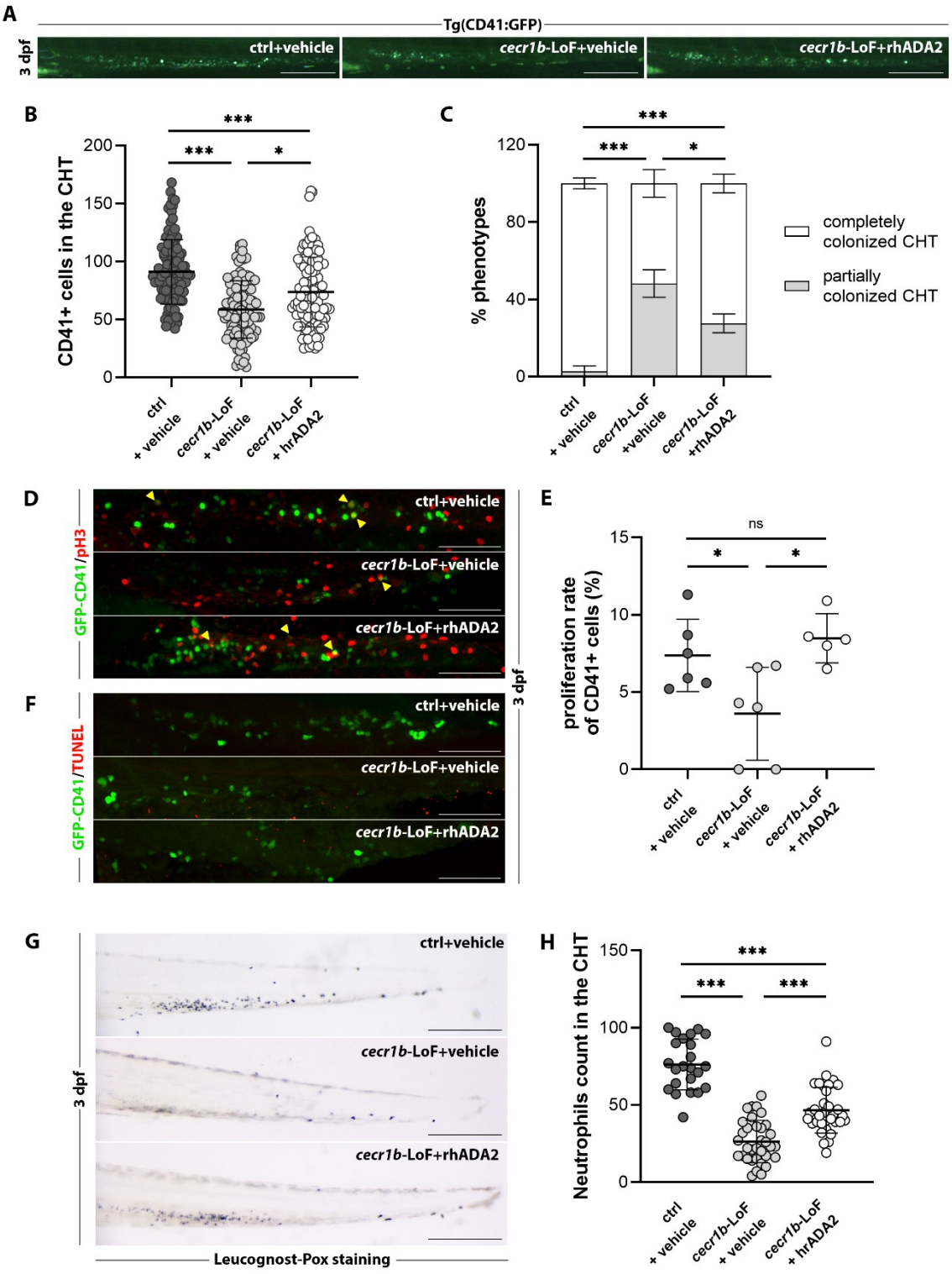

Figure 12. Recovery of the *cecr1b*-dependent hematopoietic phenotypes through supplementation of the rhADA2. (A) Representative fluorescence images of the CHT region of 3 dpf Tg(CD41:GFP) embryos of the different experimental conditions. Scale bar: 150 µm. **(B)** Quantification graph of CD41+ HSPCs in the CHT of 3 dpf embryos of the different experimental conditions. Statistical significance was assessed by Ordinary one-way ANOVA test with Tukey's correction; ***p<0.001; *p < 0.05. **(C)** Proportion of embryos showing complete or defective CHT colonization. Statistical significance was assessed by Chi-Square analysis (Fisher's exact test); ***p<0.001; *p < 0.05. **(D)** Representative confocal images of the CHT region of 2.5 dpf embryos

stained for CD41/GFP and for the proliferation marker pH3 with double immuno-fluorescence. Double CD41-GFP+/pH3+ cells are indicated by yellow arrowheads. Magnification: 20X. Scale bar: 100 μm. **(E)** Proliferation rates estimated as the number of double CD41-GFP+/pH3+ cells normalized on the total number of CD41-GFP+ in the CHT of each embryo. Statistical significance was assessed by Ordinary one-way ANOVA test with Tukey's correction; *p<0.05, ns: not significant. **(F)** Representative confocal images of the CHT region of 2.5 dpf embryos stained with the apoptotic TUNEL assay. No dying CD41-GFP+ cells have been detected. Magnification: 20X. Scale bar: 100 μm. **(G,H)** Representative brightfield images and quantification of neutrophils stained with the Leucognost-Pox colorimetric assay in the caudal hematopoietic tissue (CHT) of 3 dpf embryos. Scale bar: 300 μm. Statistical significance was assessed by Ordinary one-way ANOVA test with Tukey's correction; ***p<0.001.

2. Generation of the MCPH17 zebrafish model

2.1. Identification and targeting of the zebrafish *CIT* orthologue

Zebrafish possesses two *CIT* orthologues: *cita* (GRCz11, Chr5:2,409,554-2,636,078) and *citb* (GRCz11 Chr8:3.820134-3.923.378). To identify the paralogue with conserved function to the human one we first analysed synteny and sequence identities of transcripts and proteins. For sequence identity analyses, we performed multiple pairwise sequence alignments with the Needle (EMBOSS) tool (Clustal, EMBL-EBI(338)). The results reported in the Table of Figure 1A show that the zebrafish *cita* paralogue exhibits a higher sequence conservation with the murine and human counterparts, than the *citb.* Notably, the Citb protein completely lacks the N-terminal portion containing the kinase domain, which had been revealed essential for protein function (Figure 1B). We therefore decided to target the *cita* paralogue. We designed a knock-down strategy combining two antisense morpholinos, one targeting the intron1-exon2 boundary (sMO) and the other targeting the translation initiation region (ATG-MO). *cita*-sMO was validated by RT-PCR. Since splicing morpholinos targeting intron-exon junctions generally cause retention of the implicated intron we utilized specific primers to test for intron1 retention (360). As shown in Figure 1C, we based the validation strategy on the use of a reverse primer annealing to intron1, so that cDNA amplification can take place only if intron1 has been retained in the mature transcript. As expected, a *cita* amplicon was obtained from cDNA of embryos injected with the *cita*-sMO, but not from control embryos (Figure 1D). Sanger sequencing of the band revealed a perfect mapping of the sequence to the *cita* genomic region containing exon1-intron1 boundary, confirming intron1 retention (Figure 1E). Since no antibodies recognizing zebrafish Cita are currently available, we validated the action of *cita*-ATG-MO by comparing the resulting phenotypes with those induced by sMO (Figure 2A-C). We identified the optimal dose of morpholinos for *cita* knock-down as 0.125 pmol/embryo for ensuring the insurgence of *cit*-related-phenotypes without inducing off-target toxicity (Figure 2A-C).

A

Sequence1	vs	Sequence2	cDNA sequence identity	Protein identity	Protein similarity
zf cita		*zf citb*	52.9%	53.2%	59.7%
zf cita		mouse *Cit*	59.9%	63.3%	75.6%
zf cita		human *CIT*	55.5%	63.6%	75.9%
zf citb		mouse *Cit*	56.3%	53.7%	64.4%
zf citb		human *CIT*	38.5%	53.7%	64.5%

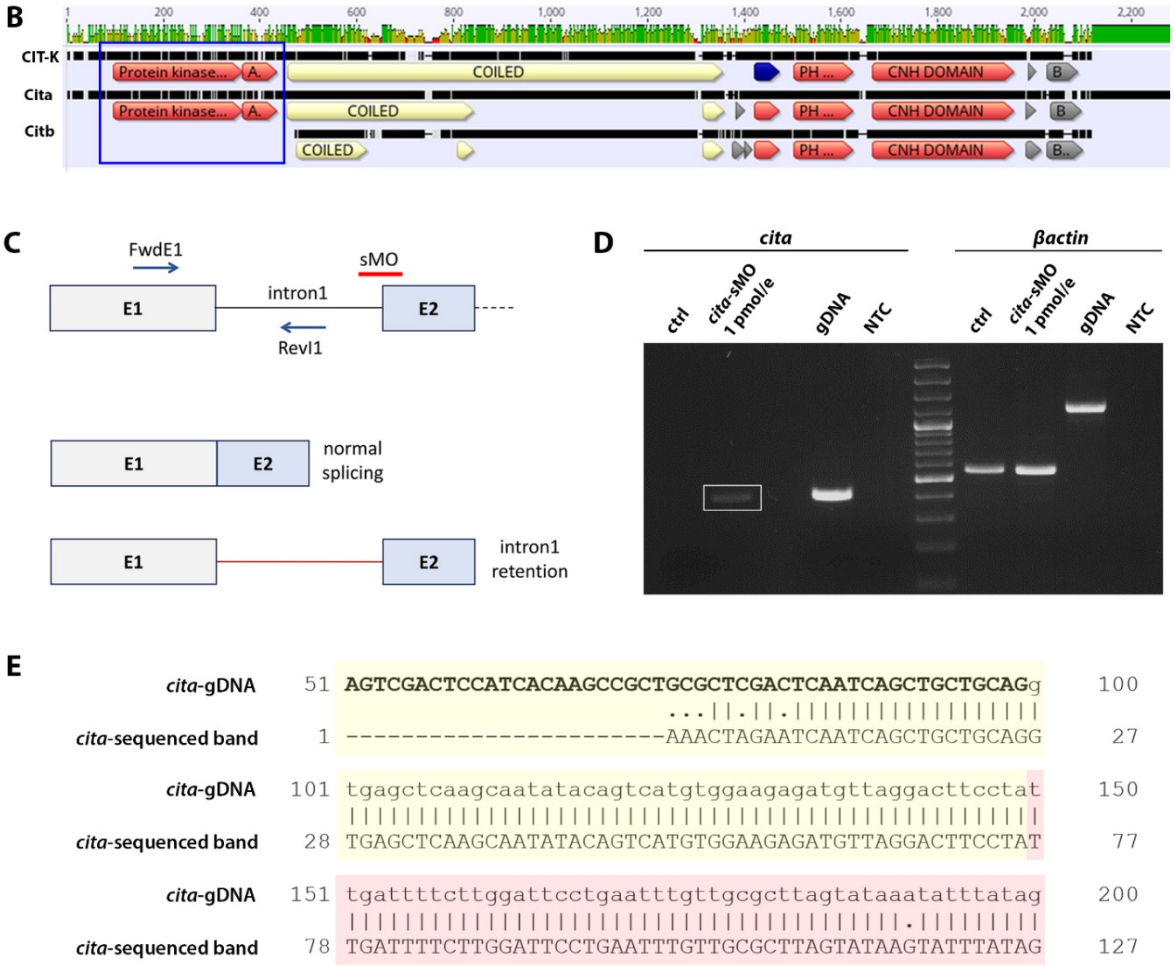

Figure 1. Analysis of sequence conservation and validation of the *cita*-sMO-mediated knock-down strategy. (A) Table reporting the results of pairwise alignments for transcript and protein sequences (Needle-EMBOSS tool - Clustal, EMBL-EBI); cDNA sequence identity, and protein sequence identity and similarity are reported. **(B)** Output of the multiple alignment results of mouse CIT-K and zebrafish Cita and Citb protein sequences aligned with Geneious Prime. Functional domains are represented by coloured blocks. The N-terminal portion containing the kinase domain is indicated by the blue rectangle. **(C)** Schematic representation of *cita*-spicing morpholino (*cita*-sMO) action and validation. *cita*-sMO, represented as a red line, recognizes and binds the intron1-exon2 boundary sequence of the cita transcript, leading to aberrant splicing and intron1 retention. PCR primers utilized for the validation strategy are represented as blue arrows. E=exon; FwdE1=forward primer mapping on exon1; RevI1= reverse primer mapping on intron1. **(D)** agarose gel showing molecular validation of the *cita*-sMO. Left side of the gel: amplification bands obtained with the FwdE1/RevI1 PCR amplification. As expected, the amplicon is obtained from cDNA of embryos injected with the *cita*-sMO (white rectangle) and from the control genomic DNA (gDNA), but not from cDNA of control embryos. Right side of the gel: amplification bands for the housekeeping gene, used as a positive control for the quality and integrity of cDNA in each sample. *βactin* PCR primers

are designed to amplify both cDNA and gDNA sequences, giving a larger product in the second case. The absence of the *βactin* larger gDNA amplification band in cDNAs samples exclude gDNA contamination. NTC = no template control. **(E)** Results of the alignment between *cita* genomic region containing exon1-intron1 junction and the *cita*-sMO aberrant band sequence, obtained by Sanger sequencing (pairwise sequence alignments with the Needle - EMBOSS - Clustal, EMBL-EBI*)*. (yellow= exon1; red= intron1)*.*

2.2. Phenotypes characterization and correction

We considered the head size as the primary phenotype for our analyses, to test for insurgence of a microcephalic condition. As expected, we observed a significant reduction of the head dimension, reminiscent of MCPH17 patients with both *cita*-ATGMO and *cita*-sMO at a dose of 0.125 pmol/embryo, without observing any gross morphological alteration **(Figure2 A-C).** For all subsequent experiments, a total dose of 0.125 pmol/embryo was achieved by combining the two morpholinos, in order to minimise off-target effects, as suggested by the guidelines for morpholinos usage (54,59). Preliminary data from our collaborators on a Cit-k deficient murine model suggested that treatment with the antioxidant N-acetylcysteine (NAC) could benefit Cit-related phenotypes (176,361). Therefore, we tested the efficacy of NAC treatments in ameliorating the microcephalic condition of our zebrafish *cita*-deficient embryos. We first tested different doses of NAC on uninjected control embryos to test for possible, dose-dependent toxicity effects. We started NAC treatments during gastrulation (50% epiboly), before neurogenesis occurs, and administrated the compound directly in the embryos' growth medium at a final concentration of 0.5 µg/ml, 1 µg/ml, 10 µg/ml, 100 µg/ml, 500 µg/ml and 1 mg/ml. We did not observe any decrease in embryo survival at 24 hpf, nor any morphological or physiological alteration (data not shown). Therefore, we proceeded with the highest tested dose of 1 mg/ml for the following experiments, administrating it from 50% epiboly and evaluating its effect on the head of *cita*-deficient embryos at 24 hpf. We observed that NAC treatment significantly recovered the head size of *cita*-deficient embryos (Figure 2 D-F). As defective neural development is associated to impaired brain functionality and seizures both in patients and in *Cit-k* deficient murine models, we assessed locomotor behaviour of *cita*-deficient larvae (164,362). We performed light/dark transition-tests through the Danio vision system (See Materials and Methods, Section 4.13) and we evaluated the distance and velocity of motion for 5 dpf larvae across 1 min intervals for 1 hour. Although *cita*-deficient larvae were still able to respond correctly to light stimuli, both the distance and velocity of motion were increased compared to controls (Figure 2 G-H). This indicated a

hyperactivity status comparable to sizures-like events (363). Notably, NAC treatment also corrected such locomotor alterations, further confirming its efficacy in treating Cit-associated abnormalities.

Morphological and behavioural defects are associated, both in patients and in *Cita*-deficient murine models, with an alteration of neuronal subtypes, particularly oligodendrocytes, but also astrocytes and microglia (164,362). Therefore, we have begun to characterize these neuronal populations by *in situ* hybridization and expression analyses via RT-qPCR. WISH analyses for the oligodendrocyte marker *olig2* revealed a decreased expression at the level of the cerebellum, eyes, and spinal cord of 2.5 dpf *cita*-deficient larvae, which is partially rescued with NAC treatment (Figure 3A). In parallel, preliminary RT-qPCR analyses revealed a decreased expression level of the oligodendrocytes (*olig2, mbp*), astrocytes (*gfap*) and microglial (*aifl1, ccr2* markers, indicative or a reduction of these cell types (Figure 3B-F).

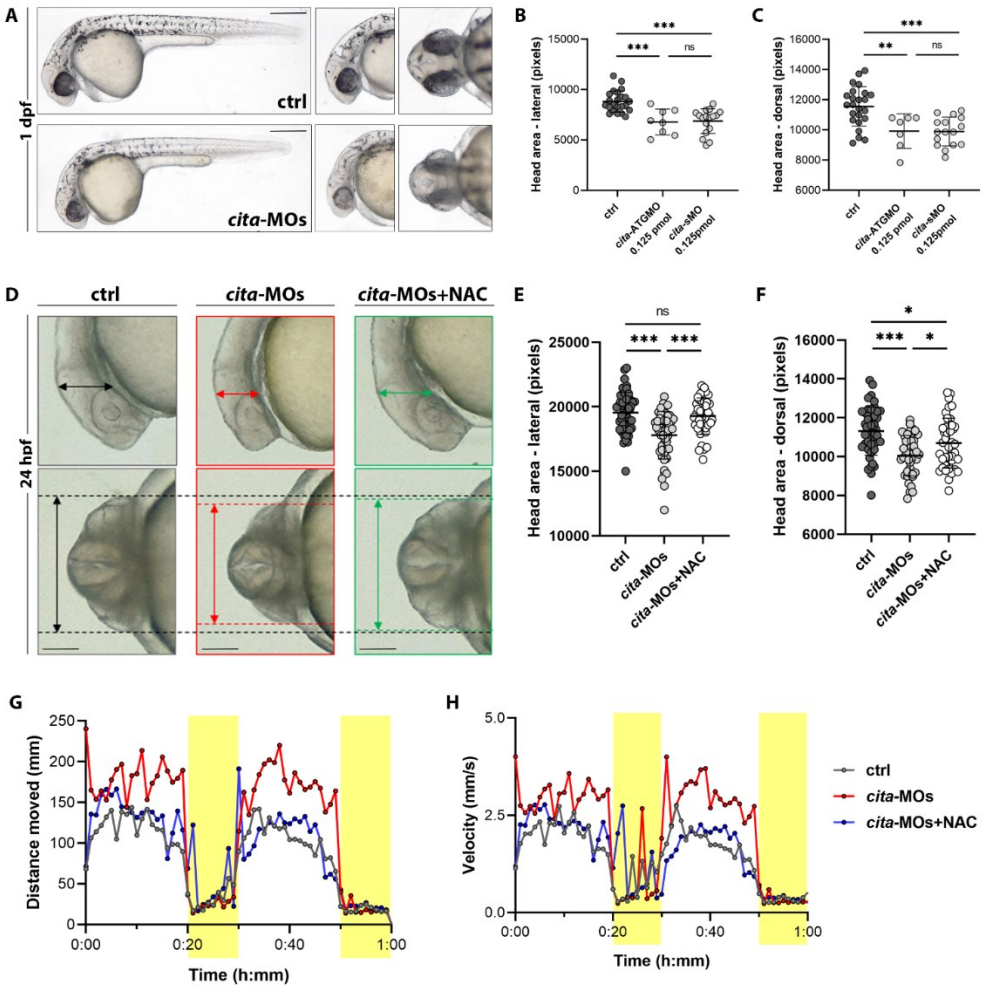

Figure 2. Microcephaly and altered locomotor behavior in *cita*-deficient larvae. (A) Representative brightfield images of control and *cita*-deficient embryos at 24 hpf, showing no

gross morphological alterations, but a decreased head size, as can be appreciated in the lateral and dorsal magnifications of the head region. Scalebar: 300µm **(B-C)** Quantification graphs of the head size (lateral and dorsal area) in controls and *cita*-ATGMO and *cita*-sMO injected embryos. Statistical significance was assessed by Ordinary one-way ANOVA test with Tukey's correction; ***p<0.001; **p < 0.002; ns = not significant. **(D**) Representative brightfield images of 24 hpf embryos of the different experimental conditions for NAC treatment experiments. Scalebar: 100µm. **(E-F)** Quantification graphs of the head size (lateral and dorsal area) of 24 hpf embryos of the different experimental conditions for NAC treatment experiments. Statistical significance was assessed by Ordinary one-way ANOVA test with Tukey's correction; ***p<0.001; *p < 0.05; ns = not significant. **(G-H)** Locomotor alterations of *cita*-deficient larvae and NAC correction. Graphs showing the results of the light/dark transition-tests. Light stimulus is indicated with the yellow colour.

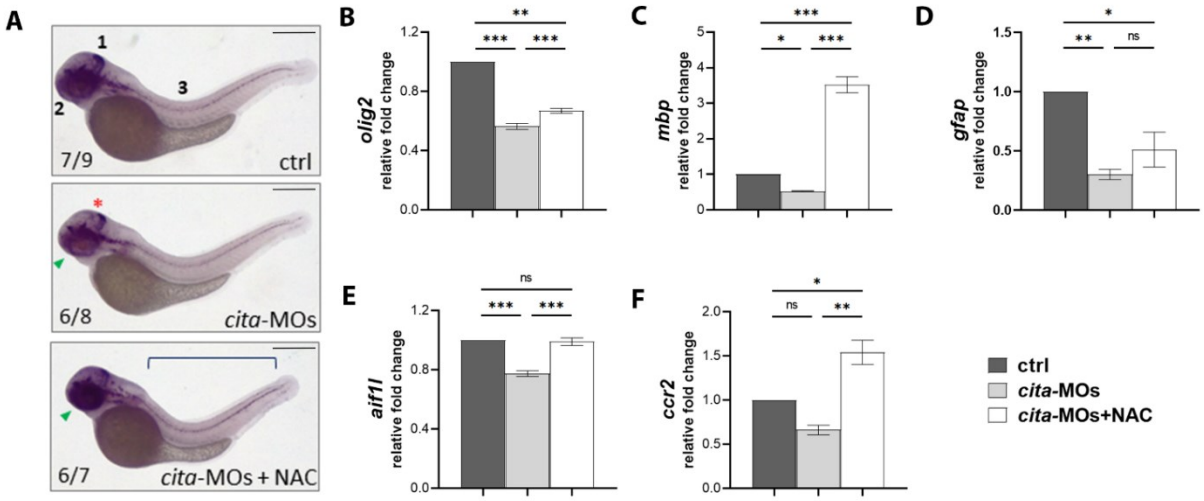

Figure 3. Expression analyses of neural subtypes markers. (A) WISH analysis of the oligodendrocyte specific marker *olig2*. Representative images of embryos of the different experimental conditions stained for *olig2. olig2* signal results decreased in all anatomical compartments of cita-deficient larvae: cerebellum (1), eye (2) and spinal cord (3). The proportion of embryos belonging to the represented phenotype in each category is indicated by the numbers in the lower left. Scalebar: 300µm. **(B-F)** Preliminary results of RT-qPCR analyses showing a decreased expression level of the analysed neuronal marker in *cita*-deficient larvae at 2 dpf, and a rescue with NAC treatment. Statistical significance was assessed by Ordinary one-way ANOVA test with Tukey's correction; ***p<0.001; **p<0.002*;* p < 0.05; ns = not significant.

3. Generation of the *GENE-X* loss-of-function zebrafish model

3.1. Set-up of the loss of function strategy

Zebrafish has a *GENE-X* orthologue, with high protein sequence conservation (Figure 1A). We developed a morpholino-mediated knock-down strategy for *gene-X*. We designed a pair of *gene-X* specific morpholinos, one targeting the ATG region (*gene-X*-ATGMO) and one targeting the exon1-intron1 splicing site (*gene-X*-sMO). We started the validation of the sMO by RT-PCR using a specific couple of PCR primers to test for its action on the transcript (Figure 1B). As *geneX*-sMO targeted the first exon, we expected an intron1 retention (360,364). We utilized a forward primer mapping on exon1 and a reverse primer mapping on intron1 to test for its presence in *gene-X* transcript (Figure 1B). As expected, we observed the appearance of an amplification band from the cDNA of embryos injected with 1 pmol or 0.5 pmol of *geneX*-sMO, but not of controls (Figure 1C). To determine the optimal dose of morpholinos to be used for functional analyses, we tested three different doses of the two morpholinos (0.25, 0.5, and 1 pmol/embryo), which we injected separately. None of the tested doses resulted in embryo toxicity, as demonstrated by the comparable survival rate at 3 dpf with all the doses. However, as the dose of morpholino increased, the percentage of embryos showing abnormal morphology increased, with a reduction in size and developmental delay. This phenotype is in line with the patient's short stature and growth delay (Figure 1D). To reduce potential morpholino non-specific effects or off-target gene knock-down, we used the lower tested dose for all the experiments shown in this report (0.25 pmol/embryo).

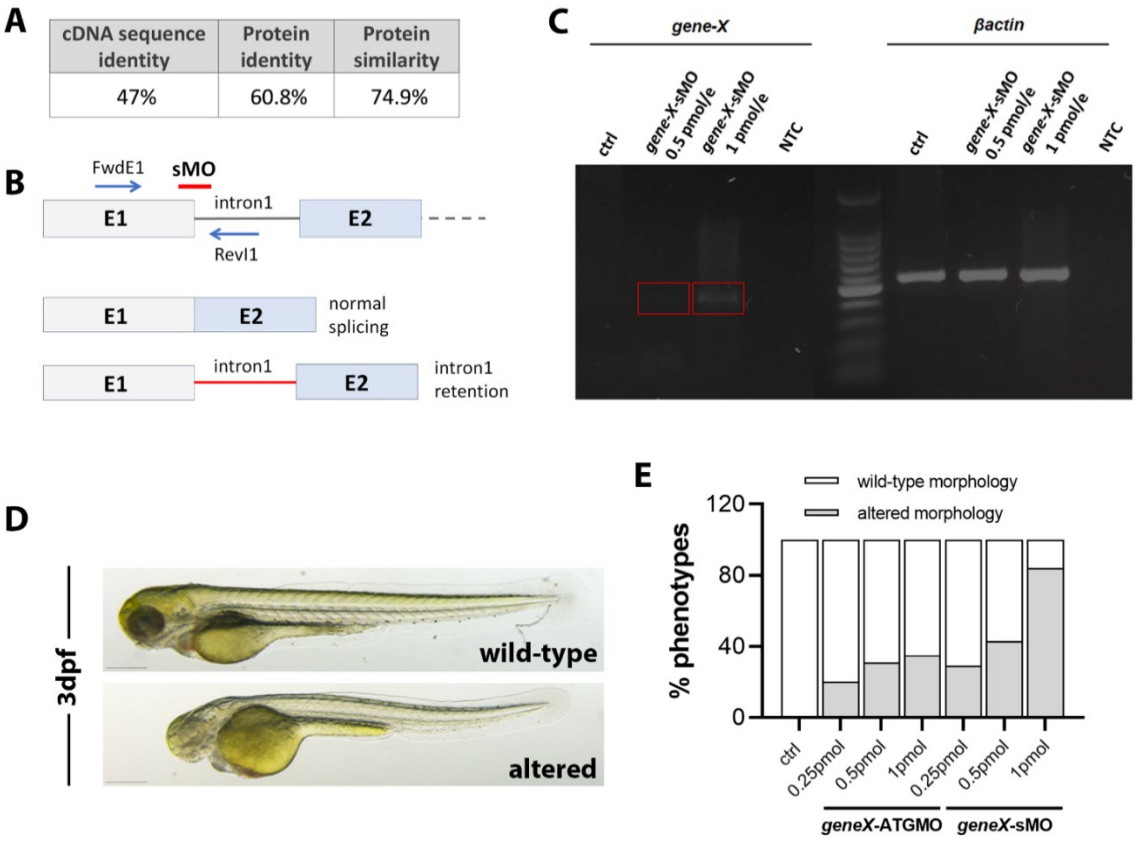

Figure 1. Set-up of the *gene-X* knock-down strategy. **(A)** Table reporting the results of pairwise alignments for human and zebrafish *GENE-X* transcripts and protein sequences (Needle-EMBOSS tool - Clustal, EMBL-EBI); cDNA sequence identity, and protein sequence identity and similarity are reported. **(B)** Schematic representation of *gene-X*-spicing morpholino (*geneX*-sMO) action and validation. *gene-X*-sMO, represented as a red line, recognizes and binds the exon1-intron1 junction of the *gene-X* transcript, leading to aberrant splicing and intron1 retention. PCR primers utilized for the validation strategy are represented as blue arrows. E=exon; FwdE1=forward primer mapping on exon1; RevI1= reverse primer mapping on intron1. **(C)** Agarose gel showing molecular validation of the *gene-X*-sMO. Left side of the gel: amplification bands obtained with the FwdE1/RevI1 PCR amplification. As expected, the amplicon is obtained from cDNA of embryos injected with the *gene-X*-sMO at the two different doses of 0.5 and 1 pmol/embryo (red rectangles). Right side of the gel: amplification bands for the housekeeping gene *βactin*, used as a positive control for the quality and integrity of cDNA in each sample. NTC = no template control **(D)** Representative brightfield images of embryos showing a wild-type or and altered morphology at 3 dpf. Scalebar: 300µm. **(E)** Graph reporting the proportion of embryos showing wild-type or altered morphology in the different experimental conditions.

3.2. Phenotypes characterization and correction

We initially verified, in our *gene-X* knock-down embryos, the occurrence of the main phenotypes reported in the patients under investigation (see introduction, section 2.3.1). We therefore analysed the vasculature, the lymphoid precursors, and the inflammatory status of *gene-X* morphants. For vascular analyses, we performed preliminary analyses on the embryos injected with the two *gene-X*-morpholinos separately, to verify the presence of phenotypes due to an effective *gene-X* knockdown and validate the dose selected. We took advantage of the specific endothelial transgenic reporter line Tg(*kdrl*:GFP);Tg(*gata1*:dsRed), and we monitored the development of the vascular tree up to 3 dpf, the stage at which the embryo's main vascular structures are formed and functional. We observed that in morphant embryos the vascular tree was correctly patterned and fully functional (data not shown), with the exception of the sub-intestinal vein plexus (SIVP), whose structure appeared altered. We stained the SIVP with the alkaline phosphatase colorimetric assay and analysed it considering the number of areas, and the presence of abnormal structures and patterns such as spikes originating from the sub-intestinal vein and ramification of the interconnecting vessels (Figure 2A). The overall areas count in the *gene-X* morphants did not differ from those of the controls, although the distribution of the areas numbers was much wider in embryos injected with the splicing morpholino (Figure 2B). On the contrary, the proportion of embryos showing structural alterations such as ventral sprouts but especially branching, was increased in morphants (Figure 2C,D), suggesting altered angiogenesis. By comparing the phenotype induced by the *gene-X*-ATGMO with that of the *geneX*-sMO which had already been validated, we obtained indirect validation of the action of the ATG-MO. From this point on, we started injecting the two morpholinos in a mix at a total dose of 0.25 pmol/e, as suggested by the morpholinos guidelines (54,59). To test for lymphoproliferation, which was present in the patient as demonstrated by diffuse lymph nodes enlargement and splenomegaly, we stained lymphocytes precursors residing in the thymus by performing WISH for the *rag1* specific marker (Figure 2E). We did not observe any alteration in the thymus area nor in the *rag1* signal intensity. Finally, we analysed the inflammatory status of *gene-X* deficient embryos by performing RT-qPCR analyses for cytokines. Preliminary analyses revealed an increase in the expression level of the proinflammatory *il1β, il6* and *tnfα* and a decrease in the anti-inflammatory *il10.*

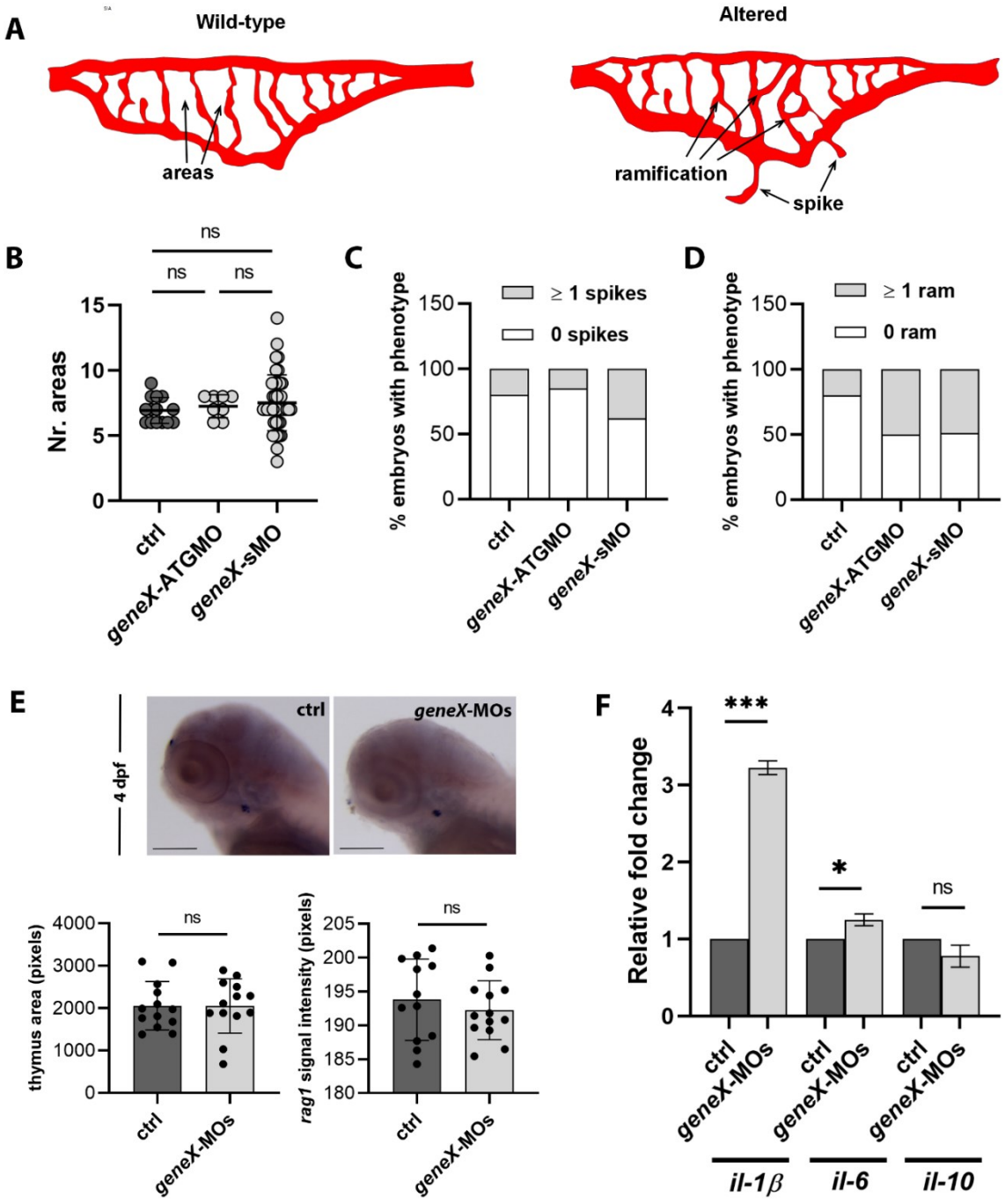

Figure 2. Preliminary characterization of the *gene-X* related phenotypes. (A) Schematic representation of the wild-type and altered SIVP structures. Areas and structural alterations as ventral spikes and ramifications are indicated with the arrows. **(B)** Quantification graphs of the SIVP areas counts in controls and *gene-X*-morphants. Statistical significance was assessed by Ordinary one-way ANOVA test with Tukey's correction; ns = not significant. **(C,D)** Proportion of embryos showing SIVPs ventral sprouts and ramifications in the different experimental conditions. **(E)** Representative brightfield images of embryos stained for the lymphocytes precursors *rag1* marker (Scalebar: 150µm) and quantification graphs of *rag1*+ area and *rag1* signal intensity. Statistical significance was assessed by Unpaired t-Student test. ns = not significant. **(F)** Preliminary results of RT-qPCR analyses of the cytokines expression in *gene-X* morphants and control embryos. Statistical significance was assessed by Unpaired t-Student test. ns = not significant. ***p<0.001; *p < 0.05; ns = not significant.

In order to demonstrate the specificity of the observed phenotypes, we used two different strategies to rescue the vascular defects. GENE-X is a negative regulator of Rho-GTPases and in its absence the Rho-GTPases pathways will be hyperactive (189,190). As the Rho kinases (ROCK) are the direct effectors of Rho-GTPases, we decided to treat *gene-X* morphant embryos with the ROCK enzyme-specific inhibitor Y27632 (192,193). One of the functions previously associated with *gene-X* is its role in erythrocyte maturation. We therefore used the erythrocyte specific transgenic line Tg(*kdrl*:GFP);Tg(*gata1*;dsREd) where we had observed a reduction of the *gata1* signal of *gene-X*-morphants, to have a direct and immediate read-out of the efficacy of Y27632. We tested different doses of the compound (10μM, 20 μM and 100 μM) on *gene-X* deficient embryos and measured the efficacy of the different doses in recovering the reduction of *gata1* signal (Figure 3A,B). The dose of 20 μM resulted as the most effective in rescuing this phenotype and therefore we selected it for further experiments. We next tested the ability of the Y27632 in correcting the vascular defects of the SIVP. We made preliminary analysis of the SIVP structure considering, in addition to the described parameters, the total extent of this vascular plexus. We noted, as previously described, an unchanged number of areas, but a significantly increased number of structural alterations (both ventral sprouts and branches). The total extension of the SIV was significantly reduced, also suggesting a defect in angiogenesis. As expected, for all parameters considered, treatment with Y27632 recovered the defects, demonstrating the specificity of the phenotypes observed with respect to the Rho-GTPase pathway. Parallel to this, we began to test the effect of the human wild-type mRNA injection on the recovery of the phenotypes. We started to consider its ability to recover the haemorrhagic events that we observed sporadically in our *gene-X*-deficient embryos using the double transgenic line Tg(*kdrl*:GFP);Tg(*gata1*;dsRed). Interestingly, we noted the complete absence of haemorrhages in the embryos co injected with the *gene-X* morpholinos and human wild-type mRNA.

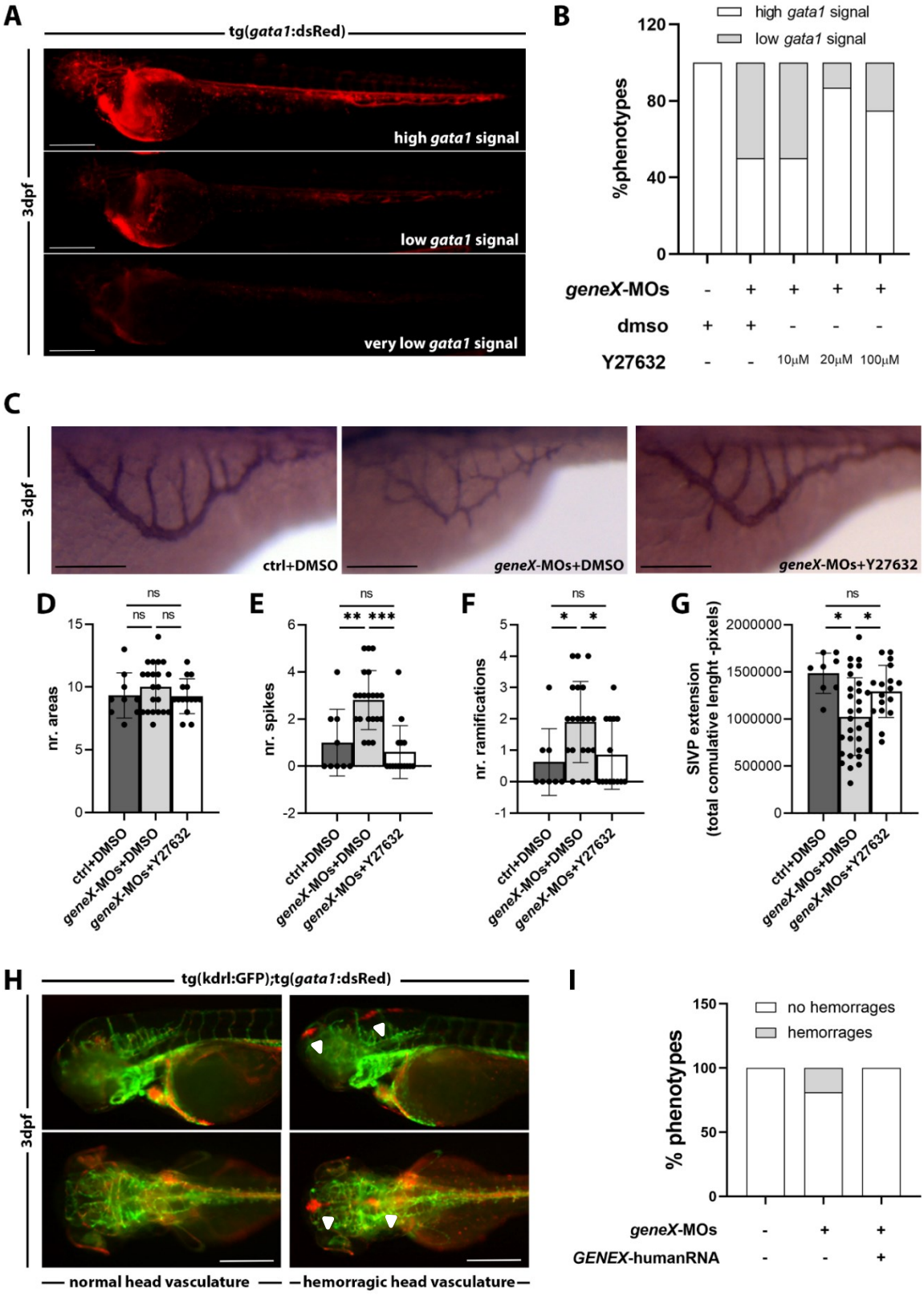

Figure 3. Correction of the *gene-X*-deficiency induced phenotypes. (A) Representative fluorescence images of 3 dpf embryos of the Tg(*kdrl*:GFP);Tg(*gata1*;dsRed) showing a normal, reduced or strongly reduced gata1 signal. Scalebar: 300μm. **(B)** Proportion of embryos of the different experimental conditions showing normal or reduced *gata1* signal for Y27632 experiments. **(C)** Representative brightfield images of the SIVP of 3 dpf embryos of the

different experimental conditions stained with the alkaline phosphatase assay. Scalebar: 100µm. **(D-G)** Quantification graphs of the parameters used for the SIVP characterization. Statistical significance was assessed by Ordinary one-way ANOVA test with Tukey's correction; ***p<0.001; **p<0.002; *p < 0.05; ns = not significant. **(H)** Representative fluorescence images of 3 dpf embryos the Tg(*kdrl*:GFP);Tg(*gata1*:dsRed) transgenic line with unaltered head vasculature or with hemorrage. Hemorrages are visible as red erythrocytes extravasating from the green endothelium and are indicated by arrowheads. Scalebar: 300µm. **(I)** Proportion of embryos of the different experimental conditions showing hemorrages.

4. Generation of a TKOS zebrafish model

4.1. Characterization of *triadin* spatio-temporal expression

In zebrafish, triadin (*trdn*) is present in a single gene copy (Chr20:40,150,612-40,231,379). We characterized *trdn* spatial and temporal expression by means of RT-PCR and WISH analyses. RT-PCR profiling outlined the temporal expression pattern of *trdn* from the onset of somitogenesis extending up to 5 dpf (Figure 1A). Accordingly, WISH analyses revealed *trdn* expression in developing somites during somitogenesis, in skeletal muscles from 24 hpf onward and in cardiac tissue from 48 hpf (Figure 1 B-F). These observations confirmed the conserved expression of zebrafish *trdn* across skeletal and cardiac muscles, mirroring the patterns observed in humans and mice.

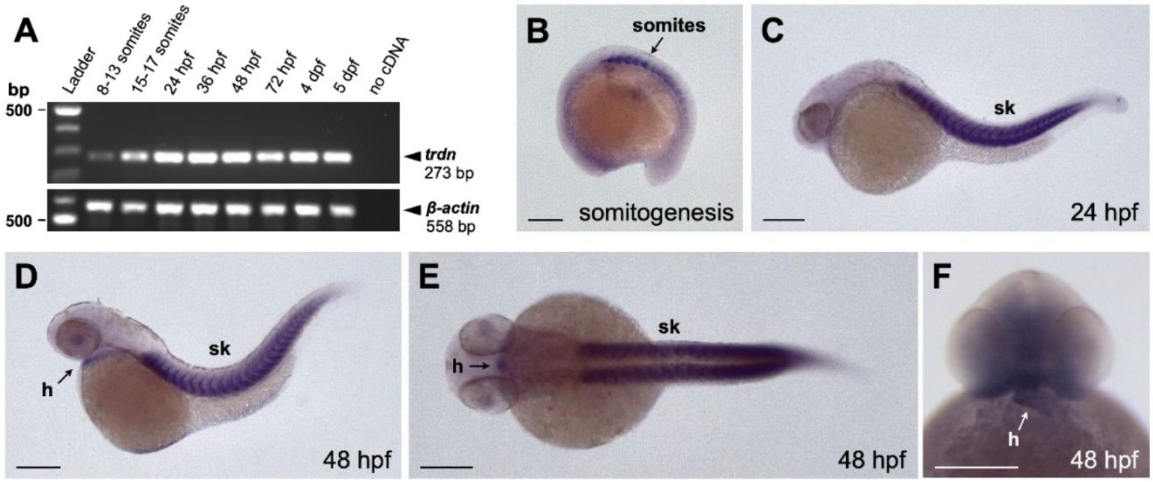

Figure 1. *trdn* expression profile. (A) Agarose gel of RT-PCR performed on RNA extracted from embryos at different developmental stages. *β-actin* was used as the loading control. **(B-F)** Representative brightfield images of *trdn* wish analyses at different developmental stages. Lateral views of 13 somite embryo **(B)**, 24 hpf **(C)**, and 48 hpf **(D)** embryos; dorsal **(E)** and frontal **(F)** perspectives of 48 hpf embryos highlighted the bilateral *trdn* expression in the skeletal muscles (sk) and the heart expression (h). Scale bars = 100 μm.

4.2. *trdn* knock-down strategy and characterization and correction of the resulting phenotypes

trdn knock-down was gained by injecting two *trdn* morpholinos (MOs) designed to target the translational start site (*trdn*-ATGMO) and the exon1-intron1 junction (*trdn*-sMO) (Figure 2A). We initially injected the two morpholinos separately, at varying

concentrations of 0.3, 0.6, and 1.2 pmol/embryo to evaluate their dose-dependent effects. Efficacy assessment of *trdn*-sMO and *trdn*-ATGMO was conducted through RT-PCR and Western blot analyses, respectively. More precisely, to assess the effect of *trdn*-sMO, RT-PCR was performed by using forward and reverse primers annealing to *trdn* exon 1 and exon 2, respectively, so that both exon 1 skipping and intron 1 (> 9000 bp length) retention determined no amplification (Figure 2A,B). Both morpholinos demonstrated efficiency and exhibited dose-dependent effects (Figure 2A-C). Most of the *trdn*-deficient embryos displayed cardiac edema and exhibited curvature in the trunk/tail region at 2 dpf (Figure 2D-E). Such abnormalities were present in a dose-dependent manner in both embryos injected with *trdn*-ATGMO and *trdn*-sMO, further demonstrating the specificity of the knock-down (Figure 2D-E). For all the following experiments we injected a mix of the *trdn*-sMO and *trdn*-ATGMO (referred to as *trdn*-MOs) at a final dose of 0.6 pmol/embryo. Given the expression of *trdn* in both the heart and skeletal muscle, we started characterizing the phenotypes induced *trdn* knockdown at 48 hpf, a developmental stage characterized by functional zebrafish hearts and the completion of the initial skeletal myogenic wave (246). *trdn*-deficient embryos displayed distinct cardiac edema and exhibited curvature in the trunk/tail region, as observed with the injection of the single *trdn* morpholinos. Utilizing these anomalies as a metric, we classified *trdn*-deficient embryos into four distinct phenotypic classes (Figure 2F-J). “Class1” embryos presented a “controls-like” morphology (Figure2F), “Class2” embryos exhibited cardiac edema (Figure2G), “Class3” embryos displayed a curved trunk and tail (Figure2H) and “Class4” embryos showed both edema and pronounced curvature in the trunk and tail region (Figure2I). We the focused on the characterization of the structure and function of the skeletal and cardiac muscles. As *trdn*-morphants often presented a curved trunk-tail region, we analysed the skeletal muscle morphology in this region of Class1 and Class3 embryos by utilizing multiple techniques. WISH staining with a probe for creatine kinase muscle (*ckma*) revealed no substantial differences in the skeletal muscle morphology between control embryos and *trdn*-morphants of both Class 1 and Class 3 (Figure 3A–C). We next performed birefringence analysis, which did not reveal any lesions in the skeletal

muscles of *trdn*-MOs-injected embryos compared to the control group (Figure 3D–F).

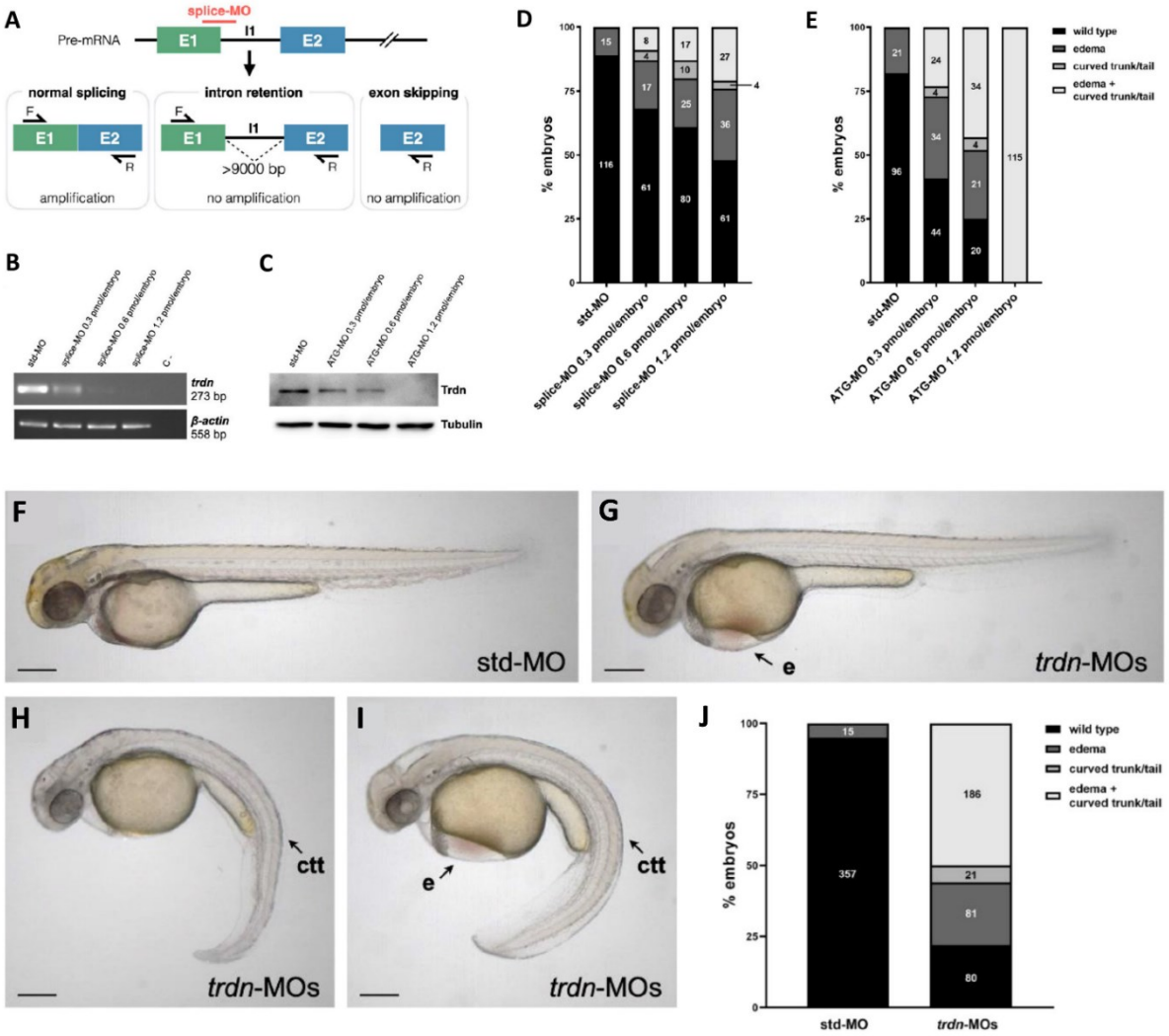

Figure 2. Molecular and functional validation of *trdn*-MOs efficacy. (A) Schematic representation of *trdn*-sMO action and validation. *trdn*-sMO, represented as a red line, recognizes and binds the exon1-intron1 junction of the *trdn* transcript, leading to aberrant splicing. PCR primers utilized for the validation strategy are represented as black arrows. E=exon; I= intron; F=forward primer mapping on exon1; R= reverse primer mapping on exon2. **(B)** agarose gel with the *trdn*-sMO validation by RT-PCR performed on cDNA derived from embryos injected with different doses of the morpholino. The housekeeping gene βactin was used as a positive control for the quality and integrity of cDNA in each sample. **(C)** Western blot analysis of Trdn expression in zebrafish embryos injected with std-MO or *trdn* ATGMO at different concentrations. Tubulin was used as internal control in each sample. **(D-E)** Quantification of embryos phenotypes following trdn splice-MO **(D)** and ATG-MO **(E)** injection. Values indicate the number of embryos for each phenotype. **(F-I)** Representative brightfield images of 48 hpf embryos injected with std-MO and *trdn*-MOs exhibiting Class1 (**F**), Class2 **(G)**, Class3 **(H)** and Class4 **(I)** phenotype. **(J)** Quantification of embryos ctrl and trdn knock-down embryos belonging to the different phenotypical classes. Classification of the phenotypes obtained with *trdn*-MOs injection. Values indicate the number of embryos for each phenotype. Scale bars indicate 100 μm. e = edema; ctt = curved trunk/tail.

Furthermore, immunofluorescence investigations employing an anti-sarcomeric myosin antibody (MF20) did not highlight any significant alteration in myosin fibers of *trdn*-morphants **(Figure 3G–I)**. These analyses suggested that, despite the observed defects in the trunk/tail region morphology, the skeletal muscle structure and integrity appeared largely unaltered in *trdn*-morphants embryos when compared to control groups.

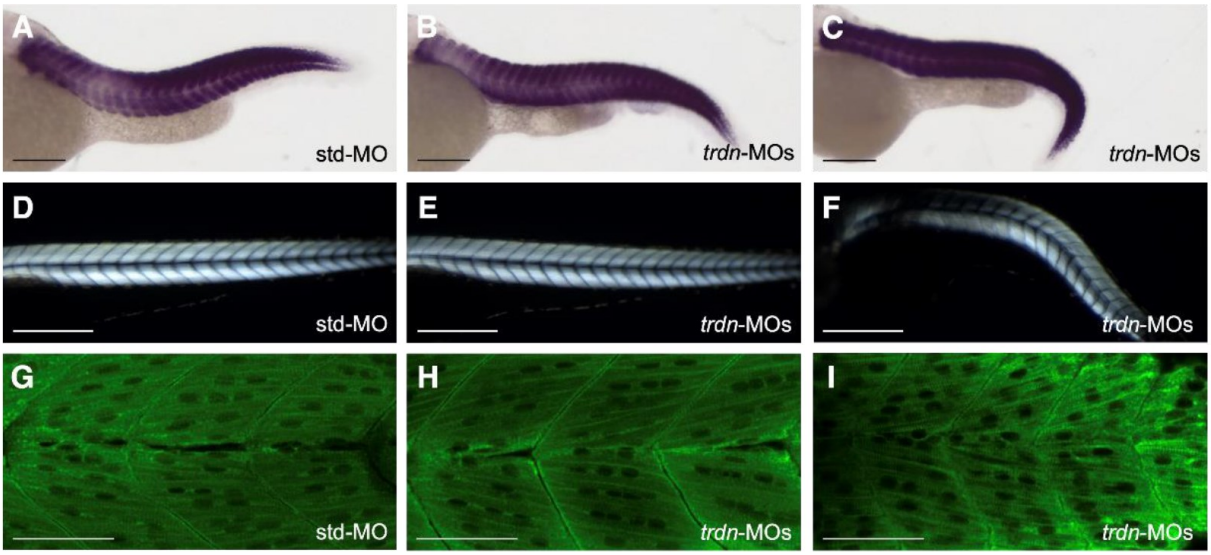

Figure 3. Characterization of the skeletal muscle structure. (A-C) Representative brightfield images of WISH analyses with the *ckma* probe of 48 hpf embryos of the control group **(A)** and of the Class1 **(B)** and Class3 **(C)** *trdn*-morphants. Scalebar 100 µm. (D-E) Representative birefringence images of 3 dpf embryos of the control group **(D)** and of the Class1 **(E)** and Class3 **(F)** *trdn*-morphants. Scalebar 100 µm. **(G-I)** Representative MF20 immunofluorescence images of control **(G)**, class1 **(H)** and class3 **(I)** *trdn*-morphants. Scalebar = 50 µm.

We next investigated the structure and function of heart in *trdn*-knock-down embryos. To examine heart looping and structure, we conducted WISH analyses using the cardiac specific probe for cardiac myosin light chain 2 (*cmlc2*), which is specifically expressed in both atrial and ventricular regions of the heart. These analyses did not reveal structural alterations in the hearts of *trdn*-morphants (Figure 4A,B). Accordingly, further analyses via semithin sections did not indicate notable morphological differences between the heart chambers of *trdn*-morphants and the control group (Figure 4C,D). Therefore, despite observing cardiac edema in *trdn*-morphants, the structural morphology of the heart, as assessed by heart-specific markers and histological sections, did not reveal evident alterations of the heart anatomical structure. We then analysed cardiac function by measuring heart rate (beats per

minute, bpm). We found a significant reduction in the heart rate of *trdn*-MO-morphants compared to controls (Figure4E), indicating an impairment in cardiac electrical function. To ascertain if this diminished heartbeat was specifically attributed to trdn loss-of-function, we co-injected the *trdn*-MOs with either the wild-type (*TRDN* WT) or the L56P mutant (*TRDN* L56P) human cardiac isoforms of TRDN mRNAs. We tested several doses of the *TRDN* mRNAs and selected the dose of 25 pmol/embryo, as higher doses induced toxicity and lethality (Figure4F). Even though not statistically significant, a partial rescue of the heart rate was observed in *trdn*-MOs + *TRDN* WT embryos, with a less pronounced effect noted in *trdn*-MOs + *TRDN* L56P embryos (Figure 4G). Notably, when considering the percentage of *trdn*-MOs + *TRDN* WT embryos with a heart rate higher than the mean of *trdn*-MOs, it increased to 78%, compared to 67% in *trdn*-MOs alone. Conversely, *trdn*-MOs + TRDN L56P embryos displayed no difference (67%) in heart rate compared to *trdn*-MOs embryos (Figure 4H).

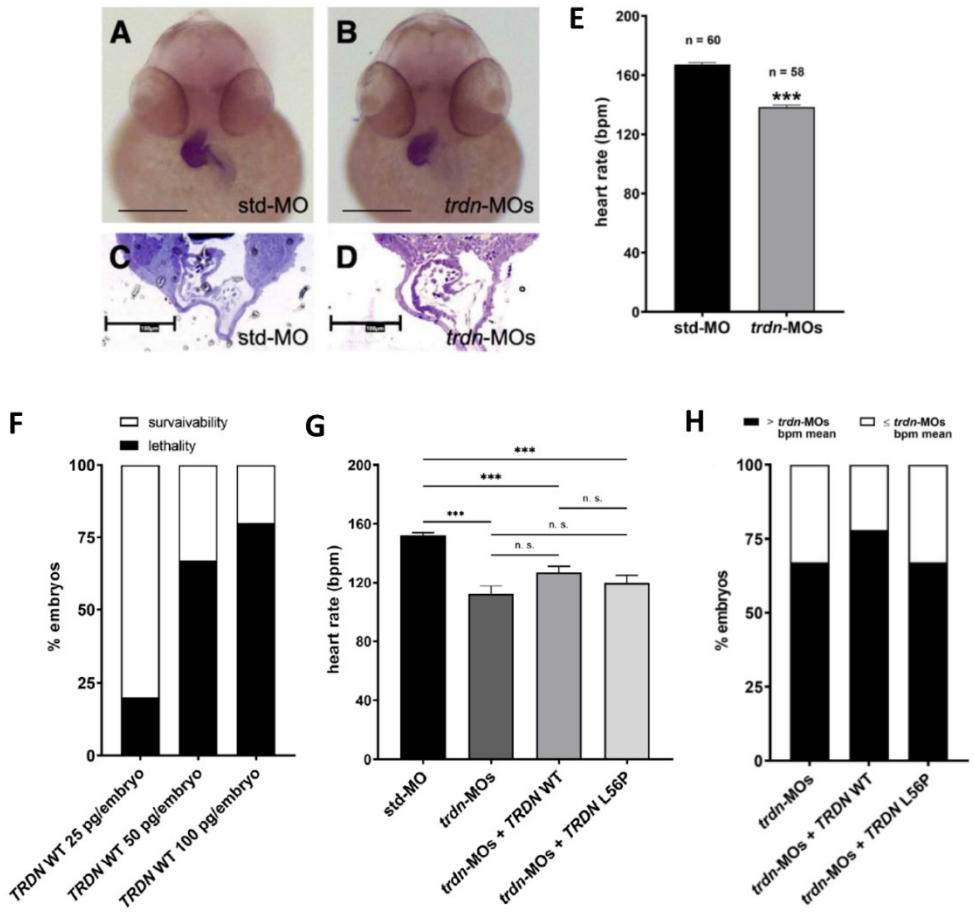

Figure 4. Evaluation of heart morphology and function. (A,B) Representative brightfield images of 48 hpf control and *trdn*-MOs embryos stained with the *cmlc2* cardiac marker via

WISH, frontal view. Scale bar = 100 µm. **(C,D)** Representative images of semithin sections of control and *trdn*-MOs embryos in the heart region. Scale bar = 100 µm. **(E)** Quantification graph of heartrate in 48 hpf control and *trdn*-MOs embryos. Statistical significance was assessed by Unpaired t-Student test. ***p<0.001. **(F)** Quantification of lethality of the different *TRDN* WT mRNA tested doses. **(G)** Quantification graphs of heart rate of embryos in the different experimental conditions for human *TRDN* mRNA rescue experiments. Statistical significance was assessed by Ordinary one-way ANOVA test with Tukey's correction; ***p<0.001; **p<0.002*p < 0.05; ns = not significant. **(H)** Proportion of embryos with a heartbeat superior to the mean of the heartbeat of *trdn*-MOs in the different experimental conditions for human *TRDN* mRNA rescue experiments.

We then investigated the potential pharmacological recovery of the *trdn*-MOs-induced heart phenotype by treating embryos with three different arrhythmic drugs: adrenaline, atropine, and isoprenaline. First, we exposed 3 dpf embryos to different concentrations of these drugs and we assessed the heartbeat rates to select the most effective doses, which we then utilized for rescue experiments on the *trdn*-morphants (Figure 4A-C). Doses of 50 mg/ml, 25 mg/ml and 50mg/ml were selected for adrenaline, isoprenaline and atropine, respectively (Figure4 A-C). We then treated *trdn*-morphants with these compounds and we observed a significant increase in heart rate upon treatment with adrenaline and isoprenaline in *trdn*-MO-injected embryos (Figure 4D). For atropine, a partial rescue of the heartbeat was observed, though it didn't reach statistical significance (Figure 4D). Given that β-blockers and sodium channel blockers are primary therapies for TKOS patients, metoprolol and flecainide were tested. Flecainide treatment led to a reduction in heartbeat in controls. Remarkably, in *trdn*-MOs-injected embryos, flecainide similarly reduced cardiac frequency, suggesting its efficacy even in the absence of Trdn function (Figure 4E). However, metoprolol did not significantly affect heartbeat in either controls or *trdn*-MOs-injected embryos (Figure 4E).

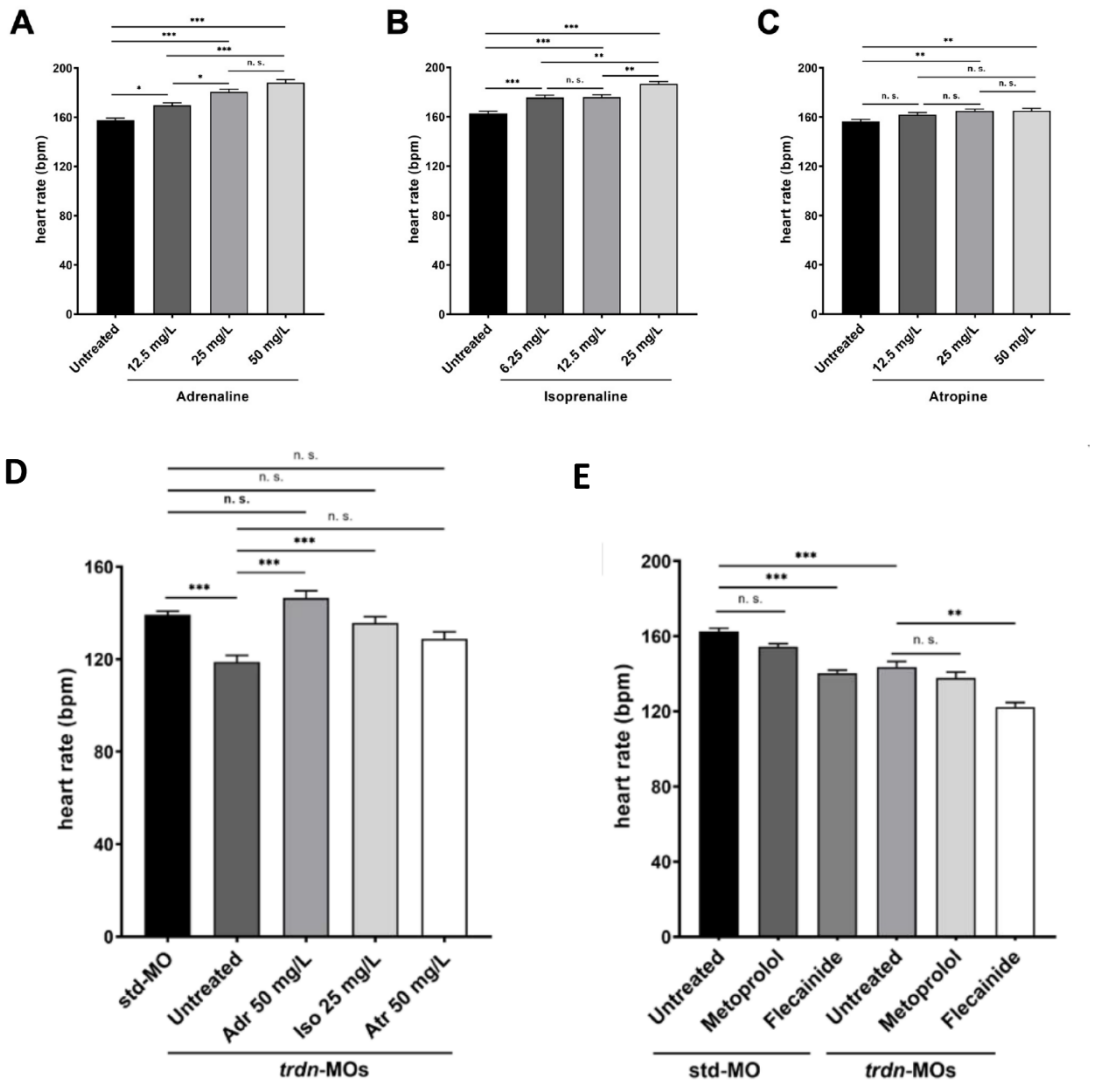

Figure 5. Pharmacological modulation of heart rate. (A-C) Quantification graphs of heart beat counts in 3 dpf larvae treated with increasing doses of adrenaline (**A**), isoprenaline (**B**) and atropine (**C**). (**D**) Quantification graphs of the heartbeat counts in 3 dpf control and *trdn*-MOs-injected larvae, untreated or treated with adrenaline, isoprenaline and atropine. (**E**) Quantification graphs of the heartbeat count in 3 dpf control and trdn-MOs-injected larvae, untreated or treated with metoprolol or flecainide. For all graphs in Figure 4, *Statistical significance was assessed by Ordinary one-way ANOVA test with Tukey's correction; ***p<0.001; **p<0.002*p < 0.05; ns = not significant* (**G**,**H**). Adr = adrenaline; Iso = isoprenaline; Atr =atropine.

Discussion and conclusions

Generation of the DADA2 zebrafish model

DADA2 is a rare, autosomal recessive genetic disease affecting the immune system. It causes excessive inflammation and immunodeficiency, and in severe cases, it results in life-threatening strokes and bone marrow failure (133–135). Currently, the only curative option is allogeneic hematopoietic stem cell transplantation (HSCT), but this is limited by the scarcity of compatible donors and by the high risk of rejection (137–139). Modelling the disease in mammalian models has not been possible as rodents lack the ADA2 gene, thus hampering the efforts to understand the pathophysiology of the disease and the development of alternative curative options. In this project, we developed a zebrafish model for the study of the molecular mechanisms underlying DADA2 and for the search of new potential therapeutic strategies. A previous zebrafish model with knock-down of *cecr1b* exhibiting neutropenia and hemorrhages had demonstrated the feasibility of the use of zebrafish to model DADA2 (131). However, this model was only exploited for testing the effects of human transcripts carrying deleterious mutations found in patients (131). We extended the characterization of the DADA2-like phenotypes induced by Cecr1b loss-of-function and investigated possible pathogenetic mechanisms underlying these defects, laying the bases for potential correction methods.

We designed and validated a knock-out strategy based on the CRISPR-Cas9 approach which would allow us to obtain, in the immediate term, a zebrafish model with transient loss-of-function of *cecr1a* and *cecr1b*, and in the long term, stable mutant lines with disruption of the catalytic domain function. In agreement with the previous work (131), we found neutropenia and vascular dysfunction only in *cecr1b*-loss-of-function (LoF) embryos but not in the *cecr1a*-LoF embryos. We then extended the characterisation of the embryos to the inflammatory state, observing also systemic inflammation predominantly mediated by activated macrophages. Unlike our zebrafish model, patients suffering from DADA2 tend to present a restricted symptomatology, with predominance of the inflammatory/vascular or of the hematological manifestations (153). This is likely due to the dual nature of ADA2, which seems to affect patients differently, depending on the residual functionality of its domains (153,365). In particular, bone marrow failure and the associated hematologic diseases are typically linked to mutations with minimal residual enzyme activity or complete loss-of-function, while inflammation and vasculitis are usually caused by ADA2 variants ensuring at

least 3% of the catalytical activity (134,153). The simultaneous presence of all the main DADA2-like phenotypes in our zebrafish model probably depends on the nature of our knock-out (KO) strategy. In fact, transient KO leads to the creation of mosaic organisms, carrying different mutations in the different cells in which the Cas9-mediated DNA nicks occurred. This is due to the error-prone DNA repair mechanisms, which induce random mutations, insertions, and deletions. In the case of our model with transient KO of *cecr1b*, the sgRNAs were designed to delete exon5 and thus gain the disruption of the catalytic domain. However, the two guides may have acted simultaneously or individually in different cells of each embryo, inducing mutations of different types. Some of these may have induced a simple reduction in the total catalytic activity of the protein, or the loss of function of a single catalytic domain or disrupted the entire structure and folding of the protein, or led to a null allele that is not expressed at all. The knock-out strategy that we applied, therefore, leads to a decrease in the global amount of functional ADA2, rather than affecting specifically one of its domains. Moreover, it is fundamental to consider that we have characterized our zebrafish model during embryogenesis, when inflammation, endothelial function and haematopoiesis are closely linked. Beside the characterization of the DADA2-like *cecr1b*-KO induced phenotypes, we also tested the two most used drugs for treating DADA2 symptoms: the human granulocyte-colony stimulating factor (hG-CSF) and the anti-TNF. Due to the absence of innate immunity in the first weeks of zebrafish development, it was possible to inject the two drugs, both of protein nature, into the circulation of our embryos, without risking an immunogenic reaction that would have impeded their action. We decided to consider the neutropenia as a first and simple readout to compare the effect of the two drugs in our model and parallel it with that in patients. As in patients, the hG-CSF was able to correct the neutropenia in our model, while the anti-TNFα therapy showed some improvement, but it did not reach statistical significance in reversing neutropenia. These data further confirm the conservation of function between Cecr1b and ADA2 and of the main mechanisms underlying DADA2, strengthening the translational potential of zebrafish for the study of this disease.

Once we had thoroughly characterised the main phenotypes of our zebrafish DADA2 model, we decided to investigate the possible molecular mechanisms underlying the onset of the phenotypes. Given the relevance of haematological disease and the curative potential of haematopoietic stem cell transplantation, we decided to analyse in detail the population of haematopoietic stem and progenitor cells (HSPCs), the first

precursors of all blood cells. The formation and homeostasis of HSPCs are regulated by a complex interplay of several intrinsic and extrinsic factors, including inflammation and extracellular adenosine, both of which are linked to the function of ADA2. Sterile inflammation and adenosine signalling play key roles in early haematopoiesis. Tnfα and Il1β are primarily responsible for this process as their action triggers the endothelial expression of *runx1*, essential for specification of the hemogenic endothelium (HE) and for endothelial-to-hematopoietic transition (EHT) (287,366,367). Parallel to this, eAdo-mediated A_{2b}r activation initiates the cAMP/PKA/*cxcl8/runx1* axis in hemogenic endothelial cells, inducing HSPCs differentiation (288). Consistent with the substantial increase in *il1β* and *tnfα* levels and with the A_{2b}r hyperactivation in *cecr1b*-deficient embryos, we found an increased expression of *scl runx1* and *cmyb*, apparently indicating and increased number of HSPCs. However, despite the overall increase in the expression of these markers, the total number of correctly specified HSPCs was reduced in *cecr1b*-LoF embryos, indicating that increased expression of these genes may not be sufficient for EHT to proceed. *runx1* expression in the HE is required for down-regulation of the arterial program which allows the establishment of the hematopoietic fate (280). Consistent with the increase in *runx1* expression, analyses of *enfb2* and *efnb4* revealed unproper arterio-venous specification of the axial vessels, supporting the hypothesis of vascular dysfunction in *cecr1b*-LoF embryos. Time lapse analyses also revealed abortive events of HSPCs budding from the HE, which can explain the reduced number of HSPCs in *cecr1b*-LoF embryos, Cecr1b deficiency then seems to force the hemogenic endothelium toward the hematopoietic fate, resulting in overexpression of these hematopoietic markers. Despite the increase in hemogenic cells markers, HSPCs fail to undergo the EHT properly and dye just after budding from the endothelium. We identified an additional vascular defect in the architecture of the caudal vein plexus (CVP), which is reduced in terms of expansion and vascularization especially in *cecr1b*-LoF embryos. The few HSPCs correctly emerged from HE, therefore, find themselves unable to proliferate and expand properly because of a defective hematopoietic niche. Given the endothelial origin of HSPCs and the importance of the vascular contribution in the hematopoietic niche (240–242), we can understand how an impairment of endothelial function can be reflected directly on the population of HSPCs at different times and regions during hematopoietic development.

However, it remains to be elucidated what the initial event is in the generation of these defects and how the key players contributing to the pathogenesis of DADA2 (inflammation, adenosine, A2br), are related to each other.

Several hypotheses can be considered to interpret our findings, considering the deleterious effects of excessive inflammation, or the possible consequences of an A_{2b}r dysregulation. The first phenotype we observed was that of inflammation, which was already detectable at around 24 hours post fertilization (hpf), before the EHT is complete and the HSPCs have emerged. Although inflammation is indispensable to produce HSPCs, it has been shown that inflammatory signals must be tightly modulated, as prenatal exposure to pro-inflammatory cytokines causes persistent impairment of the immune compartment (368,369) and chronic inflammation is deleterious for maintenance of adult HSPCs (370–372). The hyper-inflammation of *cecr1b*-LoF embryos could lead, on the one hand, to increased expression of HSPCs markers in the HE, but on the other hand it could induce dysregulation of endothelial function, or to an improper arterio-venous specification, which is also essential for HSPCs emergence (373,374). The hypothesis of endothelial dysfunction is also in line with the findings of endothelial status, which revealed, at the same time point of 34-34 hpf, increased expression of endothelial damage markers like *endothelin1* (*edn1*) and leukocytes adhesion molecules like *vcam1a*. The increased expression of endothelial activation markers, which are also upregulated in DADA2 patients (131), could be suggestive of a contribution of primitive macrophages. The action of macrophages is essential for HSPCs mobilisation and budding. Indeed, they degrade the extracellular matrix around the vessel, allowing the exit and migration of HSPCs and thus their subsequent colonisation of hematopoietic niches and the establishment of definitive hematopoiesis (375). We can therefore hypothesise that an alteration in their inflammatory state, behaviour, or recruitment to the HE may result in or contribute to an impaired emergence of the HSPCs. We plan to stain macrophages in *cecr1b*-LoF embryos of the Tg(*kdrl*:GFP) transgenic line to visualise their recruitment and action in the ventral and dorsal aorta region and highlight any alteration. Early blockage of inflammation by *tnfa* morpholino reversed the haematopoietic defects of *cecr1b*-LoF embryos, highlighting its crucial role in these processes. In contrast, later treatment of inflammation by injection of the anti-TNFα had not led to improvements in the haematopoietic compartment, showing that there is a specific time window in which these defects develop. The absence of positive effects on the neutropenia of *cecr1b*-

deficient larvae injected with anti-TNFα might be related to the time window of administration being too delayed. In the case of anti-TNFα treatments, in fact, embryos were treated from 2 days post fertilization (dpf), when the defects in HSPCs and derived cell lines are already established. We can therefore speculate that blocking inflammation is effective when used as a preventive treatment for the onset of haematopoietic phenotypes, rather than as a curative treatment.

It remains essential to clarify the role of the adenosine receptors (ARs) in these processes. $A_{2A}R$ and $A_{2B}R$, among the other ARs, mediate eAdo signaling (376) eliciting an upregulation of the cAMP/pKA pathway and they have been found to directly interact with ADA2 (145,376–378). $A_{2b}r$ is the one expressed in the zebrafish endothelium during the stages where definitive hematopoiesis commences (353). Contrary to the $A_{2A}R$ anti-inflammatory and protective action, $A_{2B}R$ has been associated to several pathological mechanisms involving precisely inflammation, leukocyte function and endothelial homeostasis (379–383). Due to its lower affinity to eAdo with respect to the other ARs, a higher and prolonged exposure to eAdo is required for its activation (378). This could be particularly relevant in the DADA2 context, as emerging evidence suggests that dysregulation of eAdo may be implicated in its pathogenesis and patients show elevated plasmatic eAdo levels (154). Interestingly, $A_{2b}R$ mediates the pro-inflammatory action of eAdo in both monocytes and endothelial cells (379–383). We can then assume that the macrophages inflammatory polarisation observed in *cecr1b*-LoF embryos from 24 hours post fertilization (hpf) could be mediated by hyperactivation of the $A_{2b}r$ pathway in the macrophages themselves. Chemical blockage of $A_{2b}r$ led to a modulation of the *il1β* and *tnfα* expression levels, demonstrating the direct involvement of this pathway in mediating inflammation associated to *cecr1b* deficiency. It would be of interest, for instance to examine whether chemical or morpholino-mediated $A_{2b}r$ inhibition can revert the polarisation of primitive macrophages. A further contribution of the $A_{2b}r$ pathway might also occur directly during EHT. eAdo is known to enhance, in synergy with TNFα signalling, the externalisation of $A_{2b}r$ on the plasma membrane, and thus its activity (384). $A_{2b}r$ is the only one among adenosine receptors to be expressed in axial vessels during the EHT process. Its specific hyperactivation, therefore, could lead to a dysregulation of this process. In agreement with this, our data indicated that early chemical modulation of the $A_{2b}r$ pathway led to an improvement in the population of

definitive HSPCs, as well as early *tnfα* inhibition. A_{2b}r could therefore be involved in both early inflammation and definitive hematopoietic defects, in a self-sustaining and self-enhancing mechanism. It remains to be clarified what the precise link between Cecr1b, A_{2b}r and inflammation and how these three factors cause haematopoietic, inflammation, and vascular defects in a DADA2-like background. In parallel, we intend to analyse primitive haematopoiesis, to check for possible alterations in these cell populations. In fact, the A_{2a}r is highly expressed in the intermediate cell mass (353), where primitive haematopoiesis takes place, and therefore it would be interesting to clarify a possible role for this receptor as well.

Besides their defects in emerging, specified Cecr1b-deficient HSPCs could have had additional defects involving their migration and colonization of the subsequent hematopoietic niches, survival, and proliferation. Regarding the migratory capacity of Cecr1b-deficient HSPCs, we found that although reduced in number, they still can migrate properly to the caudal haematopoietic tissue (CHT). Instead, we observed an alteration in their ability to colonise this region, with a tendency to accumulate in the most anterior portion. Notably, HSCs in the CHT are embedded by endothelial cells of the caudal vein plexus (CVP), which protect them and regulate their function (231,240). Considering the endothelial dysfunction demonstrated by the previous data, it is possible to hypothesise that this colonisation defect may be linked to a defective structure or function of this vascular plexus. In addition to this we found that HSPCs were defective in their proliferative potential. Beside a direct contribution of ADA2, which can act as a growth factor for HSPCs (145,146,385) we can hypothesize that the dysregulation of A_{2b}r-mediated eAdo pathway could directly contribute to this defect. eAdo modulates HSPC homeostasis through its multiple ARs (386). A_{2b}R-mediated purinergic signalling inhibits mobilization, homing, and engraftment of cultured HSPCs in a process involving inflammasomes and its inhibition has proven to be promising in hematopoietic reconstitution (157).

Finally, we tested, in our zebrafish DADA2 model, the potential of an enzyme-replacement therapy in recovering the hematopoietic defects. This therapy is currently not used to treat patients due to the very short half-life of the protein (134). In zebrafish, the vascular, immune, and haematopoietic developmental processes take place very rapidly and the respective systems and organs are completely functional within a few

days after fertilisation. In this context, the supplementation of the human recombinant protein has proved successful in correcting HSPCs defects. This finding opens the possibility, at least theoretically, to the feasibility of enzyme replacement therapy in patients as well, if a more stable form of the protein can be produced. The efficiency of the human protein in reversing the hematopoietic phenotypes in the DADA2 zebrafish model further confirms the high degree of functional conservation between the human ADA2 and the zebrafish Cecr1b and strengthens the very high translational potential of the model. The absence of an adaptive immune system during the first weeks of embryonic development allows human recombinant proteins to be administered to the zebrafish model without the risk of triggering an immune response (303). The possibility of testing recombinant human proteins or engineered antibodies is a major advantage, as it allows their direct testing in the model, shortening the gap between zebrafish and clinical research in the DADA2 field.

The zebrafish DADA2 model enabled us to delve into complex defects and relevant pathways that are challenging to study directly in patients. With this study we identified a dysregulation linked to eAdo homeostasis and its signalling mediated by the A_{2b}r receptor. These findings allowed us to identify new possible molecular mechanisms probably involved in the pathogenesis of DADA2 and so far, never explored. The study of these mechanisms, deepened by means of the *in vivo* zebrafish model and integrated with studies on cultured human cells could pave the way for the identification of new pharmacological targets and thus new therapies. Of fundamental importance, in view of the development of a possible gene therapy, such as that already developed for the other ADA-deficiency, ADA-SCID, is the study of the haematopoietic niche (387). It is indeed essential to understand whether correction of HSPCs alone is sufficient for the complete remission of the disease or whether the other bone marrow cells are also affected. Here again, the zebrafish model can support and help in understanding this by supplementing data from the characterisation of the patient's bone marrow. The haematopoietic niche of zebrafish is in fact very similar to the human one in terms of function and cell types that make it up (295,388). Unlike in the zebrafish model, in individuals with DADA2, signs of the disease are not immediately apparent at birth, likely because of ADA2 transfer from mothers through the placenta. This transfer helps regulate inflammation and supports normal development, including hematopoiesis. However, the disease can emerge in early

childhood and symptoms tend to worsen with age, suggesting a multifaceted interaction of factors. By utilizing the DADA2 zebrafish model, we've had a unique opportunity to explore how the disease affects embryonic development. During this crucial phase, inflammation, endothelial function, and hematopoiesis are closely interconnected. At this early stage, the inflammatory response primarily involves innate immune cells such as macrophages and neutrophils, as zebrafish develop their adaptive immune system (T and B lymphocytes) in adulthood (303). Absence of adaptive immune responses during embryogenesis allowed us to specifically concentrate on the role of innate immunity without the complexities introduced by adaptive immunity. However, for a comprehensive understanding of disease progression and of its effects beyond embryonic stages, further research should investigate its impact during zebrafish adult life. Establishing a stable complete *cecr1b* knockout line using the CRISPR Cas9 technique holds significant promise, allowing for a more comprehensive exploration of disease evolution. Such a knockout model could shed light on whether deficiencies in inflammation also affect the development and function of T and B lymphocytes, which are impacted in DADA2 patients. These investigations might offer crucial insights into the broader immunological implications of the disease.

We have currently generated stable homozygous mutant lines for the two *cecr1a* and *cecr1b* genes, which are viable and fertile and are currently under characterisation. The utilisation of these mutant lines will allow us to investigate the late-onset aspects of DADA2 disease and to test possible long-term corrective therapies. In addition, it is particularly interesting to reconsider the possible role of Cecr1a, given its high similarity in sequence and structure to the human ADA2 protein, which is entirely comparable to that of Cecr1b. Indeed, a compensatory gene effect between the two paralogues covering any deleterious effects of the absence of *cecr1a* cannot be completely ruled out. By crossing the two double lines and obtaining double mutant embryos it may therefore be possible to verify the occurrence of possibly more severe haematopoietic phenotypes than those observed in the single *cecr1b* mutant. In this way we would have a complete and broad view of the role of the two genes and their involvement in the mechanisms that regulate the development and maintenance of haematopoiesis, immunity and endothelial function, with particular focus on their involvement in the pathogenesis of DADA2.

Generation of the MCPH17 zebrafish model

Autosomal recessive primary microcephaly-17 (MCPH17) is a genetic condition resulting from mutations in the *CITRON* (*CIT)* gene (158–160,162). This congenital neurodevelopmental disorder is marked by a significant reduction in head circumference associated to delayed psychomotor development, intellectual disability, spasticity, reduced muscle tone and dysmorphic features (158–162). The exact mechanism causing MCPH17 remains unclear so far, and consequently available therapies only treat the symptoms (163). In this project we generated a zebrafish model of MCPH17, to support and facilitate studies in murine models by offering an additional platform to analyse easily and rapidly the CIT-associated neurodevelopmental alterations. We developed a zebrafish model with Citron deficiency by the means of a morpholino-mediated knock down approach, characterized the main anatomical, cellular and behavioural alteration paralleling with those of humans and rodent models and tested the efficacy of a novel, innovative treatment.

The human *CIT* gene encodes for two main splicing isoforms, the complete isoform CIT-K, and the shorter CIT-N lacking the kinase domain (163). Due to whole genome duplication of teleost, two orthologs of the *CIT* gene can be identified in zebrafish: *cita* and *citb*. Analyses of sequence identities and of protein domains revealed a higher sequence and structure conservation between the human complete CIT-K isoform and the zebrafish Cita. Indeed, Cita but not Citb bears the kinase domain, which has revealed to be essential for CIT to exert its main function (164,166). The presence or absence of the kinase domain suggests that the two *cita* and *citb* paralogs might have assumed the roles of the two mammalian isoforms CIT-K and CIT-N, respectively. This implies a potential functional specialization where the two genes possibly carry out distinct functions or in the organism's biological processes. There is evidence that, despite CIT-K is ubiquitously expressed, its function is required only in the developing CNS only (164,166). Remarkably, mutant mice with depleted CIT-K and physiological CIT-N levels develop microcephaly and mirror the neurodevelopmental issues typically associated with MCPH17 (164). This suggests a crucial role for CIT-K specifically in normal brain development, implicating its absence as a significant factor contributing to the observed microcephalic phenotype and associated neurological impairments. These considerations led us to identify *cita* as paralogue to the target for modelling MCPH17. We designed and validated a specific morpholino-mediated strategy to

knockdown specifically the expression of *cita.* We next analysed the effects of *cita* knock-down on head size and morphology, neuronal cells composition and motorial alterations, highlighting the potential of our model to recapitulate the main clinical features of patients and the phenotypes found in *Cit-k* deficient mice. Concerning head size, our zebrafish model showed a remarkable decrease in the head size, resembling the microcephalic typical of MCPH17. Notably, this developmental abnormality emerges as early as 24 hpf, suggesting that the causes of this defect lie in very early neurodevelopmental processes. In order to extend the characterisation of our Cita-deficient model beyond the simple morphological alteration of the head, we tested possible behavioural alterations, which may resemble those exhibited by patients and *Cit-k*$^{-/-}$ mouse murine models. Indeed, defective neural development probably underlies the impaired brain function observed in patients carrying mutations in the *CIT* gene and mimicked by *Cit-k* $^{-/-}$ mice exhibiting ataxia and epilepsy (164–166). We verified the presence of similar behavioural alterations in our zebrafish model. We took advantage of the DasioVision system to perform light/dark transition tests, which revealed altered motor behaviour in *cita*-morphants. Cita-deficient embryos showed unaffected response to light/dark stimuli, but they exhibited unstable and uncontrolled movements resembling epileptic seizures (363). It has been reported that *CIT*-associated microcephaly could be the result of a reduction in neuronal cells number in the brain (164,362). To analyse the neuronal cell composition of our *cita*-deficient embryos, we assessed the expression levels of several neuronal markers. Preliminary qPCR findings indicated decreased expression levels of oligodendrocytes (*olig2, mbp*), astrocytes (*gfap*) and microglial (*aifl1, ccr2*) markers, indicative or a reduction of these cell types. These preliminary results support the hypothesis that the CIT-associated defective neurodevelopment may be influenced by the numerical and spatial alteration of neuronal cells. These defects could, in turn, be due to defective or incomplete cytokinesis, given the direct implication of CIT in this process. It is then crucial to consider the potential association between the observed defects and incomplete cytokinesis. Referring to the existing literature (see Introduction, Section 2.2.2), the distinct role of CIT-K in modelling the architecture of the central body prompts us to investigate potential alterations in the cytokinesis process in our model. This could potentially lead to reduced proliferation of neuronal cells, thus contributing to the observed defects. Notably, treatment of the embryos with N-acetylcysteine (NAC) was able to rescue significantly either head size, behavioural alterations, and defects in

neuronal markers of *cita*-deficient embryos. Given the antioxidant potential of NAC, oxidative stress is somehow linked to the role of Citron and to the pathogenesis of MCPH17. In line with this, recent evidence described higher levels of reactive oxygen species ROS have been described in the Cit-k-/- mouse model (176). These points remain to be clarified in order to identify the association between CIT function, oxidative stress and defective cytokinesis.

The creation of a zebrafish model that recapitulates the main phenotypes of MCPH17 brings some notable advantages which can simplify and support studies conducted on mouse models. Zebrafish has become increasingly valuable as a model organism for studying neurodevelopmental disorders due to its practical advantages and its striking resemblance to the human nervous system (see Introduction, Section 3.3.). As MCPH17 is a congenital disorder, it implies the emergence of neurodevelopmental abnormalities during embryonic development. Investigating the processes contributing to MCPH17 abnormal neurodevelopment during the embryonic stages is therefore crucial for the comprehension of MCPH17 pathogenesis. Zebrafish, due to its specific embryonic characteristics, could serve as a potent tool to directly observe and analyse these mechanisms. Moreover, utilizing a zebrafish model enables rapid and extensive high-throughput screenings of potential therapeutic compounds within a live, *in vivo* setting. Furthermore, while a potential future drug therapy for this condition might need to be administered in utero, exploring the impacts of such treatment in a model with external development could still offer valuable insights and benefits.

Generation of the *GENE-X* deficiency zebrafish model

GENE-X is a gene with currently unknown function, which was identified as a possible causative gene in a paediatric patient being treated by our collaborators and exhibiting a complex syndrome. The patient, born to consanguineous parents, displays diverse clinical manifestations including short stature, chronic inflammation, hepatosplenomegaly, lymph nodes exhibiting granulomatous formations with pronounced lymphoproliferation, dyslipidaemia and vascular anomalies accompanied by progressive occlusion of medium-calibre arteries and cerebral ischemia with haemorrhagic events. Following genetic analyses, an unidentified homozygous missense mutation within the functional domain of *GENE-X* was identified. Presently, treatment of the patient relies on anti-inflammatory medications, failing to alleviate the progressively deteriorating vascular alterations. This experimental study aimed to identify the functional role of *gene-X* by employing the zebrafish model and to explore additional therapeutic strategies.

We generated a zebrafish model with loss of function of *gene-X*, utilizing a morpholino-mediated knock-down approach. Following the development and validation of the efficiency of the knock-down strategy, we started the characterisation of the resulting phenotypes. With preliminary analyses we found morphological aspects that can be paralleled to those described in the patient. Indeed, *gene-X* morphants presented reduced size, inflammation, head hemorrages and significative vascular alterations in the sub-intestinal vein plexus (SIVP). The SIVP is the vascular bed responsible for the reabsorption of lipids from the yolk during the first days of development of zebrafish embryos (226,233). The SIVP structure is highly plastic and is continuously remodelled during the first days of embryonic development (233). Therefore, it is directly affected by possible alterations in vascular homeostasis and the interaction between the cytoskeleton of endothelial cells and their extracellular matrix. Notably, GENE-X belongs to the Rho GTPase protein family, which is directly involved in the remodelling of the cytoskeleton. Furthermore, the remodelling processes of SIVP are directly influenced by alterations in physiological lipid levels (234–236). VEGF/R -mediated angiogenetic processes are responsible for regulating the structure and extent of SIVP in response to the demand for increased or decreased lipid reabsorption from the yolk (235). The structural alterations we observed in this vascular district could therefore be attributed either to a defect in regulation of the cytoskeleton, adhesion, migration and

cell polarity of endothelial cells or to an imbalance in lipid levels that the SIVP attempts to rebalance. As mentioned above, *gene-X* encodes for a GTPase activating protein (GAP), which belongs to the Rho GTPase family of regulators, and which is responsible for the inhibition of Rho activity (190). The reduction of *gene-X* expression, as well as the mutation in its functional domain identified in the patient, should lead to a hyperactivation of the Rho-signalling pathway. The direct downstream effectors of Rho GTPases are Rho-associated serine-threonine kinases (ROCKs) (192,193). We therefore decided to test a treatment with Y27632, a selective inhibitor of the ROCK enzyme. As expected, treatments with the inhibitor led to a recovery of the morphological defects of SIVP, demonstrating the specificity of the observed vascular phenotypes and confirming their dependence on an over-activation of the Rho signalling pathway. Furthermore, the recovery of SIPV alterations obtained with ROCK inhibition suggests that pharmacological modulation of the Rho signalling pathway may represent a possible therapeutic strategy for patients, in line with the results of some works that have tested the clinical use of these inhibitors.

Considering the results obtained, we planned to extend the characterisation of the embryo phenotypes for *gene-X* to highlight the presence of any additional clinical phenotypes found in the patient. In particular, we propose to carry out lipidomic analyses to reveal possible alterations in lipidaemia and to test the efficacy of the Y27632 inhibitor in treating inflammation and haemorrhages. Once the characterisation of these aspects has been completed, we propose to utilize our zebrafish model to validate the pathogenicity of the mutation described in the patient through rescue experiments with human and mutated human mRNA. Finally, we aim to investigate in more detail the molecular mechanisms involved in the onset of vascular phenotypes determined by the loss of function of *gene-X*. We will analyse the state of activation of the endothelium by analysing the expression of specific markers such as endoglin (*edn, eng, sele, vcam1*, etc.) and of genes involved in the regulation of the processes of angiogenesis and vascular homeostasis (*vegfr1/vegfr2, vecdn, efnb2, fli1a*) by means of RT-qPCR techniques.

This zebrafish model with loss of function of *gene-x* could be used in the future to study in detail the precise function of *GENE-X* and the pathogenic mechanisms associated with its loss of function. In addition to this, it could be used to verify the pathogenic effects of new *GENE-X* variants found in patients and to test the efficacy of new drug

therapies in a simple, rapid and cost-effective way, accelerating the process of identifying new therapeutic targets.

Generation of the TKOS deficiency zebrafish model

TRIADIN knock out syndrome (TKOS) is a rare cardiac arrhythmogenic disorder exhibiting T-wave inversions, transient long QT, and exercise-induced cardiac arrest (194–196) . The exact mechanisms underlying TKOS remain largely unknown, and conventional antiarrhythmic drugs have shown no efficacy in treating it, making cardioverter defibrillator implantation the only viable approach (194,197), especially given TKOS occurrence in pediatric patients. TRIADIN is a single-pass transmembrane protein derived from the TRDN gene, which is expressed exclusively in skeletal and cardiac muscle tissues (206,389). Its role in maintaining the cardiac ryanodine receptor complex (CRC) and modulating excitation-contraction coupling has been established (196,208,389), yet its precise function remains to be fully characterized.

Zebrafish serves as an established model for studying cardiac physiology and related disorders (246), offering a valuable avenue to explore the repercussions of *trdn* dysregulation. We developed and characterized a zebrafish model for *trdn* loss-of-function. Similar to humans, mice, and other animal models (390,391), *trdn* expression in zebrafish was specifically observed in skeletal muscle and the heart from somitogenesis to 5 dpf. We induced *trdn* knockdown in zebrafish embryos using a cocktail of *trdn* morpholinos (MOs). Patients with TKOS carry mutations often leading to complete loss of cardiac and skeletal muscle TRIADIN (194,197,199,200). Consequently, both an ATG-MO and a splice-MO targeting exon 1-intron 1 splice site were utilized to achieve knockdown of all three zebrafish *trdn* isoforms. Embryos injected with *trdn*-MOs exhibited altered morphology, displaying edema and trunk/tail curvature. Importantly, lethality rates did not significantly differ between controls and *trdn*-MOs-injected embryos, similarly to Trdn-/- mice, which showed no embryonic lethality (202,203). The observed morphant embryo phenotype exhibited variability, with instances of edema and trunk/tail curvature appearing individually or concurrently. Notably, such variability parallels findings in TKOS patients, among whom only six cases to date have reported skeletal myopathy alongside cardiac events (194).

Interestingly, the proportion of trdn-MOs embryos showing trunk/tail curvature (~56%) was notably higher compared to TKOS patients (<30%). Several factors might contribute to this discrepancy. Firstly, the limited number of available clinical records relative to the extensive analysis of zebrafish embryos suggests an incomplete characterization of the TKOS phenotype in humans. Moreover, the considerable variability in the TKOS phenotype might obscure subtler skeletal muscle impairments. Additionally, there's a lack of information about *TRDN* mutations in patients experiencing myopathy without heart function irregularities. Our observation of a few *trdn*-MO-injected embryos displaying trunk/tail defects without cardiac edema suggests a rare possibility that TRDN loss might occasionally impact skeletal muscle without involvement of the heart muscle. Further studies are essential to comprehensively understand the molecular basis behind TKOS phenotype variability. Future whole-genome sequencing analyses in myopathy patients may offer insights into this aspect. To evaluate the potential of our *trdn* knockdown zebrafish as an *in vivo* TKOS model, we analysed both the skeletal muscle and heart phenotypes of *trdn*-MOs embryos. Employing various techniques, we discovered that the general structure of skeletal muscle in *trdn*-MO-injected embryos remains largely unaffected. Similarly, there were no noticeable alterations in heart formation, looping, or chamber organization. These data are in line with those of a previous Trdn-/- mouse model not exhibiting significant anatomical changes in the heart and skeletal muscles but showing irregularities in cardiac function, with a decreased heart rate compared to control mice. Despite the usual expectation of increased heart rate (tachycardia) with TRDN loss, these mice surprisingly display sinus bradycardia, contradicting prior assumptions. There's evidence suggesting that an excess of TRDN could lead to heart rhythm issues in rat cardiac cells. The absence of TRDN function might contribute to a reduced ability for heart contraction, potentially predisposing to heart rhythm disorders. In support to this hypothesis, two TKOS patients suffered from in utero bradycardia (195,199).

To test the specific impact of *trdn*-loss-of-function on heart rate, we introduced the wild-type form of the human cardiac *TRDN* isoform. However, this human *TRDN* mRNA only partially rescued the heartbeat irregularities of *trdn*-loss-of-function embryos. It is worth noting that the amino acid sequence similarity between human and zebrafish *TRDN* was only around 30%, and therefore the human mRNA could only partially compensate for the absence of the zebrafish endogenous protein. Another possibility

is that the dosage of human *TRDN* mRNA might not have been adequate to fully restore the phenotype. Unfortunately, injection of higher doses of the WT *TRDN* mRNA resulted toxic for the embryos. The injection of the mutated cardiac isoform carrying a mutation previously identified in a TKOS patient did not effectively reverse the bradycardia observed in *trdn*-loss-of-function embryos. This particular mutation was likely to affect protein mobility without having any effect on its expression or stability, potentially resulting in a gain-of-function rather than a loss-of-function phenotype. However, further investigations are required to gain a better understanding of this aspect. Even though the *trdn*-MOs embryo displayed a reduced heart rate, the heart remained functional and responsive to stimuli. Treatment with various antiarrhythmic drugs successfully restored the heart rate to a level comparable to that of control embryos. Notably, these embryos also responded to metoprolol, a β-blocker used in treating TKOS patients (194).

In summary, our zebrafish model with *trdn* deficiency represents a valuable tool for exploring the physiological role of Trdn. Zebrafish offers some advantages over mouse TKOS models due to their ease of *in vivo* assessment of heart function. The transparency of zebrafish embryos allows for quick evaluation of heartbeat, enabling cost-effective high-throughput drug screening. Moreover, more detailed analyses such as assessing myocardial wall velocity, blood flow, heartbeat regularity, and fractional area changes (as discussed in (246)) could provide deeper insights into the specific effects of TRDN on heart function. Additionally, employing *trdn* knockdown in zebrafish transgenic lines, like Tg(*vmhc*:eGFP) labelling the ventricle and Tg(*amhc*:eGFP) labelling the atrium, could help distinguish the precise roles of Trdn in different heart regions. Crucially, by introducing specific mRNAs through microinjection, our model offers a valuable platform to validate *TRDN* mutations identified in individuals with TKOS, aiding in confirming the causative nature of these mutations.

References

1. Ericsson AC, Crim MJ, Franklin CL. A brief history of animal modeling. Mo Med [Internet]. 2013;110(3):201–5. Available from: http://www.ncbi.nlm.nih.gov/pubmed/23829102

2. Mukherjee P, Roy S, Ghosh D, Nandi SK. Role of animal models in biomedical research: a review. Lab Anim Res [Internet]. 2022 Dec 1;38(1):18. Available from: https://labanimres.biomedcentral.com/articles/10.1186/s42826-022-00128-1

3. Reza Khorramizadeh M, Saadat F. Animal models for human disease. In: Animal Biotechnology [Internet]. Elsevier; 2020. p. 153–71. Available from: https://linkinghub.elsevier.com/retrieve/pii/B9780128117101000082

4. Singh VK, Seed TM. How necessary are animal models for modern drug discovery? Expert Opin Drug Discov [Internet]. 2021 Dec 2;16(12):1391–7. Available from: https://www.tandfonline.com/doi/full/10.1080/17460441.2021.1972255

5. Szabo M, Svensson Akusjärvi S, Saxena A, Liu J, Chandrasekar Janebjer G, Kitambi SS. Cell and small animal models for phenotypic drug discovery. Drug Des Devel Ther [Internet]. 2017 Jun;Volume 11:1957–67. Available from: https://www.dovepress.com/cell-and-small-animal-models-for-phenotypic-drug-discovery-peer-reviewed-article-DDDT

6. Chan ET, Quon GT, Chua G, Babak T, Trochesset M, Zirngibl RA, et al. Conservation of core gene expression in vertebrate tissues. J Biol [Internet]. 2009;8(3):33. Available from: http://jbiol.biomedcentral.com/articles/10.1186/jbiol130

7. Alföldi J, Lindblad-Toh K. Comparative genomics as a tool to understand evolution and disease. Genome Res [Internet]. 2013 Jul 1;23(7):1063–8. Available from: http://genome.cshlp.org/lookup/doi/10.1101/gr.157503.113

8. Hickman DL, Johnson J, Vemulapalli TH, Crisler JR, Shepherd R. Commonly Used Animal Models. In: Principles of Animal Research [Internet]. Elsevier; 2017. p. 117–75. Available from: https://linkinghub.elsevier.com/retrieve/pii/B9780128021514000074

9. Davidson MK, Lindsey JR, Davis JK. Requirements and selection of an animal model. Isr J Med Sci [Internet]. 1987 Jun;23(6):551–5. Available from: http://www.ncbi.nlm.nih.gov/pubmed/3312096

10. Dodds WJ, Abelseth MK. Criteria for selecting the animal to meet the research need. Lab Anim Sci [Internet]. 1980 Apr;30(2 Pt 2):460–5. Available from: http://www.ncbi.nlm.nih.gov/pubmed/6221157

11. Patton EE, Tobin DM. Spotlight on zebrafish: the next wave of translational research. Dis Model Mech [Internet]. 2019 Mar 1;12(3). Available from: https://journals.biologists.com/dmm/article/12/3/dmm039370/19928/Spotlight-on-zebrafish-the-next-wave-of

12. Adhish M, Manjubala I. Effectiveness of zebrafish models in understanding human diseases—A review of models. Heliyon [Internet]. 2023 Mar;9(3):e14557. Available from: https://linkinghub.elsevier.com/retrieve/pii/S2405844023017644

13. Santoriello C, Zon LI. Hooked! Modeling human disease in zebrafish. J Clin Invest [Internet]. 2012 Jul 2;122(7):2337–43. Available from: http://www.jci.org/articles/view/60434

14. Choi T-Y, Choi T-I, Lee Y-R, Choe S-K, Kim C-H. Zebrafish as an animal model for biomedical research. Exp Mol Med [Internet]. 2021 Mar 1;53(3):310–7. Available from: https://www.nature.com/articles/s12276-021-00571-5

15. Howe K, Clark MD, Torroja CF, Torrance J, Berthelot C, Muffato M, et al. The zebrafish reference genome sequence and its relationship to the human genome. Nature [Internet]. 2013 Apr 25;496(7446):498–503. Available from: https://www.nature.com/articles/nature12111

16. Kettleborough RNW, Busch-Nentwich EM, Harvey SA, Dooley CM, de Bruijn E, van Eeden F, et al. A systematic genome-wide analysis of zebrafish protein-coding gene function. Nature [Internet]. 2013 Apr 17;496(7446):494–7. Available from: https://www.nature.com/articles/nature11992

17. Deo RC, MacRae CA. The zebrafish:scalable in vivo modeling for systems biology. WIREs Syst Biol Med [Internet]. 2011 May 29;3(3):335–46. Available from: https://wires.onlinelibrary.wiley.com/doi/10.1002/wsbm.117

18. Fuentes R, Letelier J, Tajer B, Valdivia LE, Mullins MC. Fishing forward and reverse: Advances in zebrafish phenomics. Mech Dev [Internet]. 2018 Dec;154:296–308. Available from: https://linkinghub.elsevier.com/retrieve/pii/S0925477318300765

19. Mushtaq MY, Verpoorte R, Kim HK. Zebrafish as a model for systems biology. Biotechnol Genet Eng Rev [Internet]. 2013 Oct;29(2):187–205. Available from: http://www.tandfonline.com/doi/abs/10.1080/02648725.2013.801238

20. Rafferty SA, Quinn TA. A beginner's guide to understanding and implementing the genetic modification of zebrafish. Prog Biophys Mol Biol [Internet]. 2018 Oct;138:3–19. Available from: https://linkinghub.elsevier.com/retrieve/pii/S007961071830124X

21. AMSTERDAM A, HOPKINS N. Mutagenesis strategies in zebrafish for identifying genes involved in development and disease. Trends Genet [Internet]. 2006 Sep;22(9):473–8. Available from: https://linkinghub.elsevier.com/retrieve/pii/S0168952506002125

22. Kardash E. Current Methods in Zebrafish Research. Mater Methods [Internet]. 2012 Jan 1;2. Available from: http://www.labome.com/method/Current-Methods-in-Zebrafish-Research.html

23. Li Y, Jia Z, Zhang S, He X. Progress in Gene-Editing Technology of Zebrafish. Biomolecules [Internet]. 2021 Sep 1;11(9):1300. Available from: https://www.mdpi.com/2218-273X/11/9/1300

24. Hogan BM, Verkade H, Lieschke GJ, Heath JK. Manipulation of Gene Expression During Zebrafish Embryonic Development Using Transient Approaches. In 2008. p. 273–300. Available from: http://link.springer.com/10.1007/978-1-60327-469-2_19

25. Strähle U, Scholz S, Geisler R, Greiner P, Hollert H, Rastegar S, et al. Zebrafish embryos as an alternative to animal experiments—A commentary on the definition of the onset of protected life stages in animal welfare regulations. Reprod Toxicol [Internet]. 2012 Apr;33(2):128–32. Available from: https://linkinghub.elsevier.com/retrieve/pii/S0890623811002942

26. Kimmel CB, Ballard WW, Kimmel SR, Ullmann B, Schilling TF. Stages of embryonic development of the zebrafish. Dev Dyn [Internet]. 1995 Jul 3;203(3):253–310. Available from: https://anatomypubs.onlinelibrary.wiley.com/doi/10.1002/aja.1002030302

27. Lee CE, Singleton KS, Wallin M, Faundez V. Rare Genetic Diseases: Nature's Experiments on Human Development. iScience [Internet]. 2020 May;23(5):101123. Available from: https://linkinghub.elsevier.com/retrieve/pii/S2589004220303084

28. Udvadia AJ, Linney E. Windows into development: historic, current, and future perspectives on transgenic zebrafish. Dev Biol [Internet]. 2003 Apr;256(1):1–17. Available from: https://linkinghub.elsevier.com/retrieve/pii/S0012160602000830

29. Patton EE, Zon LI, Langenau DM. Zebrafish disease models in drug discovery: from preclinical modelling to clinical trials. Nat Rev Drug Discov [Internet]. 2021 Aug 11;20(8):611–28. Available from: https://www.nature.com/articles/s41573-021-00210-8

30. Dash SN, Patnaik L. Flight for fish in drug discovery: a review of zebrafish-based screening of molecules. Biol Lett [Internet]. 2023 Aug 2;19(8). Available from: https://royalsocietypublishing.org/doi/10.1098/rsbl.2022.0541

31. No Title.

32. Jackstadt MM, Chamberlain CA, Doonan SR, Shriver LP, Patti GJ. A multidimensional metabolomics workflow to image biodistribution and evaluate pharmacodynamics in adult zebrafish. Dis Model Mech [Internet]. 2022 Aug 1;15(8). Available from: https://journals.biologists.com/dmm/article/15/8/dmm049550/276339/A-multidimensional-metabolomics-workflow-to-image

33. Behjati S, Tarpey PS. What is next generation sequencing? Arch Dis Child - Educ Pract Ed [Internet]. 2013 Dec;98(6):236–8. Available from: https://ep.bmj.com/lookup/doi/10.1136/archdischild-2013-304340

34. Hu T, Chitnis N, Monos D, Dinh A. Next-generation sequencing technologies: An overview. Hum Immunol [Internet]. 2021 Nov;82(11):801–11. Available from: https://linkinghub.elsevier.com/retrieve/pii/S0198885921000628

35. Werner T. Next generation sequencing in functional genomics. Brief Bioinform [Internet]. 2010 Sep 1;11(5):499–511. Available from:

https://academic.oup.com/bib/article-lookup/doi/10.1093/bib/bbq018

36. Harrison RJ. Understanding genetic variation and function- the applications of next generation sequencing. Semin Cell Dev Biol [Internet]. 2012 Apr;23(2):230–6. Available from: https://linkinghub.elsevier.com/retrieve/pii/S1084952112000109

37. Driever W, Solnica-Krezel L, Schier AF, Neuhauss SCF, Malicki J, Stemple DL, et al. A genetic screen for mutations affecting embryogenesis in zebrafish. Development [Internet]. 1996 Dec 1;123(1):37–46. Available from: https://journals.biologists.com/dev/article/123/1/37/39342/A-genetic-screen-for-mutations-affecting

38. Haffter P, Granato M, Brand M, Mullins MC, Hammerschmidt M, Kane DA, et al. The identification of genes with unique and essential functions in the development of the zebrafish, Danio rerio. Development [Internet]. 1996 Dec 1;123(1):1–36. Available from: https://journals.biologists.com/dev/article/123/1/1/39317/The-identification-of-genes-with-unique-and

39. Ingham PW. The power of the zebrafish for disease analysis. Hum Mol Genet [Internet]. 2009 Apr 15;18(R1):R107–12. Available from: https://academic.oup.com/hmg/article-lookup/doi/10.1093/hmg/ddp091

40. Lawson ND, Wolfe SA. Forward and Reverse Genetic Approaches for the Analysis of Vertebrate Development in the Zebrafish. Dev Cell [Internet]. 2011 Jul;21(1):48–64. Available from: https://linkinghub.elsevier.com/retrieve/pii/S1534580711002413

41. Knapik EW. ENU mutagenesis in zebrafish—from genes to complex diseases. Mamm Genome [Internet]. 2000 Jul 25;11(7):511–9. Available from: http://link.springer.com/10.1007/s003350010098

42. de Bruijn E, Cuppen E, Feitsma H. Highly Efficient ENU Mutagenesis in Zebrafish. In 2009. p. 3–12. Available from: http://link.springer.com/10.1007/978-1-60327-977-2_1

43. Gaiano N, Amsterdam A, Kawakami K, Allende M, Becker T, Hopkins N. Insertional mutagenesis and rapid cloning of essential genes in zebrafish. Nature [Internet]. 1996 Oct;383(6603):829–32. Available from: https://www.nature.com/articles/383829a0

44. Nagayoshi S, Hayashi E, Abe G, Osato N, Asakawa K, Urasaki A, et al. Insertional mutagenesis by the Tol2 transposon-mediated enhancer trap approach generated mutations in two developmental genes: tcf7 and synembryn-like. Development [Internet]. 2008 Jan 1;135(1):159–69. Available from: https://journals.biologists.com/dev/article/135/1/159/64730/Insertional-mutagenesis-by-the-Tol2-transposon

45. Blum M, De Robertis EM, Wallingford JB, Niehrs C. Morpholinos: Antisense and Sensibility. Dev Cell [Internet]. 2015 Oct;35(2):145–9. Available from: https://linkinghub.elsevier.com/retrieve/pii/S1534580715006188

46. Nasevicius A, Ekker SC. Effective targeted gene ‘knockdown’ in zebrafish. Nat

Genet [Internet]. 2000 Oct;26(2):216–20. Available from: https://www.nature.com/articles/ng1000_216

47. Summerton J. Morpholino antisense oligomers: the case for an RNase H-independent structural type. Biochim Biophys Acta - Gene Struct Expr [Internet]. 1999 Dec;1489(1):141–58. Available from: https://linkinghub.elsevier.com/retrieve/pii/S0167478199001505

48. Karkare S, Bhatnagar D. Promising nucleic acid analogs and mimics: characteristic features and applications of PNA, LNA, and morpholino. Appl Microbiol Biotechnol [Internet]. 2006 Aug 9;71(5):575–86. Available from: http://link.springer.com/10.1007/s00253-006-0434-2

49. SUMMERTON J, WELLER D. Morpholino Antisense Oligomers: Design, Preparation, and Properties. Antisense Nucleic Acid Drug Dev [Internet]. 1997 Jun;7(3):187–95. Available from: http://www.liebertpub.com/doi/10.1089/oli.1.1997.7.187

50. Bill BR, Petzold AM, Clark KJ, Schimmenti LA, Ekker SC. A Primer for Morpholino Use in Zebrafish. Zebrafish [Internet]. 2009 Mar;6(1):69–77. Available from: http://www.liebertpub.com/doi/10.1089/zeb.2008.0555

51. Eisen JS, Smith JC. Controlling morpholino experiments: don't stop making antisense. Development [Internet]. 2008 May 15;135(10):1735–43. Available from: https://journals.biologists.com/dev/article/135/10/1735/64661/Controlling-morpholino-experiments-don-t-stop

52. Draper BW, Morcos PA, Kimmel CB. Inhibition of zebrafish fgf8 pre-mRNA splicing with morpholino oligos: A quantifiable method for gene knockdown. genesis [Internet]. 2001 Jul 23;30(3):154–6. Available from: https://onlinelibrary.wiley.com/doi/10.1002/gene.1053

53. Morcos PA. Achieving targeted and quantifiable alteration of mRNA splicing with Morpholino oligos. Biochem Biophys Res Commun [Internet]. 2007 Jun;358(2):521–7. Available from: https://linkinghub.elsevier.com/retrieve/pii/S0006291X07008935

54. Moulton JD. Making a Morpholino Experiment Work: Controls, Favoring Specificity, Improving Efficacy, Storage, and Dose. In 2017. p. 17–29. Available from: http://link.springer.com/10.1007/978-1-4939-6817-6_2

55. STEIN D, FOSTER E, HUANG S-B, WELLER D, SUMMERTON J. A Specificity Comparison of Four Antisense Types: Morpholino, 2′-O-Methyl RNA, DNA, and Phosphorothioate DNA. Antisense Nucleic Acid Drug Dev [Internet]. 1997 Jun;7(3):151–7. Available from: http://www.liebertpub.com/doi/10.1089/oli.1.1997.7.151

56. Moulton JD, Yan Y. Using Morpholinos to Control Gene Expression. Curr Protoc Mol Biol [Internet]. 2008 Jul;83(1). Available from: https://currentprotocols.onlinelibrary.wiley.com/doi/10.1002/0471142727.mb2608s83

57. Norris A, Streit A. Morpholinos: Studying gene function in the chick. Methods [Internet]. 2014 Apr;66(3):454–65. Available from:

https://linkinghub.elsevier.com/retrieve/pii/S1046202313004052

58. Stainier DYR, Kontarakis Z, Rossi A. Making Sense of Anti-Sense Data. Dev Cell [Internet]. 2015 Jan;32(1):7–8. Available from: https://linkinghub.elsevier.com/retrieve/pii/S1534580714008338

59. Bedell VM, Westcot SE, Ekker SC. Lessons from morpholino-based screening in zebrafish. Brief Funct Genomics [Internet]. 2011 Jul 1;10(4):181–8. Available from: https://academic.oup.com/bfg/article-lookup/doi/10.1093/bfgp/elr021

60. Stainier DYR, Raz E, Lawson ND, Ekker SC, Burdine RD, Eisen JS, et al. Guidelines for morpholino use in zebrafish. Barsh GS, editor. PLOS Genet [Internet]. 2017 Oct 19;13(10):e1007000. Available from: https://dx.plos.org/10.1371/journal.pgen.1007000

61. Ouyang X, Shestopalov IA, Sinha S, Zheng G, Pitt CLW, Li W-H, et al. Versatile Synthesis and Rational Design of Caged Morpholinos. J Am Chem Soc [Internet]. 2009 Sep 23;131(37):13255–69. Available from: https://pubs.acs.org/doi/10.1021/ja809933h

62. Yamazoe S, Shestopalov IA, Provost E, Leach SD, Chen JK. Cyclic Caged Morpholinos: Conformationally Gated Probes of Embryonic Gene Function. Angew Chemie Int Ed [Internet]. 2012 Jul 9;51(28):6908–11. Available from: https://onlinelibrary.wiley.com/doi/10.1002/anie.201201690

63. Shestopalov IA, Sinha S, Chen JK. Light-controlled gene silencing in zebrafish embryos. Nat Chem Biol [Internet]. 2007 Oct 23;3(10):650–1. Available from: https://www.nature.com/articles/nchembio.2007.30

64. Moulton J, Jiang S. Gene Knockdowns in Adult Animals: PPMOs and Vivo-Morpholinos. Molecules [Internet]. 2009 Mar 25;14(3):1304–23. Available from: http://www.mdpi.com/1420-3049/14/3/1304

65. Morcos PA, Li Y, Jiang S. Vivo-Morpholinos: A non-peptide transporter delivers Morpholinos into a wide array of mouse tissues. Biotechniques [Internet]. 2008 Dec;45(6):613–23. Available from: https://www.future-science.com/doi/10.2144/000113005

66. Al Qaryoute A, Fallatah W, Dhinoja S, Raman R, Jagadeeswaran P. Role of microRNAs and their downstream target transcription factors in zebrafish thrombopoiesis. Sci Rep [Internet]. 2023 Sep 26;13(1):16066. Available from: https://www.nature.com/articles/s41598-023-42868-7

67. Sundaramoorthi H, Fallatah W, Mary J, Jagadeeswaran P. Discovery of seven hox genes in zebrafish thrombopoiesis. Blood Cells, Mol Dis [Internet]. 2024 Jan;104:102796. Available from: https://linkinghub.elsevier.com/retrieve/pii/S1079979623000736

68. Davis EE, Frangakis S, Katsanis N. Interpreting human genetic variation with in vivo zebrafish assays. Biochim Biophys Acta - Mol Basis Dis [Internet]. 2014 Oct;1842(10):1960–70. Available from: https://linkinghub.elsevier.com/retrieve/pii/S0925443914001525

69. Niederriter AR, Davis EE, Golzio C, Oh EC, Tsai I-C, Katsanis N. In Vivo

Modeling of the Morbid Human Genome using Danio rerio. J Vis Exp [Internet]. 2013 Aug 24;(78). Available from: https://www.jove.com/t/50338/in-vivo-modeling-of-the-morbid-human-genome-using-danio-rerio

70. Koster R, Sassen WA. A molecular toolbox for genetic manipulation of zebrafish. Adv Genomics Genet [Internet]. 2015 Mar;151. Available from: http://www.dovepress.com/a-molecular-toolbox-for-genetic-manipulation-of-zebrafish-peer-reviewed-article-AGG

71. Ota S, Kawahara A. Zebrafish: A model vertebrate suitable for the analysis of human genetic disorders. Congenit Anom (Kyoto) [Internet]. 2014 Feb 25;54(1):8–11. Available from: https://onlinelibrary.wiley.com/doi/10.1111/cga.12040

72. Gaj T, Gersbach CA, Barbas CF. ZFN, TALEN, and CRISPR/Cas-based methods for genome engineering. Trends Biotechnol [Internet]. 2013 Jul;31(7):397–405. Available from: https://linkinghub.elsevier.com/retrieve/pii/S0167779913000875

73. Meng X, Noyes MB, Zhu LJ, Lawson ND, Wolfe SA. Targeted gene inactivation in zebrafish using engineered zinc-finger nucleases. Nat Biotechnol [Internet]. 2008 Jun 25;26(6):695–701. Available from: https://www.nature.com/articles/nbt1398

74. Hisano Y, Ota S, Kawahara A. Genome editing using artificial site-specific nucleases in zebrafish. Dev Growth Differ [Internet]. 2014 Jan 14;56(1):26–33. Available from: https://onlinelibrary.wiley.com/doi/10.1111/dgd.12094

75. Auer TO, Del Bene F. CRISPR/Cas9 and TALEN-mediated knock-in approaches in zebrafish. Methods [Internet]. 2014 Sep;69(2):142–50. Available from: https://linkinghub.elsevier.com/retrieve/pii/S1046202314001297

76. Blackburn PR, Campbell JM, Clark KJ, Ekker SC. The CRISPR System—Keeping Zebrafish Gene Targeting Fresh. Zebrafish [Internet]. 2013 Mar;10(1):116–8. Available from: http://www.liebertpub.com/doi/10.1089/zeb.2013.9999

77. Mino T, Aoyama Y, Sera T. Efficient double-stranded DNA cleavage by artificial zinc-finger nucleases composed of one zinc-finger protein and a single-chain FokI dimer. J Biotechnol [Internet]. 2009 Mar;140(3–4):156–61. Available from: https://linkinghub.elsevier.com/retrieve/pii/S0168165609000480

78. Guo J, Gaj T, Barbas CF. Directed Evolution of an Enhanced and Highly Efficient FokI Cleavage Domain for Zinc Finger Nucleases. J Mol Biol [Internet]. 2010 Jul;400(1):96–107. Available from: https://linkinghub.elsevier.com/retrieve/pii/S0022283610004481

79. Zhu C, Smith T, McNulty J, Rayla AL, Lakshmanan A, Siekmann AF, et al. Evaluation and application of modularly assembled zinc-finger nucleases in zebrafish. Development [Internet]. 2011 Oct 15;138(20):4555–64. Available from: https://journals.biologists.com/dev/article/138/20/4555/44711/Evaluation-and-application-of-modularly-assembled

80. Miller JC, Tan S, Qiao G, Barlow KA, Wang J, Xia DF, et al. A TALE nuclease

architecture for efficient genome editing. Nat Biotechnol [Internet]. 2011 Feb 22;29(2):143–8. Available from: https://www.nature.com/articles/nbt.1755

81. Zhang F, Cong L, Lodato S, Kosuri S, Church GM, Arlotta P. Efficient construction of sequence-specific TAL effectors for modulating mammalian transcription. Nat Biotechnol [Internet]. 2011 Feb 19;29(2):149–53. Available from: https://www.nature.com/articles/nbt.1775

82. Mussolino C, Morbitzer R, Lütge F, Dannemann N, Lahaye T, Cathomen T. A novel TALE nuclease scaffold enables high genome editing activity in combination with low toxicity. Nucleic Acids Res [Internet]. 2011 Nov;39(21):9283–93. Available from: https://academic.oup.com/nar/article-lookup/doi/10.1093/nar/gkr597

83. Sander JD, Yeh J-RJ, Peterson RT, Joung JK. Engineering Zinc Finger Nucleases for Targeted Mutagenesis of Zebrafish. In 2011. p. 51–8. Available from: https://linkinghub.elsevier.com/retrieve/pii/B9780123748140000033

84. Mani M, Kandavelou K, Dy FJ, Durai S, Chandrasegaran S. Design, engineering, and characterization of zinc finger nucleases. Biochem Biophys Res Commun [Internet]. 2005 Sep;335(2):447–57. Available from: https://linkinghub.elsevier.com/retrieve/pii/S0006291X05015652

85. Dahlem TJ, Hoshijima K, Jurynec MJ, Gunther D, Starker CG, Locke AS, et al. Simple Methods for Generating and Detecting Locus-Specific Mutations Induced with TALENs in the Zebrafish Genome. Mullins MC, editor. PLoS Genet [Internet]. 2012 Aug 16;8(8):e1002861. Available from: https://dx.plos.org/10.1371/journal.pgen.1002861

86. Juillerat A, Dubois G, Valton J, Thomas S, Stella S, Maréchal A, et al. Comprehensive analysis of the specificity of transcription activator-like effector nucleases. Nucleic Acids Res [Internet]. 2014 Apr;42(8):5390–402. Available from: https://academic.oup.com/nar/article-lookup/doi/10.1093/nar/gku155

87. Wood AJ, Lo T-W, Zeitler B, Pickle CS, Ralston EJ, Lee AH, et al. Targeted Genome Editing Across Species Using ZFNs and TALENs. Science (80-) [Internet]. 2011 Jul 15;333(6040):307–307. Available from: https://www.science.org/doi/10.1126/science.1207773

88. Doyon Y, Vo TD, Mendel MC, Greenberg SG, Wang J, Xia DF, et al. Enhancing zinc-finger-nuclease activity with improved obligate heterodimeric architectures. Nat Methods [Internet]. 2011 Jan 5;8(1):74–9. Available from: https://www.nature.com/articles/nmeth.1539

89. Matsumoto D, Tamamura H, Nomura W. TALEN-Based Chemically Inducible, Dimerization-Dependent, Sequence-Specific Nucleases. Biochemistry [Internet]. 2020 Jan 21;59(2):197–204. Available from: https://pubs.acs.org/doi/10.1021/acs.biochem.9b00798

90. Gupta RM, Musunuru K. Expanding the genetic editing tool kit: ZFNs, TALENs, and CRISPR-Cas9. J Clin Invest [Internet]. 2014 Oct 1;124(10):4154–61. Available from: http://www.jci.org/articles/view/72992

91. Boettcher M, McManus MT. Choosing the Right Tool for the Job: RNAi,

TALEN, or CRISPR. Mol Cell [Internet]. 2015 May;58(4):575–85. Available from: https://linkinghub.elsevier.com/retrieve/pii/S109727651500310X

92. Marraffini LA, Sontheimer EJ. CRISPR interference: RNA-directed adaptive immunity in bacteria and archaea. Nat Rev Genet [Internet]. 2010 Mar 2;11(3):181–90. Available from: https://www.nature.com/articles/nrg2749

93. Barrangou R, Fremaux C, Deveau H, Richards M, Boyaval P, Moineau S, et al. CRISPR Provides Acquired Resistance Against Viruses in Prokaryotes. Science (80-) [Internet]. 2007 Mar 23;315(5819):1709–12. Available from: https://www.science.org/doi/10.1126/science.1138140

94. Horvath P, Barrangou R. CRISPR/Cas, the Immune System of Bacteria and Archaea. Science (80-) [Internet]. 2010 Jan 8;327(5962):167–70. Available from: https://www.science.org/doi/10.1126/science.1179555

95. Karginov F V., Hannon GJ. The CRISPR System: Small RNA-Guided Defense in Bacteria and Archaea. Mol Cell [Internet]. 2010 Jan;37(1):7–19. Available from: https://linkinghub.elsevier.com/retrieve/pii/S109727650900968X

96. Haft DH, Selengut J, Mongodin EF, Nelson KE. A Guild of 45 CRISPR-Associated (Cas) Protein Families and Multiple CRISPR/Cas Subtypes Exist in Prokaryotic Genomes. Eisen JA, editor. PLoS Comput Biol [Internet]. 2005 Nov 11;1(6):e60. Available from: https://dx.plos.org/10.1371/journal.pcbi.0010060

97. Makarova KS, Aravind L, Wolf YI, Koonin E V. Unification of Cas protein families and a simple scenario for the origin and evolution of CRISPR-Cas systems. Biol Direct [Internet]. 2011 Dec 14;6(1):38. Available from: https://biologydirect.biomedcentral.com/articles/10.1186/1745-6150-6-38

98. Gupta D, Bhattacharjee O, Mandal D, Sen MK, Dey D, Dasgupta A, et al. CRISPR-Cas9 system: A new-fangled dawn in gene editing. Life Sci [Internet]. 2019 Sep;232:116636. Available from: https://linkinghub.elsevier.com/retrieve/pii/S0024320519305624

99. Brouns SJJ, Jore MM, Lundgren M, Westra ER, Slijkhuis RJH, Snijders APL, et al. Small CRISPR RNAs Guide Antiviral Defense in Prokaryotes. Science (80-) [Internet]. 2008 Aug 15;321(5891):960–4. Available from: https://www.science.org/doi/10.1126/science.1159689

100. Wang H, La Russa M, Qi LS. CRISPR/Cas9 in Genome Editing and Beyond. Annu Rev Biochem [Internet]. 2016 Jun 2;85(1):227–64. Available from: https://www.annualreviews.org/doi/10.1146/annurev-biochem-060815-014607

101. Jinek M, Chylinski K, Fonfara I, Hauer M, Doudna JA, Charpentier E. A Programmable Dual-RNA–Guided DNA Endonuclease in Adaptive Bacterial Immunity. Science (80-) [Internet]. 2012 Aug 17;337(6096):816–21. Available from: https://www.science.org/doi/10.1126/science.1225829

102. Hryhorowicz M, Lipiński D, Zeyland J, Słomski R. CRISPR/Cas9 Immune System as a Tool for Genome Engineering. Arch Immunol Ther Exp (Warsz) [Internet]. 2017 Jun 3;65(3):233–40. Available from: http://link.springer.com/10.1007/s00005-016-0427-5

103. Manghwar H, Lindsey K, Zhang X, Jin S. CRISPR/Cas System: Recent Advances and Future Prospects for Genome Editing. Trends Plant Sci [Internet]. 2019 Dec;24(12):1102–25. Available from: https://linkinghub.elsevier.com/retrieve/pii/S1360138519302432

104. Xue C, Greene EC. DNA Repair Pathway Choices in CRISPR-Cas9-Mediated Genome Editing. Trends Genet [Internet]. 2021 Jul;37(7):639–56. Available from: https://linkinghub.elsevier.com/retrieve/pii/S0168952521000536

105. Ran FA, Hsu PD, Wright J, Agarwala V, Scott DA, Zhang F. Genome engineering using the CRISPR-Cas9 system. Nat Protoc [Internet]. 2013 Nov 24;8(11):2281–308. Available from: https://www.nature.com/articles/nprot.2013.143

106. Chang HHY, Pannunzio NR, Adachi N, Lieber MR. Non-homologous DNA end joining and alternative pathways to double-strand break repair. Nat Rev Mol Cell Biol [Internet]. 2017 Aug 17;18(8):495–506. Available from: https://www.nature.com/articles/nrm.2017.48

107. San Filippo J, Sung P, Klein H. Mechanism of Eukaryotic Homologous Recombination. Annu Rev Biochem [Internet]. 2008 Jun 1;77(1):229–57. Available from: https://www.annualreviews.org/doi/10.1146/annurev.biochem.77.061306.125255

108. Auer TO, Duroure K, De Cian A, Concordet J-P, Del Bene F. Highly efficient CRISPR/Cas9-mediated knock-in in zebrafish by homology-independent DNA repair. Genome Res [Internet]. 2014 Jan;24(1):142–53. Available from: http://genome.cshlp.org/lookup/doi/10.1101/gr.161638.113

109. Albadri S, Del Bene F, Revenu C. Genome editing using CRISPR/Cas9-based knock-in approaches in zebrafish. Methods [Internet]. 2017 May;121–122:77–85. Available from: https://linkinghub.elsevier.com/retrieve/pii/S1046202316302833

110. Chen X, Xu F, Zhu C, Ji J, Zhou X, Feng X, et al. Dual sgRNA-directed gene knockout using CRISPR/Cas9 technology in Caenorhabditis elegans. Sci Rep [Internet]. 2014 Dec 22;4(1):7581. Available from: https://www.nature.com/articles/srep07581

111. Khan FJ, Yuen G, Luo J. Multiplexed CRISPR/Cas9 gene knockout with simple crRNA:tracrRNA co-transfection. Cell Biosci [Internet]. 2019 Dec 20;9(1):41. Available from: https://cellandbioscience.biomedcentral.com/articles/10.1186/s13578-019-0304-0

112. Gagnon JA, Valen E, Thyme SB, Huang P, Ahkmetova L, Pauli A, et al. Efficient Mutagenesis by Cas9 Protein-Mediated Oligonucleotide Insertion and Large-Scale Assessment of Single-Guide RNAs. Riley B, editor. PLoS One [Internet]. 2014 May 29;9(5):e98186. Available from: https://dx.plos.org/10.1371/journal.pone.0098186

113. Li M, Zhao L, Page-McCaw PS, Chen W. Zebrafish Genome Engineering Using the CRISPR–Cas9 System. Trends Genet [Internet]. 2016

Dec;32(12):815–27. Available from: https://linkinghub.elsevier.com/retrieve/pii/S0168952516301378

114. Postlethwait JH, Yan Y-L, Gates MA, Horne S, Amores A, Brownlie A, et al. Vertebrate genome evolution and the zebrafish gene map. Nat Genet [Internet]. 1998 Apr 1;18(4):345–9. Available from: https://www.nature.com/articles/ng0498-345

115. Vogan K. Zebrafish mutants versus morphants. Nat Genet [Internet]. 2015 Feb 28;47(2):105–105. Available from: https://www.nature.com/articles/ng.3208

116. Lawson ND. Reverse Genetics in Zebrafish: Mutants, Morphants, and Moving Forward. Trends Cell Biol [Internet]. 2016 Feb;26(2):77–9. Available from: https://linkinghub.elsevier.com/retrieve/pii/S0962892415002366

117. Kontarakis Z, Stainier DYR. Genetics in Light of Transcriptional Adaptation. Trends Genet [Internet]. 2020 Dec;36(12):926–35. Available from: https://linkinghub.elsevier.com/retrieve/pii/S0168952520302080

118. El-Brolosy MA, Stainier DYR. Genetic compensation: A phenomenon in search of mechanisms. Moens C, editor. PLOS Genet [Internet]. 2017 Jul 13;13(7):e1006780. Available from: https://dx.plos.org/10.1371/journal.pgen.1006780

119. Sztal TE, Stainier DYR. Transcriptional adaptation: a mechanism underlying genetic robustness. Development [Internet]. 2020 Aug 1;147(15). Available from: https://journals.biologists.com/dev/article/147/15/dev186452/143912/Transcriptional-adaptation-a-mechanism-underlying

120. El-Brolosy MA, Kontarakis Z, Rossi A, Kuenne C, Günther S, Fukuda N, et al. Genetic compensation triggered by mutant mRNA degradation. Nature [Internet]. 2019 Apr 3;568(7751):193–7. Available from: https://www.nature.com/articles/s41586-019-1064-z

121. Lykke-Andersen S, Jensen TH. Nonsense-mediated mRNA decay: an intricate machinery that shapes transcriptomes. Nat Rev Mol Cell Biol [Internet]. 2015 Nov;16(11):665–77. Available from: http://www.ncbi.nlm.nih.gov/pubmed/26397022

122. Akimitsu N. Messenger RNA surveillance systems monitoring proper translation termination. J Biochem [Internet]. 2008 Jan;143(1):1–8. Available from: http://www.ncbi.nlm.nih.gov/pubmed/17981821

123. Harigaya Y, Parker R. No-go decay: a quality control mechanism for RNA in translation. Wiley Interdiscip Rev RNA [Internet]. 2010;1(1):132–41. Available from: http://www.ncbi.nlm.nih.gov/pubmed/21956910

124. Kumari P, Sturgeon M, Bonde G, Cornell RA. Generating Zebrafish RNA-Less Mutant Alleles by Deleting Gene Promoters with CRISPR/Cas9. In 2022. p. 91–106. Available from: https://link.springer.com/10.1007/978-1-0716-1847-9_8

125. Tromp A, Robinson K, Hall TE, Mowry B, Giacomotto J. Pipeline for generating stable large genomic deletions in zebrafish, from small domains to whole gene

excisions. Yáñez J, editor. G3 Genes|Genomes|Genetics [Internet]. 2021 Dec 8;11(12). Available from: https://academic.oup.com/g3journal/article/doi/10.1093/g3journal/jkab321/6367779

126. van Eeden FJM, Granato M, Odenthal J, Haffter P. Chapter 2 Developmental Mutant Screens in the Zebrafish. In 1998. p. 21–41. Available from: https://linkinghub.elsevier.com/retrieve/pii/S0091679X08618920

127. Patton EE, Zon LI. The art and design of genetic screens: zebrafish. Nat Rev Genet [Internet]. 2001 Dec;2(12):956–66. Available from: https://www.nature.com/articles/35103567

128. Abrams EW, Mullins MC. Early zebrafish development: It's in the maternal genes. Curr Opin Genet Dev [Internet]. 2009 Aug;19(4):396–403. Available from: https://linkinghub.elsevier.com/retrieve/pii/S0959437X09001142

129. Shi D-L. Circumventing Zygotic Lethality to Generate Maternal Mutants in Zebrafish. Biology (Basel) [Internet]. 2022 Jan 10;11(1):102. Available from: https://www.mdpi.com/2079-7737/11/1/102

130. Morcos PA, Vincent AC, Moulton JD. Gene Editing Versus Morphants. Zebrafish [Internet]. 2015 Oct;12(5):319–319. Available from: http://www.liebertpub.com/doi/10.1089/zeb.2015.1114

131. Zhou Q, Yang D, Ombrello AK, Zavialov A V., Toro C, Zavialov A V., et al. Early-onset stroke and vasculopathy associated with mutations in ADA2. N Engl J Med. 2014;

132. Navon Elkan P, Pierce SB, Segel R, Walsh T, Barash J, Padeh S, et al. Mutant Adenosine Deaminase 2 in a Polyarteritis Nodosa Vasculopathy. N Engl J Med [Internet]. 2014 Mar 6;370(10):921–31. Available from: http://www.nejm.org/doi/10.1056/NEJMoa1307362

133. Ben-Ami T, Revel-Vilk S, Brooks R, Shaag A, Hershfield MS, Kelly SJ, et al. Extending the Clinical Phenotype of Adenosine Deaminase 2 Deficiency. J Pediatr [Internet]. 2016 Oct;177:316–20. Available from: https://linkinghub.elsevier.com/retrieve/pii/S0022347616304875

134. Meyts I, Aksentijevich I. Deficiency of adenosine deaminase 2 (DADA2): Updates on the phenotype, genetics, pathogenesis, and treatment. Journal of Clinical Immunology. 2018.

135. Sahin S, Adrovic A, Barut K, Ugurlu S, Turanli ET, Ozdogan H, et al. Clinical, imaging and genotypical features of three deceased and five surviving cases with ADA2 deficiency. Rheumatol Int [Internet]. 2018 Jan 17;38(1):129–36. Available from: http://link.springer.com/10.1007/s00296-017-3740-3

136. Cooray S, Omyinmi E, Hong Y, Papadopoulou C, Harper L, Al-Abadi E, et al. Anti-tumour necrosis factor treatment for the prevention of ischaemic events in patients with deficiency of adenosine deaminase 2 (DADA2). Rheumatology [Internet]. 2021 Sep 1;60(9):4373–8. Available from: https://academic.oup.com/rheumatology/article/60/9/4373/6071499

137. Hashem H, Kumar AR, Müller I, Babor F, Bredius R, Dalal J, et al. Hematopoietic stem cell transplantation rescues the hematological, immunological, and vascular phenotype in DADA2. Blood [Internet]. 2017 Dec 14;130(24):2682–8. Available from: https://ashpublications.org/blood/article/130/24/2682/36885/Hematopoietic-stem-cell-transplantation-rescues

138. Hashem H, Bucciol G, Ozen S, Unal S, Bozkaya IO, Akarsu N, et al. Hematopoietic Cell Transplantation Cures Adenosine Deaminase 2 Deficiency: Report on 30 Patients. J Clin Immunol [Internet]. 2021 Oct 29;41(7):1633–47. Available from: https://link.springer.com/10.1007/s10875-021-01098-0

139. Majhail NS. Long-term complications after hematopoietic cell transplantation. Hematol Oncol Stem Cell Ther [Internet]. 2017 Dec;10(4):220–7. Available from: https://linkinghub.elsevier.com/retrieve/pii/S1658387617300456

140. S Bagheri, A A Saboury TH. Adenosine deaminase inhibition. Int J Biol Macromol . 2019;

141. Kaljas Y, Liu C, Skaldin M, Wu C, Zhou Q, Lu Y, et al. Human adenosine deaminases ADA1 and ADA2 bind to different subsets of immune cells. Cell Mol Life Sci. 2017;74(3):555–70.

142. Liu C, Skaldin M, Wu C, Lu Y, Zavialov A V. Application of ADA1 as a new marker enzyme in sandwich ELISA to study the effect of adenosine on activated monocytes. Sci Rep [Internet]. 2016 Aug 11;6(1):31370. Available from: https://www.nature.com/articles/srep31370

143. Flinn AM, Gennery AR. Adenosine deaminase deficiency: a review. Orphanet J Rare Dis [Internet]. 2018 Dec 24;13(1):65. Available from: https://ojrd.biomedcentral.com/articles/10.1186/s13023-018-0807-5

144. Bradford KL, Moretti FA, Carbonaro-Sarracino DA, Gaspar HB, Kohn DB. Adenosine Deaminase (ADA)-Deficient Severe Combined Immune Deficiency (SCID): Molecular Pathogenesis and Clinical Manifestations. J Clin Immunol [Internet]. 2017 Oct 25;37(7):626–37. Available from: http://link.springer.com/10.1007/s10875-017-0433-3

145. Zavialov A V., Gracia E, Glaichenhaus N, Franco R, Zavialov A V., Lauvau G. Human adenosine deaminase 2 induces differentiation of monocytes into macrophages and stimulates proliferation of T helper cells and macrophages. J Leukoc Biol [Internet]. 2010 Aug 1;88(2):279–90. Available from: http://doi.wiley.com/10.1189/jlb.1109764

146. Zavialov A V., Yu X, Spillmann D, Lauvau G, Zavialov A V. Structural Basis for the Growth Factor Activity of Human Adenosine Deaminase ADA2. J Biol Chem [Internet]. 2010 Apr;285(16):12367–77. Available from: https://linkinghub.elsevier.com/retrieve/pii/S002192581961118X

147. Zavialov A V., Engström Å. Human ADA2 belongs to a new family of growth factors with adenosine deaminase activity. Biochem J [Internet]. 2005 Oct 1;391(1):51–7. Available from: https://portlandpress.com/biochemj/article/391/1/51/78742/Human-ADA2-belongs-to-a-new-family-of-growth

148. Lee PY, Aksentijevich I, Zhou Q. Mechanisms of vascular inflammation in deficiency of adenosine deaminase 2 (DADA2). Semin Immunopathol [Internet]. 2022 May 17;44(3):269–80. Available from: https://link.springer.com/10.1007/s00281-022-00918-8

149. Zoccolillo M, Brigida I, Barzaghi F, Scala S, Hernández RJ, Basso-Ricci L, et al. Lentiviral correction of enzymatic activity restrains macrophage inflammation in adenosine deaminase 2 deficiency. Blood Adv [Internet]. 2021;5(16):3174–87. Available from: http://www.ncbi.nlm.nih.gov/pubmed/34424322

150. Saghiri R, Ghashghai N, Movaseghi S, Poursharifi P, Jalilfar S, Bidhendi MA, et al. Serum adenosine deaminase activity in patients with systemic lupus erythematosus: a study based on ADA1 and ADA2 isoenzymes pattern. Rheumatol Int [Internet]. 2012 Jun 25;32(6):1633–8. Available from: http://link.springer.com/10.1007/s00296-011-1836-8

151. Chittiprol S, Satishchandra P, Bhimasenarao RS, Rangaswamy GR, Sureshbabu SV, Subbakrishna DK, et al. Plasma adenosine deaminase activity among HIV1 Clade C seropositives: Relation to CD4 T cell population and antiretroviral therapy. Clin Chim Acta [Internet]. 2007 Feb;377(1–2):133–7. Available from: https://linkinghub.elsevier.com/retrieve/pii/S0009898106006097

152. Zemlin AE, Burgess LJ, Carstens ME. The diagnostic utility of adenosine deaminase isoenzymes in tuberculous pleural effusions. Int J Tuberc Lung Dis [Internet]. 2009 Feb;13(2):214–20. Available from: http://www.ncbi.nlm.nih.gov/pubmed/19146750

153. Lee PY, Kellner ES, Huang Y, Furutani E, Huang Z, Bainter W, et al. Genotype and functional correlates of disease phenotype in deficiency of adenosine deaminase 2 (DADA2). J Allergy Clin Immunol [Internet]. 2020 Jun;145(6):1664-1672.e10. Available from: https://linkinghub.elsevier.com/retrieve/pii/S0091674920300300

154. Carmona-Rivera C, Khaznadar SS, Shwin KW, Irizarry-Caro JA, O'Neil LJ, Liu Y, et al. Deficiency of adenosine deaminase 2 triggers adenosine-mediated NETosis and TNF production in patients with DADA2. Blood [Internet]. 2019 Jul 25;134(4):395–406. Available from: https://ashpublications.org/blood/article/134/4/395/260700/Deficiency-of-adenosine-deaminase-2-triggers

155. Adamiak M, Bujko K, Cymer M, Plonka M, Glaser T, Kucia M, et al. Novel evidence that extracellular nucleotides and purinergic signaling induce innate immunity-mediated mobilization of hematopoietic stem/progenitor cells. Leukemia [Internet]. 2018 Sep 30;32(9):1920–31. Available from: https://www.nature.com/articles/s41375-018-0122-0

156. Ratajczak MZ, Adamiak M, Thapa A, Bujko K, Brzezniakiewicz-Janus K, Lenkiewicz AM. NLRP3 inflammasome couples purinergic signaling with activation of the complement cascade for the optimal release of cells from bone marrow. Leukemia [Internet]. 2019 Apr 7;33(4):815–25. Available from: https://www.nature.com/articles/s41375-019-0436-6

157. Thapa A, Abdelbaset-Ismail A, Chumak V, Adamiak M, Brzezniakiewicz-Janus

K, Ratajczak J, et al. Extracellular Adenosine (eAdo) - A2B Receptor Axis Inhibits in Nlrp3 Inflammasome-dependent Manner Trafficking of Hematopoietic Stem/progenitor Cells. Stem Cell Rev Reports [Internet]. 2022 Dec 23;18(8):2893–911. Available from: https://link.springer.com/10.1007/s12015-022-10417-w

158. Basit S, Al-Harbi KM, Alhijji SAM, Albalawi AM, Alharby E, Eldardear A, et al. CIT, a gene involved in neurogenic cytokinesis, is mutated in human primary microcephaly. Hum Genet [Internet]. 2016 Oct 12;135(10):1199–207. Available from: http://link.springer.com/10.1007/s00439-016-1724-0

159. Harding BN, Moccia A, Drunat S, Soukarieh O, Tubeuf H, Chitty LS, et al. Mutations in Citron Kinase Cause Recessive Microlissencephaly with Multinucleated Neurons. Am J Hum Genet [Internet]. 2016 Aug;99(2):511–20. Available from: https://linkinghub.elsevier.com/retrieve/pii/S0002929716302750

160. Li H, Bielas SL, Zaki MS, Ismail S, Farfara D, Um K, et al. Biallelic Mutations in Citron Kinase Link Mitotic Cytokinesis to Human Primary Microcephaly. Am J Hum Genet [Internet]. 2016 Aug;99(2):501–10. Available from: https://linkinghub.elsevier.com/retrieve/pii/S0002929716302762

161. Shaheen R, Hashem A, Abdel-Salam GMH, Al-Fadhli F, Ewida N, Alkuraya FS. Mutations in CIT, encoding citron rho-interacting serine/threonine kinase, cause severe primary microcephaly in humans. Hum Genet [Internet]. 2016 Oct 8;135(10):1191–7. Available from: http://link.springer.com/10.1007/s00439-016-1722-2

162. Mahmood S, Ahmad W, Hassan MJ. Autosomal recessive primary microcephaly (MCPH): clinical manifestations, genetic heterogeneity and mutation continuum. Orphanet J Rare Dis [Internet]. 2011 Dec 13;6(1):39. Available from: https://ojrd.biomedcentral.com/articles/10.1186/1750-1172-6-39

163. Bianchi FT, Gai M, Berto GE, Di Cunto F. Of rings and spines: The multiple facets of Citron proteins in neural development. Small GTPases [Internet]. 2020 Mar 3;11(2):122–30. Available from: https://www.tandfonline.com/doi/full/10.1080/21541248.2017.1374325

164. Di Cunto F, Imarisio S, Hirsch E, Broccoli V, Bulfone A, Migheli A, et al. Defective Neurogenesis in Citron Kinase Knockout Mice by Altered Cytokinesis and Massive Apoptosis. Neuron [Internet]. 2000 Oct;28(1):115–27. Available from: https://linkinghub.elsevier.com/retrieve/pii/S0896627300000908

165. Roberts MR, Bittman K, Li W-W, French R, Mitchell B, LoTurco JJ, et al. The Flathead Mutation Causes CNS-Specific Developmental Abnormalities and Apoptosis. J Neurosci [Internet]. 2000 Mar 15;20(6):2295–306. Available from: https://www.jneurosci.org/lookup/doi/10.1523/JNEUROSCI.20-06-02295.2000

166. Sarkisian MR, Li W, Di Cunto F, D'Mello SR, LoTurco JJ. Citron-Kinase, A Protein Essential to Cytokinesis in Neuronal Progenitors, Is Deleted in the Flathead Mutant Rat. J Neurosci [Internet]. 2002 Apr 15;22(8):RC217–RC217. Available from: https://www.jneurosci.org/lookup/doi/10.1523/JNEUROSCI.22-08-j0001.2002

167. Di Cunto F, Calautti E, Hsiao J, Ong L, Topley G, Turco E, et al. Citron Rho-

interacting Kinase, a Novel Tissue-specific Ser/Thr Kinase Encompassing the Rho-Rac-binding Protein Citron. J Biol Chem [Internet]. 1998 Nov;273(45):29706–11. Available from: https://linkinghub.elsevier.com/retrieve/pii/S0021925819593723

168. Madaule P, Eda M, Watanabe N, Fujisawa K, Matsuoka T, Bito H, et al. Role of citron kinase as a target of the small GTPase Rho in cytokinesis. Nature [Internet]. 1998 Jul;394(6692):491–4. Available from: https://www.nature.com/articles/28873

169. Yamashiro S, Totsukawa G, Yamakita Y, Sasaki Y, Madaule P, Ishizaki T, et al. Citron Kinase, a Rho-dependent Kinase, Induces Di-phosphorylation of Regulatory Light Chain of Myosin II. Mol Biol Cell [Internet]. 2003 May;14(5):1745–56. Available from: https://www.molbiolcell.org/doi/10.1091/mbc.e02-07-0427

170. Bassi ZI, Audusseau M, Riparbelli MG, Callaini G, D'Avino PP. Citron kinase controls a molecular network required for midbody formation in cytokinesis. Proc Natl Acad Sci [Internet]. 2013 Jun 11;110(24):9782–7. Available from: https://pnas.org/doi/full/10.1073/pnas.1301328110

171. Gai M, Camera P, Dema A, Bianchi F, Berto G, Scarpa E, et al. Citron kinase controls abscission through RhoA and anillin. Kaibuchi K, editor. Mol Biol Cell [Internet]. 2011 Oct 15;22(20):3768–78. Available from: https://www.molbiolcell.org/doi/10.1091/mbc.e10-12-0952

172. Madaule P, Furuyashiki T, Reid T, Ishizaki T, Watanabe G, Morii N, et al. A novel partner for the GTP-bound forms of rho and rac. FEBS Lett [Internet]. 1995 Dec 18;377(2):243–8. Available from: https://febs.onlinelibrary.wiley.com/doi/10.1016/0014-5793%2895%2901351-2

173. Furuyashiki T, Fujisawa K, Fujita A, Madaule P, Uchino S, Mishina M, et al. Citron, a Rho-Target, Interacts with PSD-95/SAP-90 at Glutamatergic Synapses in the Thalamus. J Neurosci [Internet]. 1999 Jan 1;19(1):109–18. Available from: https://www.jneurosci.org/lookup/doi/10.1523/JNEUROSCI.19-01-00109.1999

174. Camera P, Schubert V, Pellegrino M, Berto G, Vercelli A, Muzzi P, et al. The RhoA-associated protein Citron-N controls dendritic spine maintenance by interacting with spine-associated Golgi compartments. EMBO Rep [Internet]. 2008 Apr 29;9(4):384–92. Available from: https://www.embopress.org/doi/10.1038/embor.2008.21

175. Mitchell BD, Gibbons B, Allen LR, Stella J, D'Mello SR. Aberrant apoptosis in the neurological mutant Flathead is associated with defective cytokinesis of neural progenitor cells. Dev Brain Res [Internet]. 2001 Sep;130(1):53–63. Available from: https://linkinghub.elsevier.com/retrieve/pii/S0165380601002061

176. Boda E, Lorenzati M, Parolisi R, Harding B, Pallavicini G, Bonfanti L, et al. Molecular and functional heterogeneity in dorsal and ventral oligodendrocyte progenitor cells of the mouse forebrain in response to DNA damage. Nat Commun [Internet]. 2022 Apr 28;13(1):2331. Available from: https://www.nature.com/articles/s41467-022-30010-6

177. Halcrow EFJ, Mazza R, Diversi A, Enright A, D'Avino PP. Midbody Proteins Display Distinct Dynamics during Cytokinesis. Cells [Internet]. 2022 Oct 22;11(21):3337. Available from: https://www.mdpi.com/2073-4409/11/21/3337

178. D'Avino PP, Capalbo L. Regulation of midbody formation and function by mitotic kinases. Semin Cell Dev Biol [Internet]. 2016 May;53:57–63. Available from: https://linkinghub.elsevier.com/retrieve/pii/S1084952116300180

179. Bassi ZI, Verbrugghe KJ, Capalbo L, Gregory S, Montembault E, Glover DM, et al. Sticky/Citron kinase maintains proper RhoA localization at the cleavage site during cytokinesis. J Cell Biol [Internet]. 2011 Nov 14;195(4):595–603. Available from: https://rupress.org/jcb/article/195/4/595/36631/Sticky-Citron-kinase-maintains-proper-RhoA

180. McKenzie C, Bassi ZI, Debski J, Gottardo M, Callaini G, Dadlez M, et al. Cross-regulation between Aurora B and Citron kinase controls midbody architecture in cytokinesis. Open Biol [Internet]. 2016 Mar;6(3):160019. Available from: https://royalsocietypublishing.org/doi/10.1098/rsob.160019

181. Gai M, Bianchi FT, Vagnoni C, Vernì F, Bonaccorsi S, Pasquero S, et al. <scp>ASPM</scp> and <scp>CITK</scp> regulate spindle orientation by affecting the dynamics of astral microtubules. EMBO Rep [Internet]. 2016 Oct 25;17(10):1396–409. Available from: https://www.embopress.org/doi/10.15252/embr.201541823

182. Sgrò F, Bianchi FT, Falcone M, Pallavicini G, Gai M, Chiotto AMA, et al. Tissue-specific control of midbody microtubule stability by Citron kinase through modulation of TUBB3 phosphorylation. Cell Death Differ [Internet]. 2016 May 20;23(5):801–13. Available from: https://www.nature.com/articles/cdd2015142

183. Bianchi FT, Tocco C, Pallavicini G, Liu Y, Vernì F, Merigliano C, et al. Citron Kinase Deficiency Leads to Chromosomal Instability and TP53-Sensitive Microcephaly. Cell Rep [Internet]. 2017 Feb;18(7):1674–86. Available from: https://linkinghub.elsevier.com/retrieve/pii/S2211124717301110

184. Hall A. Rho family GTPases. Biochem Soc Trans [Internet]. 2012 Dec 1;40(6):1378–82. Available from: https://portlandpress.com/biochemsoctrans/article/40/6/1378/66742/Rho-family-GTPases

185. Jaffe AB, Hall A. RHO GTPASES: Biochemistry and Biology. Annu Rev Cell Dev Biol [Internet]. 2005 Nov 1;21(1):247–69. Available from: https://www.annualreviews.org/doi/10.1146/annurev.cellbio.21.020604.150721

186. Etienne-Manneville S, Hall A. Rho GTPases in cell biology. Nature [Internet]. 2002 Dec;420(6916):629–35. Available from: https://www.nature.com/articles/nature01148

187. Mosaddeghzadeh N, Ahmadian MR. The RHO Family GTPases: Mechanisms of Regulation and Signaling. Cells [Internet]. 2021 Jul 20;10(7):1831. Available from: https://www.mdpi.com/2073-4409/10/7/1831

188. BISHOP AL, HALL A. Rho GTPases and their effector proteins. Biochem J

[Internet]. 2000 Jun 1;348(2):241–55. Available from: https://portlandpress.com/biochemj/article/348/2/241/38427/Rho-GTPases-and-their-effector-proteins

189. Hodge RG RA. Regulating Rho GTPases and their regulators. Nat Rev Mol Cell Biol. 2016;17(8):496-.

190. Rossman KL, Der CJ, Sondek J. GEF means go: turning on RHO GTPases with guanine nucleotide-exchange factors. Nat Rev Mol Cell Biol [Internet]. 2005 Feb;6(2):167–80. Available from: https://www.nature.com/articles/nrm1587

191. Garcia-Mata R, Boulter E, Burridge K. The “invisible hand”: regulation of RHO GTPases by RHOGDIs. Nat Rev Mol Cell Biol [Internet]. 2011 Aug 22;12(8):493–504. Available from: https://www.nature.com/articles/nrm3153

192. Julian L, Olson MF. Rho-associated coiled-coil containing kinases (ROCK). Small GTPases [Internet]. 2014 Apr 3;5(2):e29846. Available from: http://www.tandfonline.com/doi/full/10.4161/sgtp.29846

193. Amano M, Nakayama M, Kaibuchi K. Rho-kinase/ROCK: A key regulator of the cytoskeleton and cell polarity. Cytoskeleton [Internet]. 2010 Sep 23;67(9):545–54. Available from: https://onlinelibrary.wiley.com/doi/10.1002/cm.20472

194. Clemens DJ, Tester DJ, Giudicessi JR, Bos JM, Rohatgi RK, Abrams DJ, et al. International Triadin Knockout Syndrome Registry. Circ Genomic Precis Med [Internet]. 2019 Feb;12(2). Available from: https://www.ahajournals.org/doi/10.1161/CIRCGEN.118.002419

195. Altmann HM, Tester DJ, Will ML, Middha S, Evans JM, Eckloff BW, et al. Homozygous/Compound Heterozygous Triadin Mutations Associated With Autosomal-Recessive Long-QT Syndrome and Pediatric Sudden Cardiac Arrest. Circulation [Internet]. 2015 Jun 9;131(23):2051–60. Available from: https://www.ahajournals.org/doi/10.1161/CIRCULATIONAHA.115.015397

196. Roux-Buisson N, Cacheux M, Fourest-Lieuvin A, Fauconnier J, Brocard J, Denjoy I, et al. Absence of triadin, a protein of the calcium release complex, is responsible for cardiac arrhythmia with sudden death in human. Hum Mol Genet [Internet]. 2012 Jun 15;21(12):2759–67. Available from: https://academic.oup.com/hmg/article-lookup/doi/10.1093/hmg/dds104

197. Sarquella-Brugada G, Fernandez-Falgueras A, Cesar S, Arbelo E, Jordà P, García-Álvarez A, et al. Pediatric Malignant Arrhythmias Caused by Rare Homozygous Genetic Variants in TRDN: A Comprehensive Interpretation. Front Pediatr [Internet]. 2021 Feb 22;8. Available from: https://www.frontiersin.org/articles/10.3389/fped.2020.601708/full

198. Sulu A, Karacan M, Ergul Y. A very rare cause of sudden cardiac arrest in children: triadin knockout syndrome. Cardiol Young [Internet]. 2023 Jan 28;33(1):130–2. Available from: https://www.cambridge.org/core/product/identifier/S1047951122001226/type/journal_article

199. Clemens DJ, Tester DJ, Marty I, Ackerman MJ. Phenotype-guided whole

genome analysis in a patient with genetically elusive long QT syndrome yields a novel TRDN-encoded triadin pathogenetic substrate for triadin knockout syndrome and reveals a novel primate-specific cardiac TRDN transcript. Hear Rhythm [Internet]. 2020 Jun;17(6):1017–24. Available from: https://linkinghub.elsevier.com/retrieve/pii/S1547527120300254

200. Rossi D, Gigli L, Gamberucci A, Bordoni R, Pietrelli A, Lorenzini S, et al. A novel homozygous mutation in the TRDN gene causes a severe form of pediatric malignant ventricular arrhythmia. Hear Rhythm [Internet]. 2020 Feb;17(2):296–304. Available from: https://linkinghub.elsevier.com/retrieve/pii/S1547527119307507

201. Engel AG, Redhage KR, Tester DJ, Ackerman MJ, Selcen D. Congenital myopathy associated with the triadin knockout syndrome. Neurology [Internet]. 2017 Mar 21;88(12):1153–6. Available from: https://www.neurology.org/doi/10.1212/WNL.0000000000003745

202. Oddoux S, Brocard J, Schweitzer A, Szentesi P, Giannesini B, Brocard J, et al. Triadin Deletion Induces Impaired Skeletal Muscle Function. J Biol Chem [Internet]. 2009 Dec;284(50):34918–29. Available from: https://linkinghub.elsevier.com/retrieve/pii/S0021925820376158

203. Shen X, Franzini-Armstrong C, Lopez JR, Jones LR, Kobayashi YM, Wang Y, et al. Triadins Modulate Intracellular Ca2+ Homeostasis but Are Not Essential for Excitation-Contraction Coupling in Skeletal Muscle. J Biol Chem [Internet]. 2007 Dec;282(52):37864–74. Available from: https://linkinghub.elsevier.com/retrieve/pii/S0021925820777410

204. Chopra N, Yang T, Asghari P, Moore ED, Huke S, Akin B, et al. Ablation of triadin causes loss of cardiac Ca 2+ release units, impaired excitation–contraction coupling, and cardiac arrhythmias. Proc Natl Acad Sci [Internet]. 2009 May 5;106(18):7636–41. Available from: https://pnas.org/doi/full/10.1073/pnas.0902919106

205. Caswell AH, Brandt NR, Brunschwig JP, Purkerson S. Localization and partial characterization of the oligomeric disulfide-linked molecular weight 95,000 protein (triadin) which binds the ryanodine and dihydropyridine receptors in skeletal muscle triadic vesicles. Biochemistry [Internet]. 1991 Jul 30;30(30):7507–13. Available from: https://pubs.acs.org/doi/abs/10.1021/bi00244a020

206. Thevenon D, Smida-Rezgui S, Chevessier F, Groh S, Henry-Berger J, Beatriz Romero N, et al. Human skeletal muscle triadin: gene organization and cloning of the major isoform, Trisk 51. Biochem Biophys Res Commun [Internet]. 2003 Apr;303(2):669–75. Available from: https://linkinghub.elsevier.com/retrieve/pii/S0006291X03004066

207. Barone V, Randazzo D, Del Re V, Sorrentino V, Rossi D. Organization of junctional sarcoplasmic reticulum proteins in skeletal muscle fibers. J Muscle Res Cell Motil [Internet]. 2015 Dec 15;36(6):501–15. Available from: http://link.springer.com/10.1007/s10974-015-9421-5

208. Zhang L, Kelley J, Schmeisser G, Kobayashi YM, Jones LR. Complex

Formation between Junctin, Triadin, Calsequestrin, and the Ryanodine Receptor. J Biol Chem [Internet]. 1997 Sep;272(37):23389–97. Available from: https://linkinghub.elsevier.com/retrieve/pii/S0021925819655936

209. Guo W, Jorgensen AO, Jones LR, Campbell KP. Biochemical Characterization and Molecular Cloning of Cardiac Triadin. J Biol Chem [Internet]. 1996 Jan;271(1):458–65. Available from: https://linkinghub.elsevier.com/retrieve/pii/S0021925818953639

210. Knollmann BC. New roles of calsequestrin and triadin in cardiac muscle. J Physiol [Internet]. 2009 Jul 30;587(13):3081–7. Available from: https://physoc.onlinelibrary.wiley.com/doi/10.1113/jphysiol.2009.172098

211. Chopra N, Knollmann BC. Triadin regulates cardiac muscle couplon structure and microdomain Ca2+ signalling: a path towards ventricular arrhythmias. Cardiovasc Res [Internet]. 2013 May 1;98(2):187–91. Available from: https://academic.oup.com/cardiovascres/article-lookup/doi/10.1093/cvr/cvt023

212. Bowley G, Kugler E, Wilkinson R, Lawrie A, van Eeden F, Chico TJA, et al. Zebrafish as a tractable model of human cardiovascular disease. Br J Pharmacol [Internet]. 2022 Mar 10;179(5):900–17. Available from: https://bpspubs.onlinelibrary.wiley.com/doi/10.1111/bph.15473

213. Gauvrit S, Bossaer J, Lee J, Collins MM. Modeling Human Cardiac Arrhythmias: Insights from Zebrafish. J Cardiovasc Dev Dis [Internet]. 2022 Jan 5;9(1):13. Available from: https://www.mdpi.com/2308-3425/9/1/13

214. Gore A V., Pillay LM, Venero Galanternik M, Weinstein BM. The zebrafish: A fintastic model for hematopoietic development and disease. WIREs Dev Biol [Internet]. 2018 May 13;7(3). Available from: https://onlinelibrary.wiley.com/doi/10.1002/wdev.312

215. Xie Y, Meijer AH, Schaaf MJM. Modeling Inflammation in Zebrafish for the Development of Anti-inflammatory Drugs. Front Cell Dev Biol [Internet]. 2021 Jan 15;8. Available from: https://www.frontiersin.org/articles/10.3389/fcell.2020.620984/full

216. Traver D, Herbomel P, Patton EE, Murphey RD, Yoder JA, Litman GW, et al. The zebrafish as a model organism to study development of the immune system. Adv Immunol [Internet]. 2003;81:253–330. Available from: http://www.ncbi.nlm.nih.gov/pubmed/14711058

217. de Abreu MS, Genario R, Giacomini ACVV, Demin KA, Lakstygal AM, Amstislavskaya TG, et al. Zebrafish as a Model of Neurodevelopmental Disorders. Neuroscience [Internet]. 2020 Oct;445:3–11. Available from: https://linkinghub.elsevier.com/retrieve/pii/S0306452219306074

218. Wilkinson RN, van Eeden FJM. The Zebrafish as a Model of Vascular Development and Disease. In 2014. p. 93–122. Available from: https://linkinghub.elsevier.com/retrieve/pii/B9780123869302000057

219. Isogai S, Lawson ND, Torrealday S, Horiguchi M, Weinstein BM. Angiogenic network formation in the developing vertebrate trunk. Development [Internet]. 2003 Nov 1;130(21):5281–90. Available from:

https://journals.biologists.com/dev/article/130/21/5281/52159/Angiogenic-network-formation-in-the-developing

220. Galanternik MV, Stratman AN, Weinstein BM. The Zebrafish Cardiovascular System. In: The Zebrafish in Biomedical Research [Internet]. Elsevier; 2020. p. 131–43. Available from: https://linkinghub.elsevier.com/retrieve/pii/B9780128124314000142

221. Poon KL, Brand T. The zebrafish model system in cardiovascular research: A tiny fish with mighty prospects. Glob Cardiol Sci Pract [Internet]. 2013 Mar;2013(1):4. Available from: http://www.qscience.com/doi/abs/10.5339/gcsp.2013.4

222. González-Rosa JM. Zebrafish Models of Cardiac Disease: From Fortuitous Mutants to Precision Medicine. Circ Res [Internet]. 2022 Jun 10;130(12):1803–26. Available from: https://www.ahajournals.org/doi/10.1161/CIRCRESAHA.122.320396

223. Pelster B, Burggren WW. Disruption of Hemoglobin Oxygen Transport Does Not Impact Oxygen-Dependent Physiological Processes in Developing Embryos of Zebra Fish (Danio rerio). Circ Res [Internet]. 1996 Aug;79(2):358–62. Available from: https://www.ahajournals.org/doi/10.1161/01.RES.79.2.358

224. Bang A, Grønkjær P, Malte H. Individual variation in the rate of oxygen consumption by zebrafish embryos. J Fish Biol [Internet]. 2004 May 27;64(5):1285–96. Available from: https://onlinelibrary.wiley.com/doi/10.1111/j.0022-1112.2004.00391.x

225. Strecker R, Seiler T-B, Hollert H, Braunbeck T. Oxygen requirements of zebrafish (Danio rerio) embryos in embryo toxicity tests with environmental samples. Comp Biochem Physiol Part C Toxicol Pharmacol [Internet]. 2011 Apr;153(3):318–27. Available from: https://linkinghub.elsevier.com/retrieve/pii/S153204561000205X

226. Isogai S, Horiguchi M, Weinstein BM. The Vascular Anatomy of the Developing Zebrafish: An Atlas of Embryonic and Early Larval Development. Dev Biol [Internet]. 2001 Feb;230(2):278–301. Available from: https://linkinghub.elsevier.com/retrieve/pii/S0012160600999950

227. Gore A V., Monzo K, Cha YR, Pan W, Weinstein BM. Vascular Development in the Zebrafish. Cold Spring Harb Perspect Med [Internet]. 2012 May 1;2(5):a006684–a006684. Available from: http://perspectivesinmedicine.cshlp.org/lookup/doi/10.1101/cshperspect.a006684

228. Vogeli KM, Jin S-W, Martin GR, Stainier DYR. A common progenitor for haematopoietic and endothelial lineages in the zebrafish gastrula. Nature [Internet]. 2006 Sep;443(7109):337–9. Available from: https://www.nature.com/articles/nature05045

229. Hogan BM, Schulte-Merker S. How to Plumb a Pisces: Understanding Vascular Development and Disease Using Zebrafish Embryos. Dev Cell [Internet]. 2017 Sep;42(6):567–83. Available from: https://linkinghub.elsevier.com/retrieve/pii/S1534580717306755

230. Bautch VL, Caron KM. Blood and Lymphatic Vessel Formation. Cold Spring Harb Perspect Biol [Internet]. 2015 Mar 2;7(3):a008268. Available from: http://cshperspectives.cshlp.org/lookup/doi/10.1101/cshperspect.a008268

231. Eberlein J, Herdt L, Malchow J, Rittershaus A, Baumeister S, Helker CS. Molecular and Cellular Mechanisms of Vascular Development in Zebrafish. Life [Internet]. 2021 Oct 15;11(10):1088. Available from: https://www.mdpi.com/2075-1729/11/10/1088

232. Schuermann A, Helker CSM, Herzog W. Angiogenesis in zebrafish. Semin Cell Dev Biol [Internet]. 2014 Jul;31:106–14. Available from: https://linkinghub.elsevier.com/retrieve/pii/S1084952114001086

233. Goi M, Childs SJ. Patterning mechanisms of the sub-intestinal venous plexus in zebrafish. Dev Biol [Internet]. 2016 Jan;409(1):114–28. Available from: https://linkinghub.elsevier.com/retrieve/pii/S0012160615302414

234. Fang L, Liu C, Miller YI. Zebrafish models of dyslipidemia: relevance to atherosclerosis and angiogenesis. Transl Res [Internet]. 2014 Feb;163(2):99–108. Available from: https://linkinghub.elsevier.com/retrieve/pii/S1931524413002971

235. Avraham-Davidi I, Ely Y, Pham VN, Castranova D, Grunspan M, Malkinson G, et al. ApoB-containing lipoproteins regulate angiogenesis by modulating expression of VEGF receptor 1. Nat Med [Internet]. 2012 Jun 13;18(6):967–73. Available from: http://www.nature.com/articles/nm.2759

236. Fang L, Choi S-H, Baek JS, Liu C, Almazan F, Ulrich F, et al. Control of angiogenesis by AIBP-mediated cholesterol efflux. Nature [Internet]. 2013 Jun 29;498(7452):118–22. Available from: https://www.nature.com/articles/nature12166

237. Sant KE, Timme-Laragy AR. Zebrafish as a Model for Toxicological Perturbation of Yolk and Nutrition in the Early Embryo. Curr Environ Heal Reports [Internet]. 2018 Mar 7;5(1):125–33. Available from: http://link.springer.com/10.1007/s40572-018-0183-2

238. Link V, Shevchenko A, Heisenberg C-P. Proteomics of early zebrafish embryos. BMC Dev Biol [Internet]. 2006 Dec 13;6(1):1. Available from: https://bmcdevbiol.biomedcentral.com/articles/10.1186/1471-213X-6-1

239. Wilson C. Aspects of Larval Rearing. ILAR J [Internet]. 2012 Jun 1;53(2):169–78. Available from: https://academic.oup.com/ilarjournal/article-lookup/doi/10.1093/ilar.53.2.169

240. Tamplin OJ, Durand EM, Carr LA, Childs SJ, Hagedorn EJ, Li P, et al. Hematopoietic Stem Cell Arrival Triggers Dynamic Remodeling of the Perivascular Niche. Cell [Internet]. 2015 Jan;160(1–2):241–52. Available from: https://linkinghub.elsevier.com/retrieve/pii/S0092867414016389

241. Xue Y, Lv J, Zhang C, Wang L, Ma D, Liu F. The Vascular Niche Regulates Hematopoietic Stem and Progenitor Cell Lodgment and Expansion via klf6a-ccl25b. Dev Cell [Internet]. 2017 Aug;42(4):349-362.e4. Available from: https://linkinghub.elsevier.com/retrieve/pii/S1534580717305543

242. Theodore LN, Hagedorn EJ, Cortes M, Natsuhara K, Liu SY, Perlin JR, et al. Distinct Roles for Matrix Metalloproteinases 2 and 9 in Embryonic Hematopoietic Stem Cell Emergence, Migration, and Niche Colonization. Stem Cell Reports [Internet]. 2017 May;8(5):1226–41. Available from: https://linkinghub.elsevier.com/retrieve/pii/S2213671117301224

243. karthik S, Djukic T, Kim J-D, Zuber B, Makanya A, Odriozola A, et al. Synergistic interaction of sprouting and intussusceptive angiogenesis during zebrafish caudal vein plexus development. Sci Rep [Internet]. 2018 Jun 29;8(1):9840. Available from: https://www.nature.com/articles/s41598-018-27791-6

244. Kemmler CL, Riemslagh FW, Moran HR, Mosimann C. From Stripes to a Beating Heart: Early Cardiac Development in Zebrafish. J Cardiovasc Dev Dis [Internet]. 2021 Feb 10;8(2):17. Available from: https://www.mdpi.com/2308-3425/8/2/17

245. Staudt D, Stainier D. Uncovering the Molecular and Cellular Mechanisms of Heart Development Using the Zebrafish. Annu Rev Genet [Internet]. 2012 Dec 15;46(1):397–418. Available from: https://www.annualreviews.org/doi/10.1146/annurev-genet-110711-155646

246. Yalcin HC, Amindari A, Butcher JT, Althani A, Yacoub M. Heart function and hemodynamic analysis for zebrafish embryos. Dev Dyn [Internet]. 2017 Nov 11;246(11):868–80. Available from: https://anatomypubs.onlinelibrary.wiley.com/doi/10.1002/dvdy.24497

247. Bakkers J. Zebrafish as a model to study cardiac development and human cardiac disease. Cardiovasc Res [Internet]. 2011 Jul 15;91(2):279–88. Available from: https://academic.oup.com/cardiovascres/article-lookup/doi/10.1093/cvr/cvr098

248. Brown D, Samsa L, Qian L, Liu J. Advances in the Study of Heart Development and Disease Using Zebrafish. J Cardiovasc Dev Dis [Internet]. 2016 Apr 9;3(2):13. Available from: http://www.mdpi.com/2308-3425/3/2/13

249. Chi NC, Shaw RM, Jungblut B, Huisken J, Ferrer T, Arnaout R, et al. Genetic and Physiologic Dissection of the Vertebrate Cardiac Conduction System. Hogan BL., editor. PLoS Biol [Internet]. 2008 May 13;6(5):e109. Available from: https://dx.plos.org/10.1371/journal.pbio.0060109

250. Tessadori F, van Weerd JH, Burkhard SB, Verkerk AO, de Pater E, Boukens BJ, et al. Identification and Functional Characterization of Cardiac Pacemaker Cells in Zebrafish. Barbuti A, editor. PLoS One [Internet]. 2012 Oct 16;7(10):e47644. Available from: https://dx.plos.org/10.1371/journal.pone.0047644

251. Stoyek MR, Croll RP, Smith FM. Intrinsic and extrinsic innervation of the heart in zebrafish (<scp> *D* </scp> *anio rerio*). J Comp Neurol [Internet]. 2015 Aug 9;523(11):1683–700. Available from: https://onlinelibrary.wiley.com/doi/10.1002/cne.23764

252. Sampurna B, Audira G, Juniardi S, Lai Y-H, Hsiao C-D. A Simple ImageJ-Based Method to Measure Cardiac Rhythm in Zebrafish Embryos. Inventions

[Internet]. 2018 Apr 10;3(2):21. Available from: http://www.mdpi.com/2411-5134/3/2/21

253. Forouhar AS, Hove JR, Calvert C, Flores J, Jadvar H, Gharib M. Electrocardiographic Characterization of Embryonic Zebrafish. In: The 26th Annual International Conference of the IEEE Engineering in Medicine and Biology Society [Internet]. IEEE; p. 3615–7. Available from: http://ieeexplore.ieee.org/document/1404016/

254. Genge CE, Lin E, Lee L, Sheng X, Rayani K, Gunawan M, et al. The Zebrafish Heart as a Model of Mammalian Cardiac Function. In 2016. p. 99–136. Available from: http://link.springer.com/10.1007/112_2016_5

255. De Luca E, Zaccaria GM, Hadhoud M, Rizzo G, Ponzini R, Morbiducci U, et al. ZebraBeat: a flexible platform for the analysis of the cardiac rate in zebrafish embryos. Sci Rep [Internet]. 2014 May 9;4(1):4898. Available from: https://www.nature.com/articles/srep04898

256. Verkerk AO, Remme CA. Zebrafish: a novel research tool for cardiac (patho)electrophysiology and ion channel disorders. Front Physiol [Internet]. 2012;3. Available from: http://journal.frontiersin.org/article/10.3389/fphys.2012.00255/abstract

257. Milan DJ, MacRae CA. Zebrafish genetic models for arrhythmia. Prog Biophys Mol Biol [Internet]. 2008 Oct;98(2–3):301–8. Available from: https://linkinghub.elsevier.com/retrieve/pii/S0079610709000121

258. Vornanen M, Hassinen M. Zebrafish heart as a model for human cardiac electrophysiology. Channels [Internet]. 2016 Mar 3;10(2):101–10. Available from: https://www.tandfonline.com/doi/full/10.1080/19336950.2015.1121335

259. Echeazarra L, Hortigón-Vinagre MP, Casis O, Gallego M. Adult and Developing Zebrafish as Suitable Models for Cardiac Electrophysiology and Pathology in Research and Industry. Front Physiol [Internet]. 2021 Jan 13;11. Available from: https://www.frontiersin.org/articles/10.3389/fphys.2020.607860/full

260. Ravens U. Ionic basis of cardiac electrophysiology in zebrafish compared to human hearts. Prog Biophys Mol Biol [Internet]. 2018 Oct;138:38–44. Available from: https://linkinghub.elsevier.com/retrieve/pii/S0079610718300907

261. Brette F, Luxan G, Cros C, Dixey H, Wilson C, Shiels HA. Characterization of isolated ventricular myocytes from adult zebrafish (Danio rerio). Biochem Biophys Res Commun [Internet]. 2008 Sep;374(1):143–6. Available from: https://linkinghub.elsevier.com/retrieve/pii/S0006291X08012928

262. Orkin SH. Hematopoiesis: how does it happen? Curr Opin Cell Biol [Internet]. 1995;7(6):870–7. Available from: https://linkinghub.elsevier.com/retrieve/pii/0955067495800727

263. Lieschke GJ. Zebrafish—an emerging genetic model for the study of cytokines and hematopoiesis in the era of functional genomics. Int J Hematol [Internet]. 2001 Jan;73(1):23–31. Available from: http://link.springer.com/10.1007/BF02981899

264. Elsaid R, Soares-da-Silva F, Peixoto M, Amiri D, Mackowski N, Pereira P, et al. Hematopoiesis: A Layered Organization Across Chordate Species. Front Cell Dev Biol [Internet]. 2020 Dec 16;8. Available from: https://www.frontiersin.org/articles/10.3389/fcell.2020.606642/full

265. Jagannathan-Bogdan M, Zon LI. Hematopoiesis. Development [Internet]. 2013 Jun 15;140(12):2463–7. Available from: https://journals.biologists.com/dev/article/140/12/2463/45708/Hematopoiesis

266. Robertson AL, Avagyan S, Gansner JM, Zon LI. Understanding the regulation of vertebrate hematopoiesis and blood disorders – big lessons from a small fish. FEBS Lett [Internet]. 2016 Nov 25;590(22):4016–33. Available from: https://febs.onlinelibrary.wiley.com/doi/10.1002/1873-3468.12415

267. Golub R, Cumano A. Embryonic hematopoiesis. Blood Cells, Mol Dis [Internet]. 2013 Dec;51(4):226–31. Available from: https://linkinghub.elsevier.com/retrieve/pii/S1079979613002015

268. Lacaud G, Kouskoff V. Hemangioblast, hemogenic endothelium, and primitive versus definitive hematopoiesis. Exp Hematol [Internet]. 2017 May;49:19–24. Available from: https://linkinghub.elsevier.com/retrieve/pii/S0301472X16307779

269. Davidson AJ, Zon LI. The 'definitive' (and 'primitive') guide to zebrafish hematopoiesis. Oncogene [Internet]. 2004 Sep 20;23(43):7233–46. Available from: https://www.nature.com/articles/1207943

270. de Jong JLO, Zon LI. Use of the Zebrafish System to Study Primitive and Definitive Hematopoiesis. Annu Rev Genet [Internet]. 2005 Dec 1;39(1):481–501. Available from: https://www.annualreviews.org/doi/10.1146/annurev.genet.39.073003.095931

271. Paik EJ, Zon LI. Hematopoietic development in the zebrafish. Int J Dev Biol [Internet]. 2010;54(6–7):1127–37. Available from: http://www.intjdevbiol.com/paper.php?doi=093042ep

272. Bennett CM, Kanki JP, Rhodes J, Liu TX, Paw BH, Kieran MW, et al. Myelopoiesis in the zebrafish, Danio rerio. Blood [Internet]. 2001 Aug 1;98(3):643–51. Available from: https://ashpublications.org/blood/article/98/3/643/53338/Myelopoiesis-in-the-zebrafish-Danio-rerio

273. Lieschke GJ, Oates AC, Paw BH, Thompson MA, Hall NE, Ward AC, et al. Zebrafish SPI-1 (PU.1) Marks a Site of Myeloid Development Independent of Primitive Erythropoiesis: Implications for Axial Patterning. Dev Biol [Internet]. 2002 Jun;246(2):274–95. Available from: https://linkinghub.elsevier.com/retrieve/pii/S0012160602906573

274. Berman JN, Kanki JP, Look AT. Zebrafish as a model for myelopoiesis during embryogenesis. Exp Hematol [Internet]. 2005 Sep;33(9):997–1006. Available from: https://linkinghub.elsevier.com/retrieve/pii/S0301472X05002924

275. McGrath KE, Frame JM, Fromm GJ, Koniski AD, Kingsley PD, Little J, et al. A transient definitive erythroid lineage with unique regulation of the β-globin locus

in the mammalian embryo. Blood [Internet]. 2011 Apr 28;117(17):4600–8. Available from: https://ashpublications.org/blood/article/117/17/4600/20858/A-transient-definitive-erythroid-lineage-with

276. Bertrand JY, Kim AD, Violette EP, Stachura DL, Cisson JL, Traver D. Definitive hematopoiesis initiates through a committed erythromyeloid progenitor in the zebrafish embryo. Development [Internet]. 2007 Dec 1;134(23):4147–56. Available from: https://journals.biologists.com/dev/article/134/23/4147/64562/Definitive-hematopoiesis-initiates-through-a

277. Eaves CJ. Hematopoietic stem cells: concepts, definitions, and the new reality. Blood [Internet]. 2015 Apr 23;125(17):2605–13. Available from: https://ashpublications.org/blood/article/125/17/2605/34110/Hematopoietic-stem-cells-concepts-definitions-and

278. Dzierzak E. The emergence of definitive hematopoietic stem cells in the mammal. Curr Opin Hematol [Internet]. 2005 May;12(3):197–202. Available from: http://journals.lww.com/00062752-200505000-00001

279. de Bruijn MFTR. Definitive hematopoietic stem cells first develop within the major arterial regions of the mouse embryo. EMBO J [Internet]. 2000 Jun 1;19(11):2465–74. Available from: http://emboj.embopress.org/cgi/doi/10.1093/emboj/19.11.2465

280. Kissa K, Herbomel P. Blood stem cells emerge from aortic endothelium by a novel type of cell transition. Nature [Internet]. 2010 Mar 14;464(7285):112–5. Available from: https://www.nature.com/articles/nature08761

281. Sugden WW, North TE. Making Blood from the Vessel: Extrinsic and Environmental Cues Guiding the Endothelial-to-Hematopoietic Transition. Life [Internet]. 2021 Sep 29;11(10):1027. Available from: https://www.mdpi.com/2075-1729/11/10/1027

282. Wu Y, Hirschi KK. Regulation of Hemogenic Endothelial Cell Development and Function. Annu Rev Physiol [Internet]. 2021 Feb 10;83(1):17–37. Available from: https://www.annualreviews.org/doi/10.1146/annurev-physiol-021119-034352

283. Samarakkody AS, Cantor AB. Opening the window for endothelial-to-hematopoietic transition. Genes Dev [Internet]. 2021 Nov 1;35(21–22):1398–400. Available from: http://genesdev.cshlp.org/lookup/doi/10.1101/gad.349056.121

284. Ottersbach K. Endothelial-to-haematopoietic transition: an update on the process of making blood. Biochem Soc Trans [Internet]. 2019 Apr 30;47(2):591–601. Available from: https://portlandpress.com/biochemsoctrans/article/47/2/591/219681/Endothelial-to-haematopoietic-transition-an-update

285. He Q, Zhang C, Wang L, Zhang P, Ma D, Lv J, et al. Inflammatory signaling regulates hematopoietic stem and progenitor cell emergence in vertebrates. Blood [Internet]. 2015 Feb 12;125(7):1098–106. Available from: https://ashpublications.org/blood/article/125/7/1098/34186/Inflammatory-

signaling-regulates-hematopoietic

286. Li Y, Esain V, Teng L, Xu J, Kwan W, Frost IM, et al. Inflammatory signaling regulates embryonic hematopoietic stem and progenitor cell production. Genes Dev [Internet]. 2014 Dec 1;28(23):2597–612. Available from: http://genesdev.cshlp.org/lookup/doi/10.1101/gad.253302.114

287. Espín-Palazón R, Stachura DL, Campbell CA, García-Moreno D, Del Cid N, Kim AD, et al. Proinflammatory Signaling Regulates Hematopoietic Stem Cell Emergence. Cell [Internet]. 2014 Nov;159(5):1070–85. Available from: https://linkinghub.elsevier.com/retrieve/pii/S0092867414013191

288. Jing L, Tamplin OJ, Chen MJ, Deng Q, Patterson S, Kim PG, et al. Adenosine signaling promotes hematopoietic stem and progenitor cell emergence. J Exp Med [Internet]. 2015 May 4;212(5):649–63. Available from: https://rupress.org/jem/article/212/5/649/41999/Adenosine-signaling-promotes-hematopoietic-stem

289. Saxena S, Rönn RE, Guibentif C, Moraghebi R, Woods N-B. Cyclic AMP Signaling through Epac Axis Modulates Human Hemogenic Endothelium and Enhances Hematopoietic Cell Generation. Stem Cell Reports [Internet]. 2016 May;6(5):692–703. Available from: https://linkinghub.elsevier.com/retrieve/pii/S2213671116300017

290. Diaz MF, Li N, Lee HJ, Adamo L, Evans SM, Willey HE, et al. Biomechanical forces promote blood development through prostaglandin E2 and the cAMP–PKA signaling axis. J Exp Med [Internet]. 2015 May 4;212(5):665–80. Available from: https://rupress.org/jem/article/212/5/665/41984/Biomechanical-forces-promote-blood-development

291. North TE, Goessling W, Peeters M, Li P, Ceol C, Lord AM, et al. Hematopoietic Stem Cell Development Is Dependent on Blood Flow. Cell [Internet]. 2009 May;137(4):736–48. Available from: https://linkinghub.elsevier.com/retrieve/pii/S0092867409004486

292. Adamo L, Naveiras O, Wenzel PL, McKinney-Freeman S, Mack PJ, Gracia-Sancho J, et al. Biomechanical forces promote embryonic haematopoiesis. Nature [Internet]. 2009 Jun 13;459(7250):1131–5. Available from: https://www.nature.com/articles/nature08073

293. Rasighaemi P, Basheer F, Liongue C, Ward AC. Zebrafish as a model for leukemia and other hematopoietic disorders. J Hematol Oncol [Internet]. 2015 Dec 28;8(1):29. Available from: https://jhoonline.biomedcentral.com/articles/10.1186/s13045-015-0126-4

294. Murayama E, Kissa K, Zapata A, Mordelet E, Briolat V, Lin H-F, et al. Tracing Hematopoietic Precursor Migration to Successive Hematopoietic Organs during Zebrafish Development. Immunity [Internet]. 2006 Dec;25(6):963–75. Available from: https://linkinghub.elsevier.com/retrieve/pii/S1074761306005139

295. Wattrus SJ, Zon LI. Stem cell safe harbor: the hematopoietic stem cell niche in zebrafish. Blood Adv [Internet]. 2018 Nov 13;2(21):3063–9. Available from: https://ashpublications.org/bloodadvances/article/2/21/3063/16169/Stem-cell-safe-harbor-the-hematopoietic-stem-cell

296. Wolf A, Aggio J, Campbell C, Wright F, Marquez G, Traver D, et al. Zebrafish Caudal Haematopoietic Embryonic Stromal Tissue (CHEST) Cells Support Haematopoiesis. Sci Rep [Internet]. 2017 Mar 16;7(1):44644. Available from: https://www.nature.com/articles/srep44644

297. Forrester AM, Berman JN, Payne EM. Myelopoiesis and Myeloid Leukaemogenesis in the Zebrafish. Adv Hematol [Internet]. 2012;2012:1–12. Available from: http://www.hindawi.com/journals/ah/2012/358518/

298. Hu Y-X, Jing Q. Zebrafish: a convenient tool for myelopoiesis research. Cell Regen [Internet]. 2023 Jan 3;12(1):2. Available from: https://cellregeneration.springeropen.com/articles/10.1186/s13619-022-00139-2

299. Chen AT, Zon LI. Zebrafish blood stem cells. J Cell Biochem [Internet]. 2009 Sep 29;108(1):35–42. Available from: https://onlinelibrary.wiley.com/doi/10.1002/jcb.22251

300. Kulkeaw K, Sugiyama D. Zebrafish erythropoiesis and the utility of fish as models of anemia. Stem Cell Res Ther [Internet]. 2012 Dec 20;3(6):55. Available from: https://stemcellres.biomedcentral.com/articles/10.1186/scrt146

301. Xia J, Kang Z, Xue Y, Ding Y, Gao S, Zhang Y, et al. A single-cell resolution developmental atlas of hematopoietic stem and progenitor cell expansion in zebrafish. Proc Natl Acad Sci [Internet]. 2021 Apr 6;118(14). Available from: https://pnas.org/doi/full/10.1073/pnas.2015748118

302. Miao KZ, Kim GY, Meara GK, Qin X, Feng H. Tipping the Scales With Zebrafish to Understand Adaptive Tumor Immunity. Front Cell Dev Biol [Internet]. 2021 May 20;9. Available from: https://www.frontiersin.org/articles/10.3389/fcell.2021.660969/full

303. Willett CE, Cortes A, Zuasti A, Zapata AG. Early hematopoiesis and developing lymphoid organs in the zebrafish. Dev Dyn [Internet]. 1999 Apr;214(4):323–36. Available from: https://onlinelibrary.wiley.com/doi/10.1002/(SICI)1097-0177(199904)214:4%3C323::AID-AJA5%3E3.0.CO;2-3

304. Riera Romo M, Pérez-Martínez D, Castillo Ferrer C. Innate immunity in vertebrates: an overview. Immunology [Internet]. 2016 Jun 5;148(2):125–39. Available from: https://onlinelibrary.wiley.com/doi/10.1111/imm.12597

305. Hu C, Wang J, Hong Y, Li H, Fan D, Lin A, et al. Single-cell transcriptome profiling reveals diverse immune cell populations and their responses to viral infection in the spleen of zebrafish. FASEB J [Internet]. 2023 Jun 25;37(6). Available from: https://faseb.onlinelibrary.wiley.com/doi/10.1096/fj.202201505RRRR

306. Renshaw SA, Trede NS. A model 450 million years in the making: zebrafish and vertebrate immunity. Dis Model Mech [Internet]. 2012 Jan 1;5(1):38–47. Available from: https://journals.biologists.com/dmm/article/5/1/38/3186/A-model-450-million-years-in-the-making-zebrafish

307. Zanandrea R, Bonan CD, Campos MM. Zebrafish as a model for inflammation and drug discovery. Drug Discov Today [Internet]. 2020 Dec;25(12):2201–11.

Available from: https://linkinghub.elsevier.com/retrieve/pii/S1359644620303962

308. Trede NS, Langenau DM, Traver D, Look AT, Zon LI. The Use of Zebrafish to Understand Immunity. Immunity [Internet]. 2004 Apr;20(4):367–79. Available from: https://linkinghub.elsevier.com/retrieve/pii/S1074761304000846

309. Sullivan C, Kim CH. Zebrafish as a model for infectious disease and immune function. Fish Shellfish Immunol [Internet]. 2008 Oct;25(4):341–50. Available from: https://linkinghub.elsevier.com/retrieve/pii/S1050464808001319

310. Yoder JA, Nielsen ME, Amemiya CT, Litman GW. Zebrafish as an immunological model system. Microbes Infect [Internet]. 2002 Nov;4(14):1469–78. Available from: https://linkinghub.elsevier.com/retrieve/pii/S1286457902000291

311. Lam S., Chua H., Gong Z, Lam T., Sin Y. Development and maturation of the immune system in zebrafish, Danio rerio: a gene expression profiling, in situ hybridization and immunological study. Dev Comp Immunol [Internet]. 2004 Jan;28(1):9–28. Available from: https://linkinghub.elsevier.com/retrieve/pii/S0145305X03001034

312. Henry KM, Loynes CA, Whyte MKB, Renshaw SA. Zebrafish as a model for the study of neutrophil biology. J Leukoc Biol [Internet]. 2013 Oct 1;94(4):633–42. Available from: https://academic.oup.com/jleukbio/article/94/4/633/6959392

313. Torraca V, Masud S, Spaink HP, Meijer AH. Macrophage-pathogen interactions in infectious diseases: new therapeutic insights from the zebrafish host model. Dis Model Mech [Internet]. 2014 Jul 1;7(7):785–97. Available from: https://journals.biologists.com/dmm/article/7/7/785/3702/Macrophage-pathogen-interactions-in-infectious

314. Rosowski EE. Determining macrophage versus neutrophil contributions to innate immunity using larval zebrafish. Dis Model Mech [Internet]. 2020 Jan 1;13(1). Available from: https://journals.biologists.com/dmm/article/13/1/dmm041889/223112/Determining-macrophage-versus-neutrophil

315. Li D, Xue W, Li M, Dong M, Wang J, Wang X, et al. VCAM-1+ macrophages guide the homing of HSPCs to a vascular niche. Nature [Internet]. 2018 Dec 19;564(7734):119–24. Available from: https://www.nature.com/articles/s41586-018-0709-7

316. Chang Y, Sun L, Kokura K, Horton JR, Fukuda M, Espejo A, et al. MPP8 mediates the interactions between DNA methyltransferase Dnmt3a and H3K9 methyltransferase GLP/G9a. Nat Commun [Internet]. 2011 Nov 15;2(1):533. Available from: https://www.nature.com/articles/ncomms1549

317. Wang X, Ge X, Qin Y, Liu D, Chen C. Ifi30 Is Required for Sprouting Angiogenesis During Caudal Vein Plexus Formation in Zebrafish. Front Physiol [Internet]. 2022 Jul 13;13. Available from: https://www.frontiersin.org/articles/10.3389/fphys.2022.919579/full

318. Galanternik MV, Castranova D, Gore A V, Blewett NH, Jung HM, Stratman AN, et al. A novel perivascular cell population in the zebrafish brain. Elife [Internet].

2017 Apr 11;6. Available from: https://elifesciences.org/articles/24369

319. Palominos MF, Whitlock KE. The Olfactory Organ Is Populated by Neutrophils and Macrophages During Early Development. Front Cell Dev Biol [Internet]. 2021 Jan 18;8. Available from: https://www.frontiersin.org/articles/10.3389/fcell.2020.604030/full

320. Woo K, Fraser SE. Order and coherence in the fate map of the zebrafish nervous system. Development [Internet]. 1995 Aug 1;121(8):2595–609. Available from: https://journals.biologists.com/dev/article/121/8/2595/38825/Order-and-coherence-in-the-fate-map-of-the

321. Schmidt R, Strähle U, Scholpp S. Neurogenesis in zebrafish – from embryo to adult. Neural Dev [Internet]. 2013 Dec 21;8(1):3. Available from: https://neuraldevelopment.biomedcentral.com/articles/10.1186/1749-8104-8-3

322. Alexandre P, Reugels AM, Barker D, Blanc E, Clarke JDW. Neurons derive from the more apical daughter in asymmetric divisions in the zebrafish neural tube. Nat Neurosci [Internet]. 2010 Jun 9;13(6):673–9. Available from: https://www.nature.com/articles/nn.2547

323. Vaz R, Hofmeister W, Lindstrand A. Zebrafish Models of Neurodevelopmental Disorders: Limitations and Benefits of Current Tools and Techniques. Int J Mol Sci [Internet]. 2019 Mar 14;20(6):1296. Available from: https://www.mdpi.com/1422-0067/20/6/1296

324. Holzschuh J, Ryu S, Aberger F, Driever W. Dopamine transporter expression distinguishes dopaminergic neurons from other catecholaminergic neurons in the developing zebrafish embryo. Mech Dev [Internet]. 2001 Mar;101(1–2):237–43. Available from: https://linkinghub.elsevier.com/retrieve/pii/S0925477301002878

325. Higashijima S, Mandel G, Fetcho JR. Distribution of prospective glutamatergic, glycinergic, and GABAergic neurons in embryonic and larval zebrafish. J Comp Neurol [Internet]. 2004 Nov 29;480(1):1–18. Available from: https://onlinelibrary.wiley.com/doi/10.1002/cne.20278

326. Kaslin J, Ganz J. Zebrafish Nervous Systems. In: The Zebrafish in Biomedical Research [Internet]. Elsevier; 2020. p. 181–9. Available from: https://linkinghub.elsevier.com/retrieve/pii/B978012812431400018X

327. Low SE, Woods IG, Lachance M, Ryan J, Schier AF, Saint-Amant L. Touch responsiveness in zebrafish requires voltage-gated calcium channel 2.1b. J Neurophysiol [Internet]. 2012 Jul 1;108(1):148–59. Available from: https://www.physiology.org/doi/10.1152/jn.00839.2011

328. Kawai H, Arata N, Nakayasu H. Three-dimensional distribution of astrocytes in zebrafish spinal cord. Glia [Internet]. 2001 Dec 24;36(3):406–13. Available from: https://onlinelibrary.wiley.com/doi/10.1002/glia.1126

329. Peri F, Nüsslein-Volhard C. Live Imaging of Neuronal Degradation by Microglia Reveals a Role for v0-ATPase a1 in Phagosomal Fusion In Vivo. Cell [Internet]. 2008 May;133(5):916–27. Available from:

https://linkinghub.elsevier.com/retrieve/pii/S0092867408006119

330. Yoshida M, Macklin WB. Oligodendrocyte development and myelination in GFP-transgenic zebrafish. J Neurosci Res [Internet]. 2005 Jul 1;81(1):1–8. Available from: https://onlinelibrary.wiley.com/doi/10.1002/jnr.20516

331. Avila RL, Tevlin BR, Lees JPB, Inouye H, Kirschner DA. Myelin Structure and Composition in Zebrafish. Neurochem Res [Internet]. 2007 Feb 7;32(2):197–209. Available from: http://link.springer.com/10.1007/s11064-006-9136-5

332. Westerfield M, McMurray J, Eisen J. Identified motoneurons and their innervation of axial muscles in the zebrafish. J Neurosci [Internet]. 1986 Aug 1;6(8):2267–77. Available from: https://www.jneurosci.org/lookup/doi/10.1523/JNEUROSCI.06-08-02267.1986

333. d'Amora M, Giordani S. The Utility of Zebrafish as a Model for Screening Developmental Neurotoxicity. Front Neurosci [Internet]. 2018 Dec 18;12. Available from: https://www.frontiersin.org/article/10.3389/fnins.2018.00976/full

334. Nguyen-Chi M, Laplace-Builhe B, Travnickova J, Luz-Crawford P, Tejedor G, Phan QT, et al. Identification of polarized macrophage subsets in zebrafish. Elife. 2015;

335. Lin H-F, Traver D, Zhu H, Dooley K, Paw BH, Zon LI, et al. Analysis of thrombocyte development in CD41-GFP transgenic zebrafish. Blood [Internet]. 2005 Dec 1;106(12):3803–10. Available from: https://ashpublications.org/blood/article/106/12/3803/109769/Analysis-of-thrombocyte-development-in-CD41GFP

336. Santoro MM, Samuel T, Mitchell T, Reed JC, Stainier DYR. Birc2 (clap1) regulates endothelial cell integrity and blood vessel homeostasis. Nat Genet [Internet]. 2007 Nov 14;39(11):1397–402. Available from: http://www.nature.com/articles/ng.2007.8

337. Bonkhofer F, Rispoli R, Pinheiro P, Krecsmarik M, Schneider-Swales J, Tsang IHC, et al. Blood stem cell-forming haemogenic endothelium in zebrafish derives from arterial endothelium. Nat Commun [Internet]. 2019 Aug 8;10(1):3577. Available from: https://www.nature.com/articles/s41467-019-11423-2

338. Madeira F, Pearce M, Tivey ARN, Basutkar P, Lee J, Edbali O, et al. Search and sequence analysis tools services from EMBL-EBI in 2022. Nucleic Acids Res [Internet]. 2022 Jul 5;50(W1):W276–9. Available from: https://academic.oup.com/nar/article/50/W1/W276/6567472

339. Muffato M, Louis A, Poisnel C-E, Crollius HR. Genomicus: a database and a browser to study gene synteny in modern and ancestral genomes. Bioinformatics [Internet]. 2010 Apr 15;26(8):1119–21. Available from: https://academic.oup.com/bioinformatics/article/26/8/1119/206096

340. Nguyen NTT, Vincens P, Dufayard JF, Roest Crollius H, Louis A. Genomicus in 2022: comparative tools for thousands of genomes and reconstructed ancestors. Nucleic Acids Res [Internet]. 2022 Jan 7;50(D1):D1025–31. Available from: https://academic.oup.com/nar/article/50/D1/D1025/6430844

341. Smith LL, Gupta VA, Beggs AH. Bridging integrator 1 (Bin1) deficiency in zebrafish results in centronuclear myopathy. Hum Mol Genet [Internet]. 2014 Jul 1;23(13):3566–78. Available from: http://academic.oup.com/hmg/article/23/13/3566/661174/Bridging-integrator-1-Bin1-deficiency-in-zebrafish

342. Hall CJ, Sanderson LE, Lawrence LM, Pool B, van der Kroef M, Ashimbayeva E, et al. Blocking fatty acid–fueled mROS production within macrophages alleviates acute gouty inflammation. J Clin Invest [Internet]. 2018 May 1;128(5):1752–71. Available from: https://www.jci.org/articles/view/94584

343. Cordero-Maldonado ML, Siverio-Mota D, Vicet-Muro L, Wilches-Arizábala IM, Esguerra C V., de Witte PAM, et al. Optimization and Pharmacological Validation of a Leukocyte Migration Assay in Zebrafish Larvae for the Rapid In Vivo Bioactivity Analysis of Anti-Inflammatory Secondary Metabolites. Gong Z, editor. PLoS One [Internet]. 2013 Oct 4;8(10):e75404. Available from: https://dx.plos.org/10.1371/journal.pone.0075404

344. Thisse C, Thisse B. High-resolution in situ hybridization to whole-mount zebrafish embryos. Nat Protoc [Internet]. 2008 Jan 20;3(1):59–69. Available from: https://www.nature.com/articles/nprot.2007.514

345. Dobrzycki T, Krecsmarik M, Monteiro R. Genotyping and Quantification of In Situ Hybridization Staining in Zebrafish. J Vis Exp [Internet]. 2020 Jan 28;(155). Available from: https://www.jove.com/t/59956/genotyping-quantification-situ-hybridization-staining

346. Gierten J, Pylatiuk C, Hammouda OT, Schock C, Stegmaier J, Wittbrodt J, et al. Automated high-throughput heartbeat quantification in medaka and zebrafish embryos under physiological conditions. Sci Rep [Internet]. 2020 Feb 6;10(1):2046. Available from: https://www.nature.com/articles/s41598-020-58563-w

347. Kawahara G, Guyon JR, Nakamura Y, Kunkel LM. Zebrafish models for human FKRP muscular dystrophies. Hum Mol Genet [Internet]. 2010 Feb 15;19(4):623–33. Available from: https://academic.oup.com/hmg/article-lookup/doi/10.1093/hmg/ddp528

348. Smith LL, Beggs AH, Gupta VA. Analysis of Skeletal Muscle Defects in Larval Zebrafish by Birefringence and Touch-evoke Escape Response Assays. J Vis Exp [Internet]. 2013 Dec 13;(82). Available from: https://www.jove.com/t/50925/analysis-of-skeletal-muscle-defects-in-larval-zebrafish-by-birefringence-and-touch--evoke-escape-response-assays

349. Pezzotta A, Gentile I, Genovese D, Totaro MG, Battaglia C, Leung AY-H, et al. HDAC6 inhibition decreases leukemic stem cell expansion driven by Hedgehog hyperactivation by restoring primary ciliogenesis. Pharmacol Res [Internet]. 2022 Sep;183:106378. Available from: https://linkinghub.elsevier.com/retrieve/pii/S1043661822003231

350. Jin S-W, Beis D, Mitchell T, Chen J-N, Stainier DYR. Cellular and molecular analyses of vascular tube and lumen formation in zebrafish. Development [Internet]. 2005 Dec 1;132(23):5199–209. Available from:

https://journals.biologists.com/dev/article/132/23/5199/43152/Cellular-and-molecular-analyses-of-vascular-tube

351. Kilroy EA, Ignacz AC, Brann KL, Schaffer CE, Varney D, Alrowaished SS, et al. Beneficial impacts of neuromuscular electrical stimulation on muscle structure and function in the zebrafish model of Duchenne muscular dystrophy. Elife [Internet]. 2022 Mar 24;11. Available from: https://elifesciences.org/articles/62760

352. Cumano A, Godin I. Ontogeny of the Hematopoietic System. Annu Rev Immunol [Internet]. 2007 Apr 1;25(1):745–85. Available from: https://www.annualreviews.org/doi/10.1146/annurev.immunol.25.022106.141538

353. Boehmler W, Petko J, Woll M, Frey C, Thisse B, Thisse C, et al. Identification of zebrafish A2 adenosine receptors and expression in developing embryos. Gene Expr Patterns [Internet]. 2009 Mar;9(3):144–51. Available from: https://linkinghub.elsevier.com/retrieve/pii/S1567133X08001221

354. Adair TH. Growth regulation of the vascular system: an emerging role for adenosine. Am J Physiol Integr Comp Physiol [Internet]. 2005 Aug;289(2):R283–96. Available from: https://www.physiology.org/doi/10.1152/ajpregu.00840.2004

355. Poullet N, Golushko I, Lorman V, Travnickova J, Bureau C, Chalin D, et al. Mechanical instabilities of aorta drive blood stem cell production: a live study. Cell Mol Life Sci [Internet]. 2020 Sep 16;77(17):3453–64. Available from: http://link.springer.com/10.1007/s00018-019-03372-2

356. Gering M, Rodaway ARF, Göttgens B, Patient RK, Green AR. The SCL gene specifies haemangioblast development from early mesoderm. EMBO J [Internet]. 1998 Jul 15;17(14):4029–45. Available from: http://emboj.embopress.org/cgi/doi/10.1093/emboj/17.14.4029

357. de Bruijn M, Dzierzak E. Runx transcription factors in the development and function of the definitive hematopoietic system. Blood [Internet]. 2017 Apr 13;129(15):2061–9. Available from: https://ashpublications.org/blood/article/129/15/2061/36387/Runx-transcription-factors-in-the-development-and

358. Wang HU, Chen Z-F, Anderson DJ. Molecular Distinction and Angiogenic Interaction between Embryonic Arteries and Veins Revealed by ephrin-B2 and Its Receptor Eph-B4. Cell [Internet]. 1998 May;93(5):741–53. Available from: https://linkinghub.elsevier.com/retrieve/pii/S0092867400814361

359. Gore A V., Pillay LM, Venero Galanternik M, Weinstein BM. The zebrafish: A fintastic model for hematopoietic development and disease. WIREs Dev Biol [Internet]. 2018 May 13;7(3). Available from: https://wires.onlinelibrary.wiley.com/doi/10.1002/wdev.312

360. Primer for Morpholino Use in Zebrafish. Available from: https://www.gene-tools.com/content/splicing-outcomes-targeting-exon-skipping-or-intron-inclusion

361. Ferrara G. Abstracts of the Fifth Brainstorming Research Assembly for Young

Neuroscientists (BraYn), Italy, 28–30 September 2022. Neurol Int [Internet]. 2023 Mar 14;15(1):415–96. Available from: https://www.mdpi.com/2035-8377/15/1/28

362. Zaqout S, Morris-Rosendahl D, Kaindl A. Autosomal Recessive Primary Microcephaly (MCPH): An Update. Neuropediatrics [Internet]. 2017 Jun 11;48(03):135–42. Available from: http://www.thieme-connect.de/DOI/DOI?10.1055/s-0037-1601448

363. Griffin A, Carpenter C, Liu J, Paterno R, Grone B, Hamling K, et al. Phenotypic analysis of catastrophic childhood epilepsy genes. Commun Biol [Internet]. 2021 Jun 3;4(1):680. Available from: https://www.nature.com/articles/s42003-021-02221-y

364. Moulton JD. Using Morpholinos to Control Gene Expression. Curr Protoc Nucleic Acid Chem [Internet]. 2017 Mar 2;68(1). Available from: https://currentprotocols.onlinelibrary.wiley.com/doi/10.1002/cpnc.21

365. Pinto B, Deo P, Sharma S, Syal A, Sharma A. Expanding spectrum of DADA2: a review of phenotypes, genetics, pathogenesis and treatment. Clin Rheumatol [Internet]. 2021 Oct 31;40(10):3883–96. Available from: https://link.springer.com/10.1007/s10067-021-05711-w

366. Ketharnathan S, Rajan V, Prykhozhij S V., Berman JN. Zebrafish models of inflammation in hematopoietic development and disease. Front Cell Dev Biol [Internet]. 2022 Jul 18;10. Available from: https://www.frontiersin.org/articles/10.3389/fcell.2022.955658/full

367. Frame JM, Kubaczka C, Long TL, Esain V, Soto RA, Hachimi M, et al. Metabolic Regulation of Inflammasome Activity Controls Embryonic Hematopoietic Stem and Progenitor Cell Production. Dev Cell [Internet]. 2020 Oct;55(2):133-149.e6. Available from: https://linkinghub.elsevier.com/retrieve/pii/S153458072030589X

368. López DA, Apostol AC, Lebish EJ, Valencia CH, Romero-Mulero MC, Pavlovich P V., et al. Prenatal inflammation perturbs murine fetal hematopoietic development and causes persistent changes to postnatal immunity. Cell Rep [Internet]. 2022 Nov;41(8):111677. Available from: https://linkinghub.elsevier.com/retrieve/pii/S2211124722015510

369. King KY, Goodell MA. Inflammatory modulation of HSCs: viewing the HSC as a foundation for the immune response. Nat Rev Immunol [Internet]. 2011 Oct 9;11(10):685–92. Available from: https://www.nature.com/articles/nri3062

370. Matatall KA, Jeong M, Chen S, Sun D, Chen F, Mo Q, et al. Chronic Infection Depletes Hematopoietic Stem Cells through Stress-Induced Terminal Differentiation. Cell Rep [Internet]. 2016 Dec;17(10):2584–95. Available from: https://linkinghub.elsevier.com/retrieve/pii/S2211124716315893

371. Pietras EM, Mirantes-Barbeito C, Fong S, Loeffler D, Kovtonyuk L V., Zhang S, et al. Chronic interleukin-1 exposure drives haematopoietic stem cells towards precocious myeloid differentiation at the expense of self-renewal. Nat Cell Biol [Internet]. 2016 Jun 25;18(6):607–18. Available from: https://www.nature.com/articles/ncb3346

372. Meacham CE, Jeffery EC, Burgess RJ, Sivakumar CD, Arora MA, Stanley AM, et al. Adiponectin receptors sustain haematopoietic stem cells throughout adulthood by protecting them from inflammation. Nat Cell Biol [Internet]. 2022 May 5;24(5):697–707. Available from: https://www.nature.com/articles/s41556-022-00909-9

373. Heck AM, Ishida T, Hadland B. Location, Location, Location: How Vascular Specialization Influences Hematopoietic Fates During Development. Front Cell Dev Biol [Internet]. 2020 Nov 13;8. Available from: https://www.frontiersin.org/articles/10.3389/fcell.2020.602617/full

374. Ferri-Lagneau KF, Haider J, Sang S, Leung T. Rescue of hematopoietic stem/progenitor cells formation in plcg1 zebrafish mutant. Sci Rep [Internet]. 2019 Jan 21;9(1):244. Available from: https://www.nature.com/articles/s41598-018-36338-8

375. Travnickova J, Tran Chau V, Julien E, Mateos-Langerak J, Gonzalez C, Lelièvre E, et al. Primitive macrophages control HSPC mobilization and definitive haematopoiesis. Nat Commun [Internet]. 2015 Feb 17;6(1):6227. Available from: https://www.nature.com/articles/ncomms7227

376. Borea PA, Gessi S, Merighi S, Vincenzi F, Varani K. Pharmacology of Adenosine Receptors: The State of the Art. Physiol Rev [Internet]. 2018 Jul 1;98(3):1591–625. Available from: https://www.physiology.org/doi/10.1152/physrev.00049.2017

377. McNeill SM, Baltos J-A, White PJ, May LT. Biased agonism at adenosine receptors. Cell Signal [Internet]. 2021 Jun;82:109954. Available from: https://linkinghub.elsevier.com/retrieve/pii/S0898656821000425

378. De Filippo E, Hinz S, Pellizzari V, Deganutti G, El-Tayeb A, Navarro G, et al. A2A and A2B adenosine receptors: The extracellular loop 2 determines high (A2A) or low affinity (A2B) for adenosine. Biochem Pharmacol [Internet]. 2020 Feb;172:113718. Available from: https://linkinghub.elsevier.com/retrieve/pii/S0006295219304174

379. Sun Y, Huang P. Adenosine A2B Receptor: From Cell Biology to Human Diseases. Front Chem [Internet]. 2016 Aug 24;4. Available from: http://journal.frontiersin.org/Article/10.3389/fchem.2016.00037/abstract

380. Feoktistov I, Biaggioni I. Role of Adenosine A2B Receptors in Inflammation. In 2011. p. 115–44. Available from: https://linkinghub.elsevier.com/retrieve/pii/B9780123855268000059

381. Sun C-X. Role of A2B adenosine receptor signaling in adenosine-dependent pulmonary inflammation and injury. J Clin Invest [Internet]. 2006 Aug 1;116(8):2173–82. Available from: http://www.jci.org/cgi/doi/10.1172/JCI27303

382. Linden J. Regulation of Leukocyte Function by Adenosine Receptors. In 2011. p. 95–114. Available from: https://linkinghub.elsevier.com/retrieve/pii/B9780123855268000047

383. Ryzhov S, Zaynagetdinov R, Goldstein AE, Novitskiy S V., Blackburn MR, Biaggioni I, et al. Effect of A 2B Adenosine Receptor Gene Ablation on

Adenosine-Dependent Regulation of Proinflammatory Cytokines. J Pharmacol Exp Ther [Internet]. 2008 Feb;324(2):694–700. Available from: http://jpet.aspetjournals.org/lookup/doi/10.1124/jpet.107.131540

384. Kolachala V, Asamoah V, Wang L, Obertone TS, Ziegler TR, Merlin D, et al. TNF-α upregulates adenosine 2b (A2b) receptor expression and signaling in intestinal epithelial cells: a basis for A2bR overexpression in colitis. Cell Mol Life Sci [Internet]. 2005 Nov 2;62(22):2647–57. Available from: http://link.springer.com/10.1007/s00018-005-5328-4

385. Zurovec M, Dolezal T, Gazi M, Pavlova E, Bryant PJ. Adenosine deaminase-related growth factors stimulate cell proliferation in Drosophila by depleting extracellular adenosine. Proc Natl Acad Sci [Internet]. 2002 Apr 2;99(7):4403–8. Available from: https://pnas.org/doi/full/10.1073/pnas.062059699

386. Hofer M, Pospisil M, Weiterova L, Hoferova Z. The Role of Adenosine Receptor Agonists in Regulation of Hematopoiesis. Molecules [Internet]. 2011 Jan 17;16(1):675–85. Available from: http://www.mdpi.com/1420-3049/16/1/675

387. Calvi LM, Link DC. The hematopoietic stem cell niche in homeostasis and disease. Blood [Internet]. 2015 Nov 26;126(22):2443–51. Available from: https://ashpublications.org/blood/article/126/22/2443/34611/The-hematopoietic-stem-cell-niche-in-homeostasis

388. Stosik M, Tokarz-Deptuła B, Deptuła W. Haematopoiesis in Zebrafish (Danio Rerio). Front Immunol [Internet]. 2022 Jun 2;13. Available from: https://www.frontiersin.org/articles/10.3389/fimmu.2022.902941/full

389. Marty I. Triadin regulation of the ryanodine receptor complex. J Physiol [Internet]. 2015 Aug 20;593(15):3261–6. Available from: https://physoc.onlinelibrary.wiley.com/doi/10.1113/jphysiol.2014.281147

390. Marty I, Robert M, Ronjat M, Bally I, Arlaud G, Villaz M. Localization of the N-terminal and C-terminal ends of triadin with respect to the sarcoplasmic reticulum membrane of rabbit skeletal muscle. Biochem J [Internet]. 1995 May 1;307(3):769–74. Available from: https://portlandpress.com/biochemj/article/307/3/769/31312/Localization-of-the-N-terminal-and-C-terminal-ends

391. Marty I, Fauré J, Fourest-Lieuvin A, Vassilopoulos S, Oddoux S, Brocard J. Triadin: what possible function 20 years later? J Physiol [Internet]. 2009 Jul 30;587(13):3117–21. Available from: https://physoc.onlinelibrary.wiley.com/doi/10.1113/jphysiol.2009.171892

List of figures and tables

Dissemination of results

The results collected during the realization of this PhD project have already been partly made public to the scientific community through publication in international journals and presentations at national and international congresses. In particular, the data collected on the DADA2 project are presented in a research article that is currently under review at the peer-reviewed open-access journal of the Nature Portfolio "Communications Biology": All the raw data of this project have been uploaded to the Dataverse public repository associated with the University of Milan and will be made permanently public and accessible following publication. These data were also disseminated during the PhD period at the following conferences:

- upcoming 4th Zebrafish Italian Meeting, Palermo (Italy), 7-9 February 2024 – selected for oral presentation – **"ADA2 regulates inflammation and hematopoietic stem cells emergence via the A2bR pathway in zebrafish".**

- 7th BioMeTra Workshop (annual internal departmental workshop), Milano (Italy), 19th September 2023 - oral presentation - **"A new *in-vivo* zebrafish model with *cecr1b* deficiency fully recapitulates the pathological features of human adenosine deaminase 2 deficiency".**

- 12th European Zebrafish Meeting, Krakow (Poland), 9-13 July 2023 - poster presentation - **"A new *in-vivo* zebrafish model with *cecr1b* deficiency fully recapitulates the pathological features of human adenosine deaminase 2 deficiency".**

- MyDEV meeting 2023, Milano (Italy), 19th May 2023 - poster presentation - **"A new *in-vivo* zebrafish model with *cecr1b* deficiency fully recapitulates the pathological features of human adenosine deaminase 2 deficiency".**

- 3rd Zebrafish Italian Meeting, Napoli (Italy), 9-11 February 2022 - oral presentation - **"An *in-vivo* zebrafish model with *cecr1b* deficiency recapitulates human DADA2 phenotype".**

- Zebrafish Disease Model Society (ZDMS) Conference, Sheffield (UK), 5-8 September 2022 - poster presentation - **"A promising *ada2* loss-of-function zebrafish model to study the pathogenesis and efficiently correct the Deficiency of Adenosine Deaminase 2 (DADA2) phenotype".**

- MyDEV meeting 2021, Milano (Italy), May 2021 - poster presentation - **"An in-vivo zebrafish model with *cecr1b* deficiency recapitulates human DADA2 phenotype".**

TKOS project was concluded with a publication in the peer-reviewed access International Journal of Molecular Sciences of the MDPI group:

Vecchi, V. M., Spreafico, M., Brix, A., Santoni, A., Sala, S., Pistocchi, A., Marozzi, A., & Di Resta, C. (2021). "**Generation of a Triadin KnockOut Syndrome Zebrafish Model"** International Journal of Molecular Sciences, 22(18), 9720. https://doi.org/10.3390/ijms22189720.

Concerning the research lines related to the models for MCPH17 and GENE-X, the data collected will be included and merged with those of our collaborators for publication in peer-reviewed international scientific journals.

Lay abstract – Italiano:

Lo zebrafish (*Danio rerio*), un piccolo pesce di acqua dolce originario dell'Asia, è un animale modello per lo studio di malattie genetiche umane. La maggior parte dei geni umani si ritrovano infatti anche in questo pesce, così come la maggior parte degli organi, dei sistemi e dei meccanismi fisiologici che governano il funzionamento dell'organismo. In questo progetto di ricerca è stato usato il pesce zebrafish per la creazione di quattro diversi modelli di malattie umane: il deficit di adenosine deaminasi 2 (DADA2), la microcefalia primaria ereditaria 17 (MCPH17), la sindrome da "triadina-knockout" (TKOS) e una nuova sindrome mai descritta prima e non ancora associata ad alcuna causa certa. Queste patologie sono causate dall'assenza di specifici geni e sono accomunate dal fatto che il meccanismo molecolare che le induce non è noto e

che non sono disponibili terapie risolutive. Abbiamo quindi identificato e silenziato nel pesce zebrafish i geni che nell'uomo sono mutati in tali patologie, generando modelli-malattia che ricapitolano quanto accade nei pazienti. Tali modelli ci hanno permesso di studiare i meccanismi responsabili delle patologie in esame in modo più rapido e più semplice rispetto ai modelli murini. Abbiamo quindi la possibilità di testare in un organismo vitale l'effetto di farmaci, semplificando e accelerando il processo di creazione di nuove terapie. I risultati ottenuti, opportunamente integrati con i dati raccolti sui pazienti e sugli altri modelli in vitro e in vivo, possono contribuire significativamente all'avanzamento della ricerca biomedica e della conoscenza e cura di queste malattie.

Lay abstract – inglese:

Zebrafish (*Danio rerio*), a small freshwater fish native to Asia, is an ideal animal for studying human genetic diseases. Most human genes are also found in this fish, as are most of the organs, systems, and physiological mechanisms that govern the functioning of the body. In this research project, the zebrafish was used to create four different models of human diseases: adenosine deaminase 2 deficiency (DADA2), microcephaly primary hereditary 17 (MCPH17), triadine-knockout syndrome (TKOS) and a new complex syndrome that has never been described before and that is not yet associated with any certain cause. These diseases are caused by the absence of specific genes and are linked by the fact that the molecular mechanism inducing them is unknown and that there are no resolving therapies available. We have therefore identified and silenced in zebrafish the genes that are linked to these diseases in humans, generating disease models that recapitulate what happens in patients. These zebrafish models allowed us to study the mechanisms responsible for the disease more quickly easier than in rodent models. We have thus created valuable tools that allow us to test the effect of new drugs in a complete, living organism, simplifying and accelerating the process of creating new therapies. The results obtained, properly integrated with data collected on patients and other animal models, can contribute significantly to the advancement of biomedical research and to the advancement of knowledge and treatment of these diseases.